

**ROBUST MICRORNA DETECTION BY CAPILLARY  
ELECTROPHORESIS**

**LIANG HU**

A DISSERTATION SUBMITTED TO  
THE FACULTY OF GRADUATE STUDIES  
IN PARTIAL FULFILLMENT OF THE REQUIREMENTS  
FOR THE DEGREE OF  
DOCTOR OF PHILOSOPHY

GRADUATE PROGRAM IN CHEMISTRY  
YORK UNIVERSITY  
TORONTO, ONTARIO

© Liang Hu, 2023

## ABSTRACT

MicroRNA (miRNA) are short single-stranded RNA molecules that function as post-transcriptional regulators in gene expression. The abnormal expression of small subsets of miRNAs, termed “miRNA fingerprints”, have been found as potential biomarkers in diagnosis of various diseases including cancers. However, none of miRNA-based biomarkers has been approved yet for clinical use due to the lack of a robust quantitative method for miRNA analysis. To address this issue, there has been significant efforts towards developing robust quantitative miRNA detection methods. Among a variety of initiatives, DQAMmiR is a promising approach developed by our lab which is capable of direct, quantitative analysis of multiple miRNAs in capillary electrophoresis (CE). In my PhD project, I have been focusing on investigating and improving the robustness of DQAMmiR to increase its applicability for practical use.

Firstly, I demonstrate that DQAMmiR is capable of directly quantitating miRNA in crude cell lysates, indicating its robustness to the change of sample matrices, revealing its great potential to be used to analyzing miRNAs in biological samples directly without the need for complex sample processing. Secondly, I developed a second-generation DQAMmiR by replacing the ssDNA probes with the electrically neutral peptide nucleic acid (PNA) probes, which further improves the robustness of the assay by removing the need for single-stranded DNA binding protein (SSB) in the assay. Thirdly, to increase the applicability of the assay, I introduced a new sample preconcentration technique based on the integration of field-amplified sample stacking (FASS) and isotachopheresis (ITP) prior to CE separation in DQAMmiR, which successfully decreases its limit of quantification (LOQ) by 140 times. Lastly, I investigated the applicability of DQAMmiR for analyzing urinary miRNAs. I demonstrated that the concentration ratio of two miRNAs, miR-16 and miR-21, could be relative stable from different urine samples collected from

the same person, although the individual concentrations of these miRNAs varied significantly in these samples. These findings suggests that the ratiometric measurements between multiple miRNAs in urine would serve as better biomarkers than individual miRNA concentrations for clinical diagnostic tests. And DQAMmiR would be an ideal analytical methodology for the development and use of such tests.

## **DEDICATION**

I dedicate this thesis to the unwavering support and love of my family, whose encouragement has been the foundation of my journey.

To mom and dad, whose belief in my ability and endless sacrifices have shaped the person I am today. Your unwavering support and constant encouragement have been a beacon of strength throughout this arduous endeavor.

To my brother and sisters, who have been confidante and source of inspiration. Your unwavering support and unwavering belief in me have been a constant reminder that I am never alone on this journey.

To my wife, Jessica, whose love, patience, and understanding have sustained me during the challenging times of this pursuit. Your unwavering support, encouragement, and sacrifices have been the cornerstone of my success. Your belief in me, even when I doubted myself, has been a constant source of motivation. Thank you for standing by my side through the highs and lows of this journey.

Lastly, to my dear Ethan, who has brought immense joy and purpose to my life. Your innocence, laughter, and unwavering belief in me have fueled my determination to succeed. I dedicate this work to you, with the hope that it will inspire you to pursue your dreams fearlessly.

To my family, thank you for your unconditional love, understanding, and support. This accomplishment would not have been possible without each and every one of you. I am forever grateful for the love and strength you have provided throughout this journey.

## ACKNOWLEDGEMENTS

First and foremost, I am deeply grateful to Prof. Sergey Krylov for his invaluable guidance and unwavering support throughout my doctoral journey. Without his presence and mentorship, I would not have reached this significant milestone. Prof. Krylov's exceptional patience has enabled me to overcome challenges and complete each project, even when the timelines extended far beyond initial expectations. His vast knowledge and expertise have provided answers to all of my inquiries, further enriching my research endeavors. Moreover, his strong work ethic has served as a constant source of inspiration and motivation, propelling me forward during moments of doubt. Above all, Prof. Krylov has nurtured in me a profound sense of confidence, instilling the belief that I am capable of achieving greatness in both science and in life.

I would like to express my heartfelt gratitude to Dr. Svetlana Krylova for her exceptional guidance and support throughout my journey in the lab. Her meticulous attention to detail and insightful suggestions have been instrumental in shaping the quality and direction of my research. I am truly fortunate to have had her as my mentor, and I am immensely grateful for her invaluable contributions to my success. I also want to extend my heartfelt gratitude to the remarkable colleagues and friends who have played a pivotal role in my journey within the laboratory. To Dr. David Wegman, Dr. Mirzo Kanoatov, Dr. Alexander Stasheuski, and Dr. Sven Kochmann, my mentors during my junior years in the lab, I am profoundly grateful for your invaluable guidance. Your mentorship has been instrumental in laying the foundation of my research endeavors. I would also like to express my sincere appreciation to Stas, An, Nikita, and Jean Luc for the exhilarating experience of motivating and supporting one another. Without that, I would not have achieved what I have today. Likewise, to Tong, Mansi, Shakiba, and Eden, it has been a pleasure

collaborating with you and witnessing your growth and success. I wholeheartedly wish you all the best in your future endeavors, both personally and professionally.

To all the current and former members of the Krylov lab, I extend my deepest thanks for the enriching collaboration and friendships. Your presence has made every day in the lab an enjoyable and fulfilling experience.

I am grateful to Prof. Kathi Hudak and Philip Johnson for their valuation time and guidance. Your insightful questions and comments on my research have been immensely valuable during our interactions.

I would also like to acknowledge and express my appreciation to our funding agencies, NSERC and CREATE, for their continuous support. Your funding has been instrumental in enabling and advancing my research pursuits.

Lastly, I would like to express my appreciation to all the individuals who have contributed to my journey in ways big or small. Your support and belief in my abilities have been immeasurable.

## TABLE OF CONTENTS

ABSTRACT.....	II
DEDICATION.....	IV
ACKNOWLEDGEMENTS.....	V
TABLE OF CONTENTS .....	VII
LIST OF TABLES.....	X
LIST OF FIGURES.....	XI
COMMONLY USED ABBREVIATIONS.....	XIV
<b>CHAPTER 1. INTRODUCTION.....</b>	<b>1</b>
<b>1.1. INTRODUCTION TO miRNAs.....</b>	<b>1</b>
1.1.1. <i>Biogenesis of miRNAs</i> .....	1
1.1.2. <i>Biological functions of miRNAs</i> .....	2
1.1.3. <i>miRNAs in Disease</i> .....	3
<b>1.2. miRNA DETECTION METHODS.....</b>	<b>5</b>
1.2.1. <i>Classification of miRNA detection methods</i> .....	6
1.2.1.1. Sequencing-based methods.....	6
1.2.1.2. Signature-based methods .....	7
1.2.1.3. Hybridization-based methods .....	8
1.2.2. <i>Hybridization-based miRNA quantification in capillary electrophoresis</i> .....	18
1.2.2.1. Introduction to Capillary Electrophoresis .....	18
1.2.2.2. Hybridization Assays in CE .....	19
1.2.2.3. Direct quantitative analysis of multiple miRNAs (DQAMmiR).....	21
<b>1.3. ELECTROPHORESIS-BASED ONLINE SAMPLE PRECONCENTRATION (OSP) TECHNIQUES .....</b>	<b>24</b>
1.3.1. <i>Facilitating velocity gradient via mobility gradient <math>\partial\mu\epsilon\rho\partial x</math></i> .....	27
1.3.1.1. Charge changing-induced mobility gradient .....	27
1.3.1.2. Size changing-induced mobility gradient .....	28
1.3.2. <i>Facilitating velocity gradient via electric field gradient <math>\partial E\partial x</math></i> .....	29
1.3.2.1. Field-amplified sample stacking (FASS) .....	29
1.3.2.2. Field-amplified sample injection (FAI) .....	30
1.3.2.3. Large-volume sample stacking (LVSS) .....	31
1.3.2.4. Isotachopheresis (ITP).....	32
<b>CHAPTER 2. ACCURATE MICRORNA ANALYSIS IN CRUDE CELL LYSATE BY CAPILLARY ELECTROPHORESIS-BASED HYBRIDIZATION ASSAY IN COMPARISON WITH QUANTITATIVE REVERSE TRANSCRIPTION-POLYMERASE CHAIN REACTION.....</b>	<b>36</b>
<b>2.1. INTRODUCTION.....</b>	<b>36</b>
<b>2.2. MATERIALS AND METHODS.....</b>	<b>38</b>
2.2.1. <i>miRNAs and DNA Probe</i> .....	38
2.2.2. <i>Cell Lysate and RNA Extract</i> .....	38
2.2.3. <i>DQAMmiR</i> .....	39
2.2.4. <i>Quantitative Reverse Transcription-Polymerase Chain Reaction (qRT-PCR)</i> .....	40
<b>2.3. RESULTS AND DISCUSSION.....</b>	<b>41</b>
2.3.1. <i>Effect of sample matrix on hybridization</i> .....	42
2.3.2. <i>Effect of sample matrix on probe degradation</i> .....	44
2.3.3. <i>Effect of sample matrix on the performance of DQAMmiR in comparison to qRT-PCR</i> .....	45
<b>2.4. CONCLUSION .....</b>	<b>48</b>

<b>CHAPTER 3. DIRECT QUANTITATIVE ANALYSIS OF MULTIPLE MICRORNA (DQAMMIR) WITH PEPTIDE NUCLEIC ACID HYBRIDIZATION PROBES .....</b>	<b>49</b>
3.1. INTRODUCTION TO DQAMmiR WITH PNA PROBES.....	49
3.2. MATERIALS AND METHODS .....	51
3.2.1. <i>miRNAs and PNA probes</i> .....	51
3.2.2. <i>Hybridization reactions</i> .....	52
3.2.3. <i>Capillary electrophoresis</i> .....	52
3.2.4. <i>Derivation of the equation for the determination of concentrations of multiple miRNAs by PNA facilitated DQAMmiR</i> .....	53
3.3. RESULTS AND DISCUSSION .....	55
3.3.1. <i>Separation of the PNA probe from PNA–miRNA hybrid in CE</i> .....	55
3.3.2. <i>Theoretical estimation of the electrophoretic mobility of PNA–RNA hybrids</i> .....	56
3.3.3. <i>DQAMmiR with PNA probes</i> .....	60
3.4. CONCLUSIONS.....	64
<b>CHAPTER 4. NECESSITY AND CHALLENGES OF SAMPLE PRECONCENTRATION IN ANALYSIS OF MULTIPLE MICRORNAS BY CAPILLARY ELECTROPHORESIS .....</b>	<b>66</b>
4.1. INTRODUCTION.....	66
4.2. MATERIALS AND METHODS .....	71
4.2.1. <i>miRNAs and PNA Probes</i> .....	71
4.2.2. <i>Hybridization Reactions</i> .....	72
4.2.3. <i>Protocol of cell culture</i> .....	72
4.2.4. <i>CE-LIF Instrument</i> .....	73
4.2.5. <i>Relative quantum yields measurements</i> .....	73
4.2.6. <i>Standard CE-Based DQAMmiR</i> .....	74
4.2.7. <i>ITP-CE for DQAMmiR</i> .....	74
4.2.8. <i>FASS-ITP-CE for DQAMmiR</i> .....	75
4.2.9. <i>Quantitation of miRNA</i> .....	76
4.2.10. <i>Analyzing miRNAs in crude cell lysates</i> .....	76
4.3. RESULTS AND DISCUSSION .....	77
4.3.1. <i>ITP-CE for DQAMmiR with PNA probes</i> .....	77
4.3.2. <i>FASS-ITP-CE for DQAMmiR with PNA probes</i> .....	80
4.3.2.1. <i>Effect of sample buffer concentration on PNA/miRNA hybridization</i> .....	80
4.3.2.2. <i>Ability of retaining excess PNA probes in FASS-ITP-CE</i> .....	82
4.3.2.3. <i>Evaluation the preconcentration efficiency of FASS-ITP-CE</i> .....	84
4.3.2.4. <i>Purification of the PNA probes using FASS-ITP-CE</i> .....	85
4.3.2.5. <i>FASS-ITP-CE for DQAMmiR with PNA probes</i> .....	88
4.3.2.6. <i>Analysis of endogenous miRNAs in crude cell lysates by FASS-ITP-CE</i> .....	91
4.4. CONCLUSIONS.....	92
<b>CHAPTER 5. RATIOMETRIC ANALYSIS OF MICRORNAS IN URINE BY CAPILLARY ELECTROPHORESIS ENABLES THEIR CLINICAL USE AS NON-INVASIVE BIOMARKERS .....</b>	<b>94</b>
5.1. INTRODUCTION.....	94
5.2. MATERIALS AND METHODS .....	96
5.2.1. <i>miRNAs and DNA probes</i> .....	96
5.2.2. <i>Standard CE-Based DQAMmiR</i> .....	97
5.2.3. <i>ITP-CE for DQAMmiR</i> .....	97
5.2.4. <i>Urine Sample Collection and Processing</i> .....	97
5.3. RESULTS AND DISCUSSION .....	98

5.3.1.	<i>Implementing DQAMmiR for simultaneous quantitation of miR-16 and miR-21</i> .....	98
5.3.2.	<i>Implementing ITP-DQAMmiR for simultaneous quantitation of miR-16 and miR-21</i> .....	99
5.3.3.	<i>Analysis of miR-16 and miR-21 in urine sediments with ITP-DQAMmiR</i> .....	102
5.4.	CONCLUSIONS.....	105
	CONCLUDING REMARKS.....	106
	FUTURE PLANS .....	108
	LIST OF PUBLICATIONS.....	109
	REFERENCE .....	110

## LIST OF TABLES

Table 3.1. Detailed sequences of target miRNAs and their complementary PNA hybridization probes.	53
Table 3.2. Relative quantum yields of PNA probes for the respective miRNAs	64
Table 3.3. Quantification results of DQAMmiR measurements with PNA probes.	64
Table 4.1. Sequences of target miRNAs and their fluorescently labeled complementary PNA hybridization probes	73
Table 4.2. Relative quantum yields of PNA–miRNA hybrids (qH) with respect to their unbound PNA probes.	75
Table 4.3. Relative quantum yields of the PNA probes (qP) to the PNA probe corresponding to miR-100 for signal normalization.	75
Table 4.4. Quantitation results of the measurements.	91
Table 4.5. Concentrations of two miRNAs (miR-100 and miR-20b) in RWPE-1 cell lysates and 22Rv1 cell lysates determined by FASS-ITP-CE.	93
Table 5.1. Quantitation results of ITP-DQAMmiR for the analysis of miR-16 and miR-21 at different concentrations	102

## LIST OF FIGURES

Figure 1.1. Biogenesis of miRNA and translational repression of target mRNA.	3
Figure 1.2. Classification of all miRNAs detection techniques based on how the miRNAs sequences are exploited in the analysis.	7
Figure 1.3. Hybridization assays classified based on how the signals from the hybrid and excess unbound probe are separated.	9
Figure 1.4. Schematic of an electrochemical detection technique	11
Figure 1.5. Schematic diagram of a molecular beacon	14
Figure 1.6. Schematic illustration of hybridization analysis in CE.	21
Figure 1.7. Schematic representation of a CE-based hybridization assay for mRNA quantification.	22
Figure 1.8. Schematic representation of the direct quantitative analysis of miRNAs.	23
Figure 1.9. An illustration of peak broadening and stacking	27
Figure 1.10. Illustration of the boundary where the pH changes in dynamic pH junction.	29
Figure 1.11. Illustration of changing the mobility of an analyte via adding a pseudo-stationary (PS) phase into the BGE.	30
Figure 1.12. Illustration of facilitating electric field gradient via conductivity gradient.	31
Figure 1.13. Illustration of the discontinuous buffer system in ITP.	34
Figure 1.14. Conceptual depiction of streamlined combination of isotachopheresis (ITP) and DQAMmiR.	35
Figure 2.1. The impurity level associated with the DNA probes.	43
Figure 2.2. Effect of sample matrix on miRNA hybridization.	44
Figure 2.3. Integrity of the DNA probe in each matrix over time.	45
Figure 2.4. Example of a standard curve of qRT-PCR.	46
Figure 2.5. Electropherograms of DQAMmiR measurements in the (a) TAE buffer, (b) RNA extract, and (c) Cell lysate.	47
Figure 2.6. Comparison of miRNA recovery in DQAMmiR and qRT-PCR-based for (a) TAE buffer, (b) RNA extract, and (c) cell lysate.	48
Figure 3.1. Schematic depiction of DQAMmiR with PNA hybridization probes.	51

Figure 3.2. CE separation of a PNA probe from a PNA-miR-21 hybrid in a running buffer of 20 mM Borax, 20% acetonitrile, pH 9.0.	56
Figure 3.3. Dependence of relative mobility of a hybrid ( $\mu_{rel}$ ) with the number of base pairs of the hybrid (N <sub>hyb</sub> ).	58
Figure 3.4. Simulated electropherograms of different PNA-RNA hybrids.	59
Figure 3.5. Experimental implementation of DQAMmiR with PNA probes.	62
Figure 3.6. Results of PNA-facilitated DQAMmiR measurements.	65
Figure 4.1. Schematics of CE separation in two implementations of DQAMmiR: with DNA (A) and PNA probes (B).	68
Figure 4.2. Conceptual depiction of ITP-CE for DQAMmiR with two different types of hybridization probes: ssDNA (a) and PNA (b).	70
Figure 4.3. Conceptual depiction of the proposed FASS-ITP-CE approach for DQAMmiR utilizing PNA probes.	71
Figure 4.4. Investigation of two TE ions — Tricine and HEPES — in ITP-CE for DQAMmiR with PNA hybridization probes.	79
Figure 4.5. The effect of sample buffer concentration on PNA–miRNA hybridization.	82
Figure 4.6. Determination of the time-point (t <sub>st</sub> ) for stopping in preconcentration by FASS-ITP and starting CE by applying an electric field with a reversed polarity.	83
Figure 4.7. Proof of the ability to retain PNA probes in FASS-ITP-CE.	85
Figure 4.8. Evaluation of the preconcentration efficiency and the analytical performances of FASS-ITP-CE.	87
Figure 4.9. Electropherograms of the negative control samples before purification (bottom trace) and after purification (middle trace).	88
Figure 4.10. Electropherograms for FASS-ITP-CE of samples in pure buffer.	90
Figure 4.11. FASS-ITP-CE analysis of miR-100 and miR-20b in 22Rv1 cell lysate (red trace) and RWPE-1 cell lysate (black trace).	92
Figure 4.12. Electropherograms for FASS-ITP-CE measurements of miR-100 and miR-20b in the 22Rv1 cell lysate (bottom trace) and a positive control sample (top trace).	94
Figure 5.1. Implementation of DQAMmiR for simultaneously analysis of miR-16 and miR-21.	100
Figure 5.2. Implementation of DQAMmiR with ITP preconcentration for the analysis of miR-16 and miR-21 at different concentrations	101
Figure 5.3. Implementation of DQAMmiR with ITP preconcentration for the analysis of miR-16 and miR-21 with different concentrations of DNA probes	102
Figure 5.4. DQAMmiR with ITP preconcentration for quantitation of miR-16 and miR-21 at different concentrations	103
Figure 5.5. Sampling procedures for the analysis of endogenous miRNAs in urine sediments.	103

Figure 5.6. DQAMmiR with ITP preconcentration for quantitation of miR-16 and miR-21 in crude lysates of urine sediments	104
Figure 5.7. Illustration of complicated matrices in crude lysates of urine sediments interfering with DQAMmiR quantification.	105

## COMMONLY USED ABBREVIATIONS

A: Area of peak  
aa: Amino acid  
C: Celsius  
CE: Capillary electrophoresis  
DQAMmiR: Direct quantitative analysis of multiple microRNAs  
EOF: Electroosmotic flow  
FFPE: Formalin-fixed paraffin embedded  
HPLC: High performance liquid chromatography  
ITP: Isotachophoresis  
LE: Leading electrolyte  
LOD: Limit of detection  
LOQ: Limit of quantification  
miRNA: MicroRNA  
mRNA: Messenger RNA  
nt: Nucleotide  
P: Probe  
PCR: Polymerase Chain Reaction  
PNA: Peptide nucleic acid  
pre-miRNA: Precursor microRNA  
pri-miRNA: Primary microRNA  
*q*: Quantum yield  
qRT-PCR: quantitative reverse transcriptase polymerase chain reaction  
*R*: Resolution  
RISC: RNA-induced silencing complex  
SSB: Single strand DNA binding protein  
ssDNA: single stranded DNA  
T: Target microRNA  
TE: Trailing electrolyte  
TP: Target-probe hybrid  
UTR: Untranslated region

## CHAPTER 1. INTRODUCTION

### 1.1. Introduction to miRNAs

MicroRNAs (miRNAs) are small non-coding RNA molecules of approximately 18–25 nucleotides in length that have emerged as key regulators of gene expression at the post-transcriptional level. These molecules were first discovered in 1993 by the Ambros lab in the nematode *Caenorhabditis elegans* [1]. These small RNAs were later found to be important post-transcriptional regulators of gene expression across multiple species, including humans [2]. This section aims to provide an in-depth introduction to miRNAs, covering their biogenesis, biological functions, and their relevance in various diseases, with a particular emphasis on cancers.

#### 1.1.1. Biogenesis of miRNAs

The biogenesis of miRNAs is a multi-step process that begins in the nucleus and ends in the cytoplasm. The process initiates with the transcription of a primary miRNA (pri-miRNA) by RNA polymerase II. The pri-miRNA, which ranges from hundreds to thousands of bases long, contains a double-stranded stem with a hairpin loop (**Fig. 1.1**) [3]. Following transcription, the pri-miRNA is cleaved within the nucleus by the enzyme Drosha, producing a shorter, approximately 70-nucleotide stem-loop structure known as the precursor-miRNA (pre-miRNA) [4]. The pre-miRNA is then transported to the cytoplasm by the nuclear export factor Exportin-5. Here, it is further processed by the enzyme Dicer into a double-stranded 18–25 oligonucleotide duplex [5].

The miRNA duplex is subsequently loaded into an Argonaute (Ago) protein, a component of the RNA-induced silencing complex (RISC). One strand of the duplex, termed the guide strand or mature miRNA, is retained in the RISC, while the other strand (miRNA\*) is typically degraded.

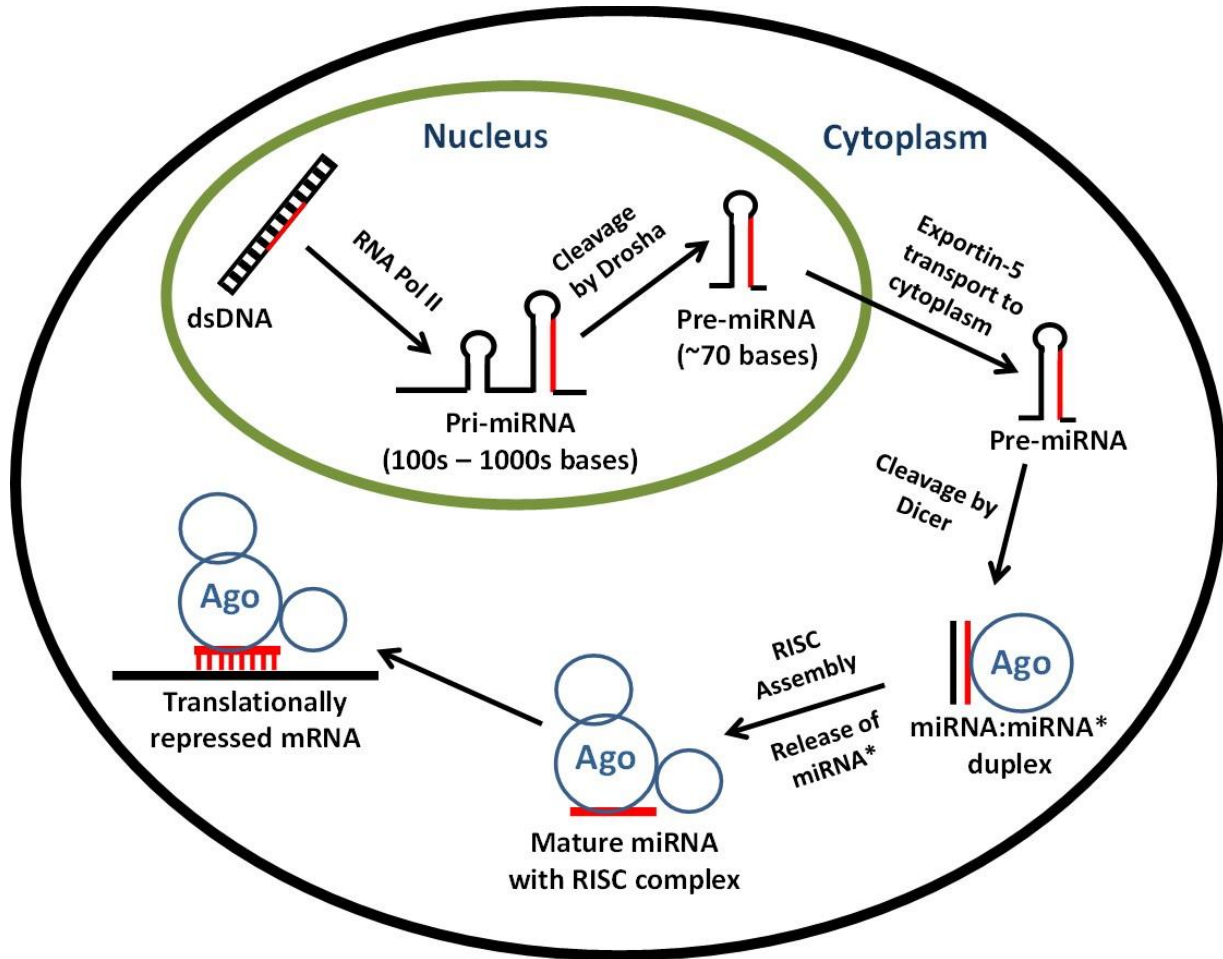


**Figure 1.1.** Biogenesis of miRNA and translational repression of target mRNA. See texts for details.

The selection of the guide strand depends on its thermodynamic stability [6]. The incorporation of the mature miRNA into RISC completes the miRNA biogenesis pathway and prepares the RISC for target mRNA recognition [7].

### 1.1.2. Biological functions of miRNAs

miRNAs play a crucial role in a multitude of biological processes due to their ability to control gene expression post-transcriptionally. This control is typically exerted through binding of the mature miRNA within the RISC to target mRNAs sequence complementarity. Typically, the “seed” region of the miRNA, nucleotides 2–8 from the 5’ end, bind to the 3’ untranslated region

(UTR) of the target mRNA, commonly without perfect complementarity. This imperfection enables a single miRNA to bind multiple target mRNAs [8]. For instance, miR-21 targets several mRNAs on the caspase activation pathway, inhibiting cellular apoptosis [9–10]. When miRNAs bind to mRNA, the outcome depends on the level of complementarity. Perfect complementarity (rare in humans) triggers mRNA degradation, while imperfect complementarity results in translation inhibition without degradation.

New proposed mechanisms suggest that miRNAs may regulate gene expression in ways beyond seed region-binding [8]. For example, miRNAs can bind to the open-reading frame, 5' UTR, and promoter of target mRNAs [11–13]. A study showed that miR-373 binds to a promoter, outcompeting a repressor and stimulating gene expression [12]. Despite these multiple binding sites complicating target prediction, they suggest a more significant impact of miRNAs on gene expression than previously thought.

### **1.1.3. miRNAs in Disease**

Given their expansive regulator roles, it's not surprising that dysregulation of miRNAs has been linked to various diseases, including cancer. Changes in miRNA expressions levels can lead to the disruption of key cellular pathways, influencing cell growth, differentiation, and apoptosis – processes that, when perturbed, can contribute to tumorigenesis [14–18].

miRNAs can act as oncogenes or tumor suppressors depending on their target genes. For instance, the overexpression of oncogenic miRNAs, often called “oncomiRs”, such as miR-21, contributes to cancer progression by downregulating tumor suppressor genes [19]. Conversely, the downregulation of tumor suppressive miRNAs, like let-7, can lead to the upregulation of oncogenes, thereby promoting cancer development [20]. These associated up- or down-regulation of miRNAs with such diseases means that miRNAs have great potential as a diagnostic or

prognostic biomarker for many human diseases. There are significant efforts directed towards combining sets of such deregulated miRNAs into fingerprints that can be used for disease diagnosis. Cancer-specific miRNA fingerprints have been found for multiple forms of cancer and even cancer subtype-specific fingerprints have been discovered [16, 21, 22]. In one example, miRNA fingerprints (of 7 miRNAs or fewer) have reliably been able to distinguish all 5 intrinsic subtypes associated with breast cancer [21].

Another advantage in the use of miRNAs as disease biomarkers is their remarkable stability in biological samples. Formalin-fixed paraffin embedded (FFPE) tissues are one of the more commonly used methods for long-term sample storage. One of the common issues with FFPE tissues is that the sample preparation process can potentially cause the degradation of cancer biomarkers [23–25]. A recent study revealed that such impact was very minimal on miRNA [26–27]. miRNAs have also been found to be remarkably stable in body fluids such as blood plasma and urine, making them potential candidates for non-invasive cancer biomarkers [28–29]. For examples, Liu *et al.* found circulating miRNA fingerprints associated with early-stage pancreatic cancer, demonstrating their potential diagnostic utility [30].

In conclusion, miRNAs are critical regulators of gene expression, affecting numerous biological processes and contributing to the pathogenesis of various diseases, including cancer. miRNA fingerprints can distinguish healthy from cancerous cells, can identify specific cancer subtypes, and are stable in body fluids showing they have potential to be very effective cancer biomarkers. Therefore, there is a strong demand for a miRNA detection method capable of detecting/identifying these fingerprints in a clinical setting.

## 1.2. miRNA detection methods

For miRNA fingerprints to be used in diagnostics, a suitable detection method is required. Such method should satisfy several key criteria including the ability to simultaneously detect multiple miRNAs, a low limit-of-detection (LOD), and high robustness to ensure reliable and reproducible results. Of particular importance is the capacity of the method to quantitatively measure miRNAs. This is essential because often the deregulation in miRNAs is subtle and such small changes in miRNA abundance can be indicative of disease. Therefore, a highly quantitative method will be more adept at analysing disease fingerprints based on such subtle changes rather than merely detecting the presence or absence of specific miRNAs.

Moreover, it is common for disease fingerprints to consist of a panel of miRNAs rather than a single miRNA species, necessitating the detection methods to avoid sequence-related biases in quantitation. Many of the current indirect detection methods involve pre-amplification of miRNAs or require enzymatic/chemical modifications which are likely to introduce such biases [31–33]. Additionally, these extra processing steps may lead to loss of miRNA samples and extend the assay time, impacting the overall efficiency of the method. Direct methods, which do not necessitate amplification or modification of miRNAs, could be a more advantageous alternative.

Currently, the two main methods of practical miRNAs analysis are microarrays and quantitative reverse transcriptase PCR (qRT-PCR). Microarrays allow simultaneous detection of hundreds to thousands of miRNAs in a single experiment and qRT-PCR allows detection of low abundance miRNA species [34–35]. These methods have been essential in identifying candidates of disease-specific miRNA fingerprints; however, due to their indirect nature and the associated lack of robustness in quantitation, their usefulness in the validation of miRNA fingerprints and miRNAs-based diagnostics is limited. We must look for other potential methods that best meet the

criteria for use in diagnostics. This section aims to provide a comprehensive review of the prevailing techniques employed in miRNA detection.

### 1.2.1. Classification of miRNA detection methods

To ensure specificity, miRNA detection methods typically sense a target miRNA based on its unique nucleotide sequence. However, the degree at which their sequence is exploited for the detection differs in different methods. Here all detection methods are classified into 3 main categories: sequencing-based methods, signature-based methods, and hybridization-based methods (**Fig. 1.2**).

#### 1.2.1.1. Sequencing-based methods

Sequencing-based methods determine the nucleotide sequence of miRNAs by converting them into their corresponding complementary DNA (cDNA) and examining it base-by-base via a

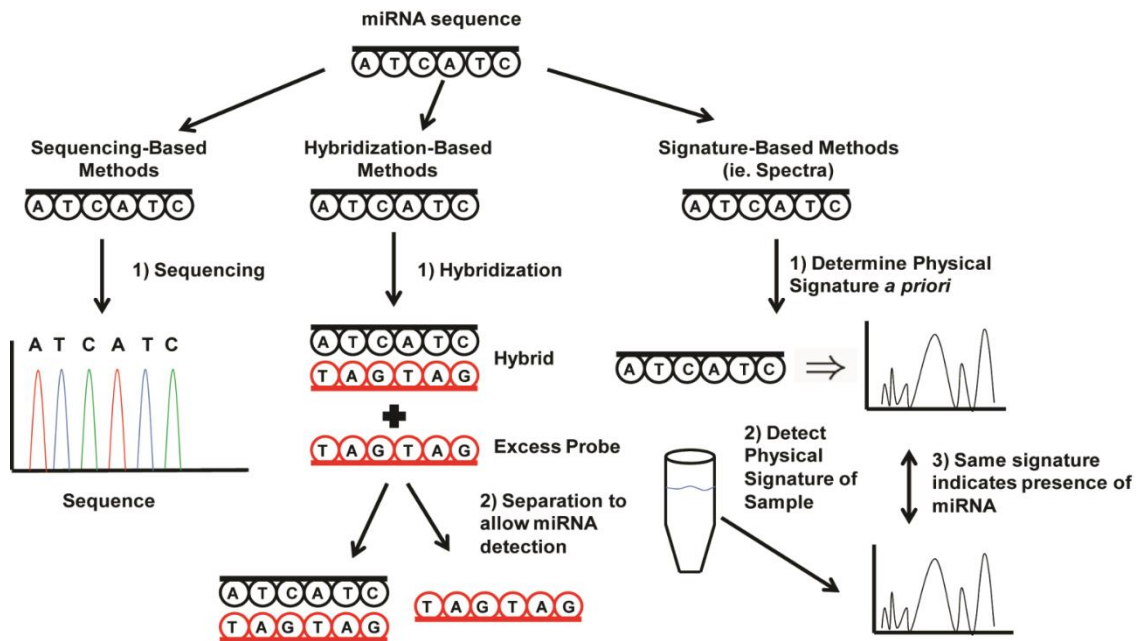


**Figure 1.2.** Classification of all miRNAs detection techniques based on how the miRNAs sequences are exploited in the analysis. (Adapted from [36]. Copyright)

DNA-sequencing method. The traditional Sanger method employs DNA chain-terminating dideoxynucleotide bases that stop DNA strand growth. These four dideoxynucleotide bases each carry a distinct fluorophore, facilitating the recognition of each successive base. Next-generation sequencing is a much more high-throughput technique that accelerates this process and reduces the sequencing costs. Although there are various forms of next-generation sequencing, most still utilize the four dye-labeled terminating bases, enabling the detection of each individual base in the sequence. The sequence-based miRNA detection techniques enable greater assurance in target specificity due to the comprehensive information provided for each miRNA species. As a result, these methods are less susceptible to false positive outcomes. Nevertheless, contemporary sequencing techniques necessitate the ligation of adaptor sequences to the miRNA target's both ends, followed by reverse transcription and PCR amplification [37–39]. Therefore, sequencing-based methods fail to satisfy our requirement of being direct. Nanopore-based sequencing methods have the potential to be direct; nonetheless, this technology is not yet adequately advanced to be practical in any practical application [40–41].

#### **1.2.1.2. Signature-based methods**

Signature-based methods identify target miRNAs *via* information – “signature” retrieved from diverse spectroscopic techniques. Instead of pinpointing the nucleotide sequence, these methods link target miRNAs to a physical attribute such as a molecule's mass, charge, or structure. For instance, Driskell *et al.* leveraged surface-enhanced Raman scattering (SERS) to generate sequence-specific spectra of miRNAs [42]. While there are ongoing efforts to incorporate other spectroscopic methods like mass spectrometry and circular dichroism for miRNAs detection, none are currently viable in diagnostics [43–44]. Unfortunately, these techniques have an intrinsic drawback of susceptibility to false positives, as non-identical miRNAs with some similarities can

yield indistinguishable signatures. Moreover, with the possibility of various molecule types mimicking miRNA signatures, this limitation is exacerbated when dealing with complex biological samples. In such scenarios, considerable effort would need to be exerted to verify the specificity of each signature, which currently hampers the application of these methods for practical miRNA analysis.

### 1.2.1.3. Hybridization-based methods

Hybridization-based methods involves the binding of the target miRNA to a complementary probe, which could be made of DNA, RNA, locked nucleic acid (LNA), or peptide nucleic acid (PNA). The presence and the quantity of miRNA are inferred from the detection of such hybrids. There are two ways to detect the presence of probe–miRNA hybrids; they can be distinguished from the unbound probe either by observing the signal changes that are dependent on hybridization, or through spatial separation of hybrids from the unbound probes. This bifurcation allows us to further classify all hybridization-based methods into two categories: detection not requiring spatial separation and detection based on spatial separation (**Fig 1.3**). In

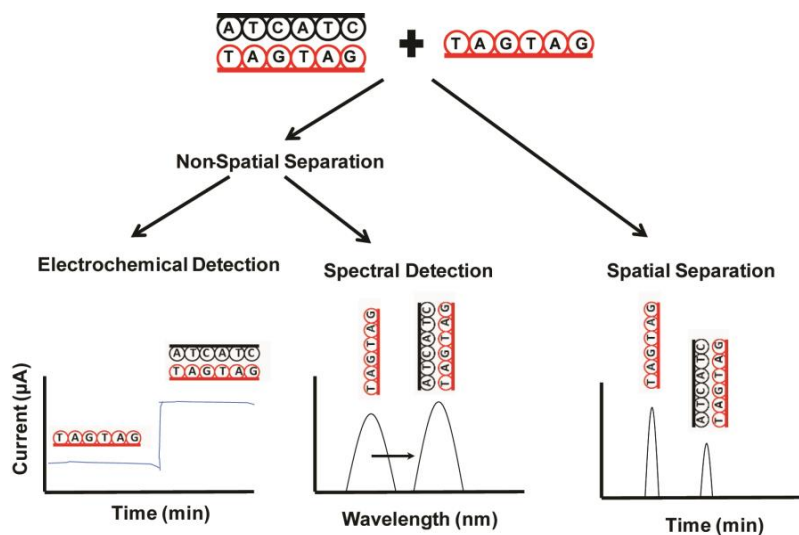


**Figure 1.3.** Hybridization assays classified based on how the signals from the hybrid and excess unbound probe are separated. (Adapted from [36]. Copyright)

the first category, hybrids are detected by observing alterations in signals dependent on hybridization, like the fluorescence or electrical conductivity of the sample. In the second category, techniques such as immobilization or electrophoresis are used to spatially separate hybrids from the unbound probes. This section aims to focus on the merits and drawbacks of each category to emphasize methods offering the greatest potential for miRNA-based diagnostic purpose.

### **1.2.1.3.1. Non-spatial separation methods**

#### **1.2.1.3.1.1. Electrochemical detection**

The electrochemical detection in hybridization assays leverages changes in circuit properties upon miRNA/probe hybridization. In these methods, miRNAs hybridize to a complementary probe that is immobilized on either an electrode or a nanowire. Depending on which technique is used, miRNA-binding causes either the promotion of oxidation on an electrode or a change in the conductance of a nanowire.

Though indirect, the first-electrochemical methods for miRNA detection was developed in 2006 by Gao *et al.*, which took advantage of a catalyzed oxidation reaction between an oxidation reagent and the target miRNA (**Fig. 1.4**) [45]. In 2009, Yang *et al.* designed a direct electrochemical detection method by constructing microelectrodes decorated with immobilized PNA probes [46]. In PNA, unlike DNA, the negative sugar-phosphate backbone is replaced with a neutral peptide backbone. Binding of miRNAs to these PNA probes resulted in an accumulation of negative charge on the electrode, which in turn, attracted  $\text{Ru}^{3+}$  redox reporter. Electrochemical reduction of  $\text{Ru}^{3+}$  to  $\text{Ru}^{2+}$  resulted in a detectable change in electrical current. With the use of a signal amplification technique, an impressive LOD of 10 aM (attomolar) was achieved, which enabled the quantification of miR-21 and miR-205 from total RNA extracts of various cell lines [46].

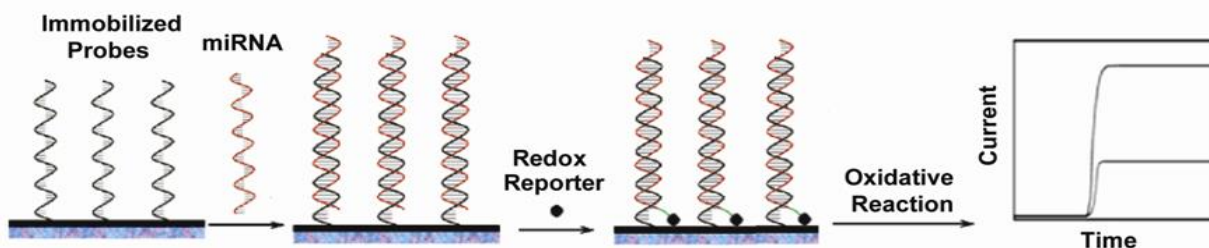


**Figure 1.4.** Schematic of an electrochemical detection technique, miRNAs are hybridized to immobilized probe, allowing for accumulation of redox reporter, causing a detectable change in circuit properties. (Adapted from [52]. Copyright [2006] American Chemical Society).

Wang et al. demonstrated a highly sensitive POC adoptable magnetic-controllable electrochemical based biosensor [47]. It presents oral cancer miRNA biomarker diagnosis in early stage that showed limit of detection (LOD) down to 0.22 aM with a recovery rate of 93% and relative standard deviation (RSD) < 6%. Additionally, Boriachek et al. reported an efficient biosensor for miRNA detection from human serum where they immobilized biotinylated complementary probes on commercial streptavidin-coated magnetic beads (MBs) [48]. The level of adsorbed miRNA was detected electrochemically in presence of the  $[\text{Fe}(\text{CN})_6]^{4-/3-}$  in redox system. The developed biosensor has a significant detection limit as low as 1.0 pM with RSD less than 5.5% that were satisfactorily observed with differential pulse voltammetry (DPV). The proposed method offers several advantages such as enhanced capture, low manufacturing cost, reduced assay time and matrix effect.

Moreover, Luo et al. revealed a LNA assisted strand displacement reaction-based ratiometric electrochemical biosensor having higher reproducibility to detect exosomal miR-21 derived from cancer with LOD of 2.3 fM [49]. They used Y-like structure facilitated by LNA that gets activated in the presence of miR-21 as a target biomarker, and detection was confirmed by electrochemical impedance spectroscopy (EIS) and DPV. Sabahi et al. recently fabricated single-wall carbon nanotubes (SWCNTs)-grafted dendritic Au nanostructure modified fluorine-doped tin

oxide (FTO) electrode-based biosensor to detect miR-21 in the range of 0.01 fM – 1  $\mu$ M with a detection limit down to 0.01 fM [50]. Furthermore, the proposed biosensor revealed an acceptable performance in human serum and good selectivity. The fabricated biosensor could potentially be used in clinical processes as a point of care device for early diagnosis of prostate cancer. Additionally, Hong et al. fabricated an ultrasensitive biosensor that can directly detect miRNA from human serum without prior treatment [51]. The self-assembled DNA concatemers can carry numerous RuHex that results in significantly enhanced electrochemical signals, leading to a high sensitivity for target miR-21 in a concentrating range from 100 aM to 100 pM with a detection limit of 100 aM.

Other forms of electrochemical detection includes the use of nanowires to sense target miRNAs [52–53]. Fan *et al.* designed an electronic circuit where a conducting polyaniline nanowire was interrupted by nanometer-sized gaps [52]. These gaps were decorated with neutral PNA hybridization probes. The negatively charged miRNAs, upon hybridization with the probes, interacted with cationic anilines and increased the conductance of the electronic circuit. Electrical conductance of the nanowire directly correlated with the amount of hybridized miRNAs, which allowed to detect miRNAs at concentrations as low as 5 fM (femtomolar). Zhang *et al.* developed a similar method, where a PNA decorated silicon nanowire was used [53]. In this technique, hybridization of negatively charged miRNAs affected the semiconductor properties of the silicon nanowires, resulting in an increased resistance of the circuit in a miRNA concentration-dependent manner.

The electrochemical methods for miRNA detection exhibit remarkable advantages such as extraordinary LODs, with capabilities reaching as low as 10 aM of miRNAs. These detection limits generally surpass those of other hybridization-based methods, allowing electrochemical

techniques to bypass the need for miRNA amplification through PCR. Moreover, electrochemical approaches demonstrate high specificity by distinguishing miRNAs with single-nucleotide differences. Nonetheless, the adoption of these electrochemical techniques in diagnostics necessitates overcoming substantial obstacles. For instance, in many existing examples, only one type of miRNA has been successfully detected. Multiplexing, or detecting multiple miRNAs simultaneously, is currently impeded by the limited dynamic range of detection and the intricate electrode manufacturing process. Moreover, present-day electrochemical techniques are not compatible with raw biological samples. Unpredictable interactions between various components of the cell lysates and the nanostructures may lead to false positive or false negative results. Therefore, miRNA extraction kits are necessary, which can introduce biases in quantification and prolong the overall assay duration. This makes electrochemical detection techniques less robust, necessitating rigorous control over clinical standards. Lastly, the lifespan of the electrode or nanowires is finite, and their complex production process continues to be a significant constraint, particularly concerning the cost of analysis.

#### **1.2.1.3.1.2. Spectral detection**

Spectral detection methods require a change in absorbance, fluorescence, refractive index or reflectivity of the sample to occur upon binding of the probe to its complementary target miRNA. The most common spectral detection techniques involves the use of molecular beacons (MBs). MBs are constructs that take advantage of phenomena such as quenching or fluorescence resonance energy transfer (FRET). A typical MBs consist of four functional parts: (i) target miRNA hybridization sequence that is complementary to the target miRNA like a hybridization probe; (ii) complementary sequences at the 5' and 3' ends; (iii) a terminal fluorophore, and (iv) a terminal quencher or acceptor (**Fig. 1.5**). When the target miRNAs are absent, a stem-loop is

formed through the hybridization of the 5–6 nucleotide-long complementary components at the ends of the construct. In this conformation, the fluorophore and the quencher are brought into close proximity, resulting in the absence of fluorescence signal. However, when a target miRNAs hybridizes to the MBs, it interferes with the stem-loop structure and results in a spatial separation of the fluorophore and quencher. Thus, the presence of target miRNAs results in an increase in fluorescence signal.

MBs have been used extensively with miRNAs in the past two decades [54–57]. Unfortunately, such methods suffer from an inherent lack of dynamic range and poor LOD due to incomplete quenching in the absence of target miRNAs. Several protocols were developed to improve the LOD of the MB techniques. Hartig, in 2004, used a signal amplifying ribozyme instead of the typical MB [58]. In such case, the target miRNA binds to the ribozyme and cause its structural change, activating the cleavage of a fluorophore/quencher-labeled substrate. This cleavage releases the fluorophore, which in turn, produces a detectable signal. Signal amplification was achieved by multiple substrates being cleaved by a single activated ribozyme. They were able to achieve an LOD of 5 nM though the dynamic range was only 2 orders of magnitude.

There are also examples of spectral techniques that do not require the use of MBs. Neely *et al.* used a single molecule detector, LNA–DNA probes, and dual fluorophore to achieve an LOD

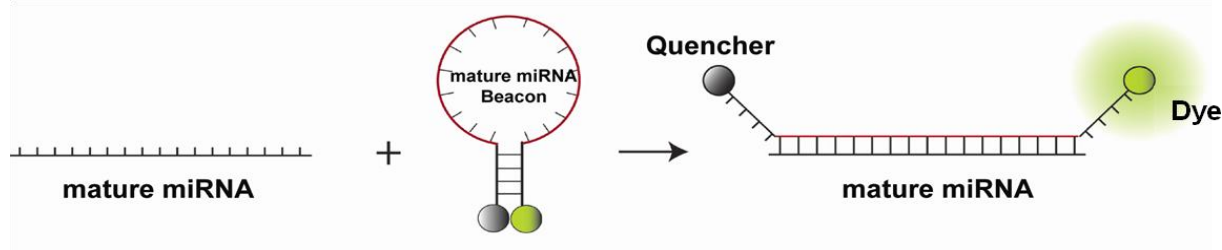


**Figure 1.5.** Schematic diagram of a molecular beacon which consists of four parts, target miRNA hybridization sequence, complementary 5-6 DNA bases at 5' and 3' ends, a fluorophore and a quencher. Upon hybridization, MB structure opens, allowing for fluorescence to occur. (Adapted from [56] by permission of Oxford University Press).

of 500 fM and a dynamic range of 3 orders of magnitude [59]. Yin *et al.* developed a signal amplification technique with the use of a Taqman probe and a duplex specific nuclease (DSN) [60]. A Taqman probe is a short DNA oligo with a fluorophore and quencher at either end that requires cleavage to fluorescence. Upon hybridization with target miRNAs, the DSN cleaves the Taqman probe, thus breaking the energy transfer connection between the fluorophore and the quencher. Thus, the presence of Taqman–miRNA hybrids results in an increased fluorescence signal. Furthermore, cleavage of Taqman releases the target miRNAs undamaged, allowing for hybridization to a new Taqman probe to occur. This signal amplification technique yielded an LOD of 100 fM and had a dynamic range of over 4 orders of magnitude.

Spectral detection methods that do not use typical MBs can have a dynamic range of up to 4 orders of magnitude, which make them suitable for detecting multiple miRNAs at different expression levels in practice. The use of multiple fluorophores or microarray format make it possible for simultaneous analysis of multiple miRNAs. Additionally, spectral methods can usually be performed with relatively inexpensive commercial equipment and some spectral methods are less prone to non-specific effects of crude biological matrices and as a result require fewer preparative steps (e.g., RNA extraction), making them especially attractive for clinical use.

Although spectral methods do not have many limitations, the high LOD due to the high background signal associated with the fluorophore-quencher systems significantly affect their potential for the diagnosis use. While there are efforts to improve these LODs, they typically result in either decreased quantitative accuracy (e.g., indirect amplification) or significantly more complex and expensive instrumentation.

#### 1.2.1.3.2. Spatial separation methods

There are two basic ways to physically separate the miRNA-probe hybrid from the excess probe. In the first category of methods, miRNAs are immobilized on a surface through various techniques and are then hybridized with labeled probes. In the second category, the hybrids are separated from the excess probe based on their inherent physical properties, such as mass or charge. For nucleic acids, one of the most efficient ways to achieve this separation is through use of electrophoretic techniques.

Northern blotting is a gold-standard immobilization technique in miRNAs detection. In this technique, the components of total RNA extracts from biological samples are separated based on size using gel electrophoresis. Afterwards, bands of separated RNA are blotted onto a nitrocellulose membrane. Labeled target-specific DNA probes are then washed over the membrane, allowing them to become immobilized through hybridization. While very popular among biologists, Northern blotting has several limitations when it comes to clinical applications, including long assay time (~24 h), large sample requirements, high LODs and dependence on radioactive probes. Variations of Northern blotting were developed to address some of these issues. For example, Varallyay was able to reduce the overall assay time down to 4 h through various improvements, including the use of LNA hybridization probes [61]. Kim *et al.* developed a non-radioactive technique through use of LNA probes, a digoxigenin (DIG) label and an improved cross-linking reagent to achieve an LOD of 0.8 pM [62]. DIG-labeling allowed for non-radioactive detection of miRNAs by using alkaline-phosphatase (AP)-labeled anti-DIG antibodies. The activity of the enzyme, AP, could then be measured to detect the presence of target miRNAs. Though LNA probes, DIG labels, and the cross-linking reagent had been used previously, the combination of the three techniques allowed for the improved LOD. The authors applied this

technique to detect low abundance miRNAs from a breast cancer cell line. Unfortunately, these improved methods still require an initial sample (5–20  $\mu\text{g}$  total RNA per lane) that is too large to be feasible for most diagnostic applications.

Sandwich assays are another form of immobilization techniques that take advantage of two different functional probes: capture and labeled probes. The capture probe typically includes regions of complementarity to both target and labeled probe. Hybridization of the labeled probe depends on the hybridization status of the target-specific region of the capture probe, through exploitation of the base-stacking phenomenon. In base-stacking, the presence of an adjacent hybrid region stabilizes hybridization of a very short nucleotide that otherwise would have been too weak to remain bound. Yang *et al.* combined the use of a sandwich assay design with gold nanoparticle labeling, and were able to achieve a 10 fM LOD through signal amplification by silver enhancement[63].

Roy *et al.* further improved the LOD of the sandwich assays by introducing an exonuclease processing step [64]. In their design, after the capture probe had a chance to hybridize with the target miRNAs, exonuclease was added to degrade any unbound capture probe. This decreased the probability of non-specific interactions between the capture and labeled probes and resulted in a lower background signal. Employing the differential interference contrast method for detection of gold nanoparticle labels, the authors were able to detect as few as 300 copies of miRNA (1 fM) without the use of any signal amplification.

Physical separation between excess probe and miRNA-probe hybrids via immobilization significantly reduces possibilities of detecting non-specific interactions, giving immobilization-based methods excellent quantitative accuracy. Like other hybridization assays, immobilization techniques are capable of 1-nt specificity. Furthermore, the dynamic range of these methods spans

up to 4 orders of magnitude, making them well-suited for simultaneous analysis of deregulated miRNAs. There have been some recently introduced immobilization techniques that have great potential for use in diagnostic assays [65–67]. The limitations of such immobilization techniques used for physical separation are that they require the use of microarrays for detection of multiple miRNAs and their hybridization times can be quite long with most commercially available microarrays requiring 16–18 h [64].

Powerful separation techniques offer similar benefits as immobilization techniques, but they eliminate the need of lengthy hybridization. There are, however, only a few physical separation techniques that do not require miRNAs immobilization. Even with the use of a powerful separation technique such as capillary electrophoresis (CE), it is difficult to separate excess probes from hybrids due to their inherently similar physical properties. Chang *et al.* were the first to use CE to separate excess DNA probe from the miRNA-probe hybrid. They did not achieve sufficient separation to accurately quantitate the miRNA showing that CE alone is not sufficient for separation [68]. To overcome this problem Khan *et al.* used various separation enhancers which altered the size to charge ratio of either the excess probe or the miRNA-probe hybrid allowing for sufficient separation of the hybrid and probe to be achieved [69]. This showed that the use of CE with separation enhancers has potential for the quantitation of miRNAs.

In the next section I will go into more detail on the use of CE for hybridization assays, specifically I will focus on how to make CE quantitative for detecting multiple miRNAs simultaneously with the use of separation enhancers.

## **1.2.2. Hybridization-based miRNA quantification in capillary electrophoresis**

### **1.2.2.1. Introduction to Capillary Electrophoresis**

Capillary electrophoresis (CE) is an analytical separation technique, which enables separation and detection of ionic species based on their differential migration velocities under an applied electric field [70]. CE is widely used in a wide variety of fields including food analysis, molecular biology, and environment monitoring for the separation and detection of ionic species ranging from small ions to macromolecules and microorganisms [71–74]. Typical CE experiments involve injection of a sample mixture as a short zone in a capillary or microchannel filled with a background electrolyte (BGE) with a concentration significantly higher than those of analytes, followed by application of an electric field. Thereafter, analyte zones separate based on their differential electrophoretic mobilities based on their charge-to-size ratios. Measured CE signals are called electropherograms, which quantify the relative heights, widths, and locations of peaks corresponding to separated analytes.

The ability of CE to distinguish separated analyte zones is characterized by its resolution, the separation between neighbouring peaks normalized by their thickness [75–76]. Peaks are said to be well-resolved if the separation between their maxima is significantly larger than their widths. The ability to identify a well-resolved analyte peak over background noise is termed detection sensitivity and is characterized by the height of the peak relative to the fluctuation magnitude of the background signal, *i.e.*, noise [76]. Design CE experiments often poses a trade-off between resolution and sensitivity: longer separation times increase peak separation, but at the cost of lower sensitivity due to increased dispersion [76]. In general, CE has very high resolving power, and in many cases higher than that of chromatographic techniques [77–78]. However, in some cases, low sensitivity of CE can limit its applicability, particularly for detection modes other than

fluorescence such as ultra-violet (UV) absorbance and various electrical detection methods (*e.g.*, conductivity detection) [79–80].

Several methods have been employed to increase the sensitivity of CE, including use of high-sensitivity detectors, and off-line and on-line sample preconcentration techniques. Direct laser-induced fluorescence (LIF) is the most sensitive method for detection in CE, and has been used for single molecule detection (*i.e.*, at ~100 aM concentration level) with on-line sample preconcentration [81]. However, in practice, many analytes of interest are either non-fluorescent or lack free chemical groups that can be derivatized with fluorophores. Even if fluorescent-labeling of analytes is possible, the inefficiencies involved in derivatization of trace species can result in unwanted artifacts, including modification of analyte mobilities and background signals resulting from unbound fluorophores and their degradation products [82–83]. Detection of many analytes using CE with local conductivity or UV absorbance detection modes is limited to analytes to order 1–100 nM or greater concentrations [79–80].

#### **1.2.2.2. Hybridization Assays in CE**

The unique capabilities of CE, including its high resolving power and versatile detection modes, have made it an ideal platform for conducting hybridization assays with spatial separation for DNA or RNA detection. **Fig. 1.6** presents the general concept of such assays. In step 1, an excess of labeled probe ( $P^*$ ) is added to a target (T)-containing sample to bind the majority of the target, resulting in a mix of  $TP^*$  hybrid and any unbound  $P^*$ . In step 2,  $TP^*$  is separated from  $P^*$  in CE to facilitate the quantitation of  $TP^*$  using the label on  $P^*$  for detection and quantification.

Using this concept, several CE-based hybridization assays have been developed including gel and gel-free assays [85–88]. One of gel-free hybridization analyses is based on separation of the unbound probe from the target–probe hybrid by affinity capillary electrophoresis mediated by a separation enhancer, single-strand DNA binding protein (SSB) (**Fig. 1.7**) [86]. In this approach, SSB is added to the hybridization mixture where it binds the single-stranded probe but does not bind the double-stranded target–probe hybrid prior injecting into CE. The SSB-bounded single-stranded probes were then separated from the target–probe hybrid in CE. Both the SSB-bounded probe and the hybrid were detected with a fluorescent label on the probe, facilitating the sensitive detection of mRNA without the need for calibration curves. With the similar concept of SSB-mediated hybridization analysis, it was also found adding the SSB directly into the electrophoresis run buffer instead of the hybridization mixture also worked for analyzing a 22-nt ssDNA target [84]. It was found that the assay could be quantitative by taking into account the quenching effects of both the target and SSB binding to the probe.

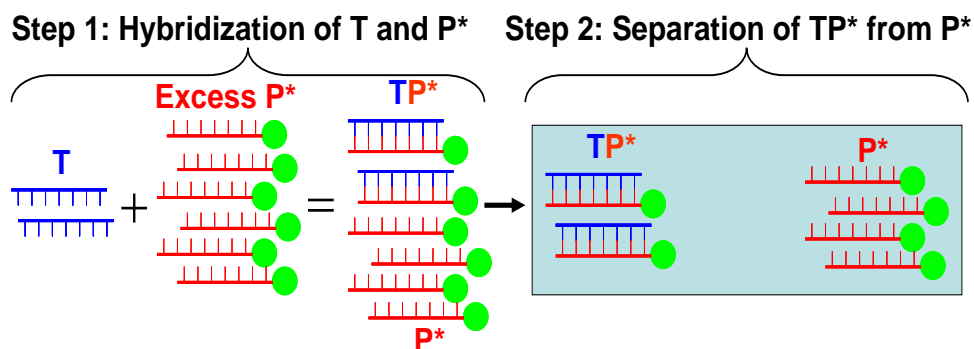


**Figure 1.6.** Schematic illustration of hybridization analysis in CE. In Step 1, the target sequence T is hybridized with a labeled probe P\* to form the target-probe hybrid, TP\*, through mixing the target with the excess of the probe. In Step 2, the unreacted probe is separated from the target-probe hybrid in CE to facilitate the quantitation of the hybrid. (Adapted from [84] by permission of American Chemical Society.)

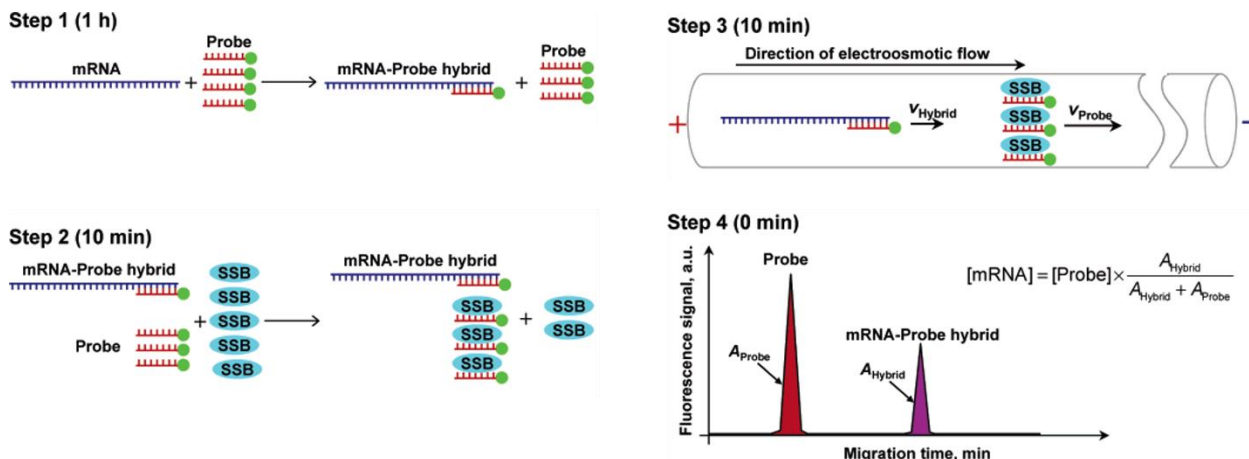


**Figure 1.7.** Schematic representation of a CE-based hybridization assay for mRNA quantification. See text for the details. (Adapted from [86] by permission of American Chemical Society)

### 1.2.2.3. Direct quantitative analysis of multiple miRNAs (DQAMmiR)

With this SSB-mediated approach, a hybridization-based method in CE for miRNA analysis was developed in 2011 by researchers in our lab [89], which was named as Direct Quantitative Analysis of Multiple MicroRNAs (DQAMmiR). This method aims to address the need for direct, quantitative and multiplexing methods for miRNA analysis in the application of miRNA fingerprints in diagnostics. DQAMmiR uses miRNAs directly, without any modification, and accurately determines concentrations of multiple miRNAs without the need for calibration curves. This was achieved by a CE-based hybridization assay with a combination of two well-known separation-enhancement approaches in CE: 1) drag tags on the DNA probes [90], and 2) SSB in the run buffer [85]. **Fig. 1.8** shows this method where the miRNAs and their complementary ssDNA probes are shown as short lines of the same color, drag tags are shown as parachutes, a fluorescent label is shown as small green circles and SSB is shown as large black circles. In the hybridization set, the excess of the probes is mixed with the miRNAs which leads to all miRNAs being hybridized but with some probes left unbound. A short plug of the

hybridization mixture is introduced into a capillary prefilled with an SSB-containing run buffer. SSB binds all ssDNA probes but doesn't bind the double-stranded miRNA–DNA hybrids. When an electric field is applied, all SSB-bound probes move faster than all the hybrids (SSB works as a propellant) [85]. Different drag tags making different hybrids move with different velocities. SSB-bound probes, however, can move even with similar velocities if the drag tags are small with respect to SSB. In such a case, a fluorescent detector at the end of the capillary detects separate signals for the hybrids and a cumulative signal for the excess of the probes (i.e., one peak or multiple peaks for all SSB-bounded probes). Thus, the amounts of each miRNA can be determined with a mathematical approach that uses the integrated peak areas from the electropherogram.

Besides the proof-of-principle work, a serial of following-up studies have been conducted to improve the DQAMmiR approach by researchers in our lab in terms of increasing number of detectable miRNAs, reducing overall assay time, and improving specificity [91–94]. By conjugating short peptides of varying length to the DNA probes, these peptides acted as drag tags which allowed for the separation and detection of 5 miRNAs [91–92]. To reduce overall assay time, an efficient purification procedure was developed to significantly reduce the impurities associated with the DNA probes, which allowed for using a higher probe concentration, which in turn, decreasing the hybridization time from 60 min down to 10 min [93]. To improve the

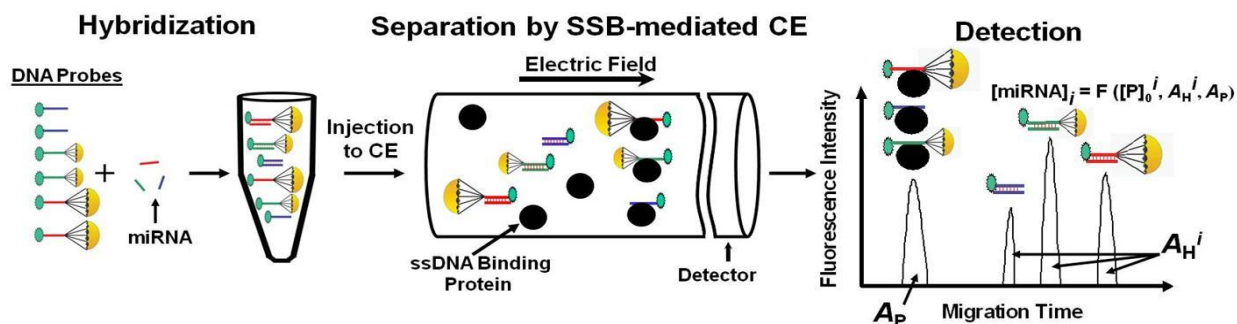


**Figure 1.8.** Schematic representation of the direct quantitative analysis of miRNAs. See text for details. (Adapted from [89] by permission of John Wiley and Sons)

specificity of DQAMmiR, LNA-incorporated DNA probes was utilized to normalize the melting temperature of all target miRNA–probe hybrids. This allowed for using a single hybridization temperature, at which all target miRNA hybrids remained intact while single nucleotide mismatches melted [94].

In several examples, it was also demonstrated that sampling the cell lysate did not affect the CE separation pattern in DQAMmiR [89, 91]. These results led us to hypothesis that DQAMmiR may be robust to changes in the sample matrix and potentially allow highly accurate miRNA analysis in crude cell lysates. In **Chapter 2**, I present my work on testing this hypothesis by investigating the influence of the sample matrix on accuracy and precision of the miRNA analysis. The results showed that DQAMmiR quantitates miRNA equally well in a pure buffer, RNA extract from the cell lysate, and the crude cell lysate, which suggest that the complexity of sample matrix has negligible effect on the analytical performance of DQAMmiR.

While the SSB-mediated DQAMmiR has shown great analytical performance in previous study, the involvement the protein, SSB, in the assay can potentially decrease the assay's robustness and increase its cost, making it less suitable for practical clinical use. To address this use, in **Chapter 3**, I present the second-generation DQAMmiR, which does not need SSB and has lesser dependence on drag tags on probes, by introducing PNA, an electrically neutral analog of DNA, as the hybridization probes. I proved that the new PNA-facilitated DQAMmiR is feasible without compromising the accuracy and LOD of the assay, making it a potential tool for practical miRNA analyses in clinical samples.

Unlike RT-PCR, DQAMmiR does not involve enzymatic reactions (which are error-prone); therefore, DQAMmiR is more robust than RT-PCR. However, its robustness comes at an expense of relatively high concentration LOD. A typical cell-lysate sample contains miRNAs at

sub-pM concentrations, while the LOQ of commercial CE-LIF instruments is in the low pM range at best. This problem could be addressed by introducing a on-column sample preconcentration (OSP) step prior to CE separation in DQAMmiR. In the next section, I am going to review different OSP methods to explore which one could be compatible with the DQAMmiR and in particular, the second generation DQAMmiR with PNA hybridization probes.

### 1.3. Electrophoresis-based online sample preconcentration (OSP) techniques

Irrespective of the method of detection, detection sensitivity of CE can be maximized by performing sample preconcentration prior to CE. While offline preconcentration techniques, such as liquid-liquid extraction and solid-phase extraction are commonly used for sample pre-treatment, these methods are often laborious, are time consuming, can require significant experimental skills, and are difficult to automate. In contrast, electrophoresis based online sample preconcentration (OSP) techniques, such as field-amplified sample stacking (FASS), dynamic pH junction, and isotachopheresis (ITP), are well suited for increasing CE sensitivity as they require little or no changes in the existing CE setups, and their coupling with CE can be mostly or completely automated [95–100]. This section aims to introduce these OSP techniques in detail by explaining how they work.

To understand how these techniques work, we can start from the conservation of mass in a mass flux. Below **Eq. 1-1** is a derivative form of conservation of mass in a mass flux, where  $c$  and  $v$  refer to the concentration and migration velocity of a species at the given position  $x$  and the given time  $t$ .

$$\frac{\partial c}{\partial t} + \frac{\partial(cv)}{\partial x} = 0 \quad (1-1)$$

Or it can be derived to:

$$\frac{\partial c}{\partial t} = -\frac{\partial(cv)}{\partial x} \quad (1-2)$$

In these equations, the term  $\frac{\partial c}{\partial t}$  refers to the species' concentration changing over time at the positive  $x$  at , and the term  $\frac{\partial(cv)}{\partial x}$  is the change rate of total quantities of the species passing through the positive  $x$ . This equation can be interpreted as that the accumulation rate of a species at a given position (i.e., sample concentration) equal to the decreasing rate of total quantities of the species between the outflux and influx to that position. **Eq. 1-2** can be further derived to:

$$\frac{\partial c}{\partial t} = -v \frac{\partial c}{\partial x} - c \frac{\partial v}{\partial x} \quad (1-3)$$

This equation tells that there are two scenarios that can cause accumulation of the species in a given position ( $\frac{\partial c}{\partial t} > 0$ ) in a flux: i) there is a negative concentration gradient across different positions in the direction which the species is moving to, *i.e.*,  $\frac{\partial c}{\partial x} < 0$ , and ii) there is a negative velocity gradient across different positions in the direction which the species is moving to, *i.e.*,  $\frac{\partial v}{\partial x} < 0$ . In the CE study, the species is typically injected in a bulk solution, where there is no concentration gradient in the injected sample plug. Thus the first scenario is not relevant here. And we will focus on the second scenario where a negative velocity gradient in the direction of movement ( $\frac{\partial v}{\partial x} < 0$ ) will cause the accumulation of a species, leading to sample stacking. While in reverse, a positive velocity gradient in the direction of movement ( $\frac{\partial v}{\partial x} > 0$ ) will cause the dispersion of the species, resulting in peak broadening. **Fig. 1.9** illustrates peak broadening and stacking of a species moving in two discontinued phases caused by velocity gradient. Almost all electrophoresis-based on-line sample preconcentration techniques set up this velocity gradients for



**Figure 1.9.** An illustration of peak broadening and stacking for a species moving in two discontinued phases  $\alpha$  and  $\beta$ .  $v_\alpha$  and  $v_\beta$  refer to the migration velocities of the species in phase  $\alpha$  and  $\beta$ , respectively. Peak broadening will be observed at the boundary of two phases if there is a positive velocity gradient in the direction of movement ( $v_\alpha < v_\beta$ ). Stacking will be observed if the velocity gradient in the direction of movement is negative ( $v_\alpha > v_\beta$ ).

the analytes in specific regions, wherein analytes undergo a net accumulation. The major difference between these methods is the strategies they used to facilitate such gradients.

Because the electrophoretic migration velocity of an ionic species ( $v_{ep}$ ) is the product of its electrophoretic mobility  $\mu_{ep}$  and the local electric field  $E$  (**Eq. 1-4**), the velocity gradient can be created by either a gradient in local electric field ( $\frac{\partial E}{\partial x}$ ) or a mobility gradient ( $\frac{\partial \mu_{ep}}{\partial x}$ ) or a gradient in local electric field ( $\frac{\partial E}{\partial x}$ ) as shown in **Eq. 1-5**.

$$v_{ep} = \mu_{ep} E \quad (1-4)$$

$$\frac{\partial v_{ep}}{\partial x} = E \frac{\partial \mu_{ep}}{\partial x} + \mu_{ep} \frac{\partial E}{\partial x} \quad (1-5)$$

### 1.3.1. Facilitating velocity gradient via mobility gradient $\frac{\partial \mu_{ep}}{\partial x}$

The velocity of an ions can be altered via the changes to their electrophoretic mobilities, i.e., facilitating a mobility gradient in capillary. To understand how this can be achieved, let's look back to the equation of electrophoretic mobility of an ion. As shown in **Eq. 1-6**, the electrophoretic mobility of an ion is related to its charge,  $q$ , and its size,  $r$ . This means that the electrophoretic mobility of an analyte can be changed by either changing its charge or its size. Depending on which strategy is used to alter the mobility of the ions, the OSP methods with mobility gradient can be further classified to two groups, charge-induced and size-induced.

$$\mu_{ep} = f(q, r) \quad (1-6)$$

#### 1.3.1.1. Charge changing-induced mobility gradient

One method to alter the charge of an ion is to change the pH of the buffers, which leads to another electrophoresis based OSP methods called dynamic pH junction [97–98]. The dynamic pH junction involves creating a “junction” or boundary in the capillary where the pH changes, leading to a change in the charge state of the analytes (**Fig. 1.10**).

In dynamic pH junction, the capillary is typically filled with a BGE that has a pH either lower or higher than the pKa of the analytes. The sample, on the other hand, should be prepared in a buffer that has a pH on the other side of the pKa. This results in change to the analytes's ionization state when they passes through the sample/BGE boundary, leading to significant alternation of their electrophoretic mobilities, which cause concentration and focusing with a factor of 10–100 times or even more [97–98]. One of the advantages of dynamic pH junction is that it works with high ionic strength samples, making it useful for clinical diagnostic applications as biological samples such as blood and urine have high ionic strength. And it can be used for a wide range of

$$pH_{\alpha} < pH_{\beta}, q_{\alpha} > q_{\beta}, \mu_{\alpha} > \mu_{\beta}$$

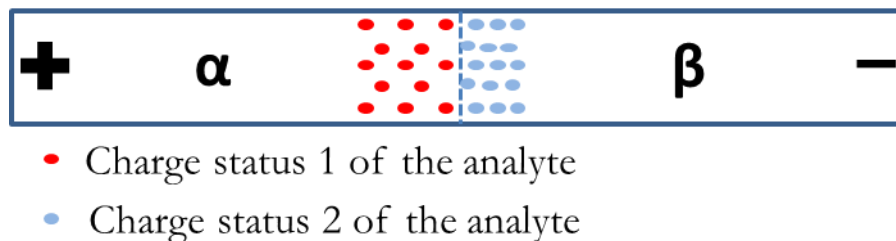


**Figure 1.10.** Illustration of the boundary where the pH changes in dynamic pH junction.

analytes, as long as their charge state can be manipulated by changing the pH, making them been applied in various applications, including biochemical analysis to detect amino acids, peptides, and proteins, pharmaceutical analysis to quantify drugs and their metabolites, and environment and food analysis [101–104].

### 1.3.1.2. Size changing-induced mobility gradient

The electrophoretic mobility of an ionic can also be altered by changing its size, which can be achieved by adding a pseudo-stationary (PS) phase which the analyte interacts with into the BGE (**Fig. 1.11**). This approach was originally introduced by Terabe *et al.* as micellar electrokinetic chromatography (MEKC) to analyze neutral compounds by SDS micelles as PS phase [105–106]. A decade later, PS phases evolved into being used in preconcentration mechanisms by virtue of their interaction with the compound of interest. The OSP technique that employ this mechanism is sweeping, which involves the injection of sample solution devoid of the PS phase [107–108]. When the electric field is applied, the micelles present in the BGE penetrate the sample zone, and subsequently pick and accumulate the analytes into a narrow band. Then enrichment of the analytes is largely dependent on the analyte-micelle interaction. Since its introduction in 1990s, sweeping has grown to be one of the most prominent and universal OSP

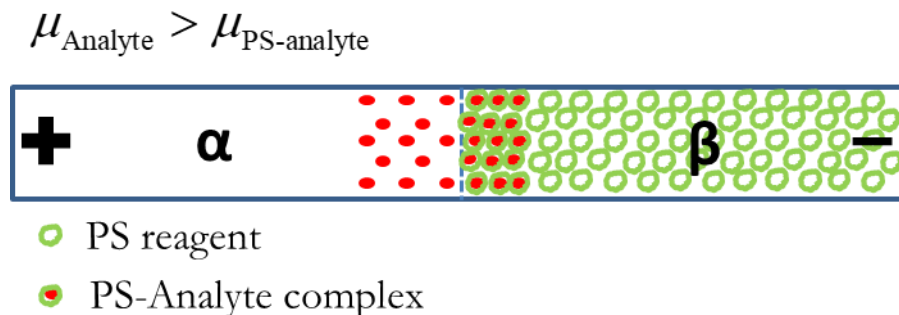


**Figure 1.11.** Illustration of changing the mobility of an analyte via adding a pseudo-stationary (PS) phase into the BGE.

techniques in the field because of its applicability to both charged and neutral species and its tolerance of high ionic strength samples.

### 1.3.2. Facilitating velocity gradient via electric field gradient $\frac{\partial E}{\partial x}$

The electric field gradient can be achieved when the two discontinued phases have different conductivity as shown in **Fig. 1.12**. According to a variation of Ohm's law:  $J = \sigma E$ , where  $J$  is the current density,  $\sigma$  is the conductivity, and  $E$  is electric field strength, the local electric field is inversely proportional to the conductivity. Thus, a smaller conductivity in phase  $\alpha$  causes a stronger local electric field in phase  $\alpha$  (i.e.,  $\sigma_{\alpha} < \sigma_{\beta}, E_{\alpha} > E_{\beta}$ ). As a result, the ionic analytes have a larger electrophoretic velocity in phase  $\alpha$  than that in phase  $\beta$ , i.e.,  $v_{\alpha} > v_{\beta}$ . Thus, when the analytes moving from phase  $\alpha$  to phase  $\beta$ , the analytes will be accumulated by staking at the boundary between two phases leading to analytes concentration.

#### 1.3.2.1. Field-amplified sample stacking (FASS)

One OSP technique that using this strategy is field-amplified sample stacking (FASS). In FASS, the analytes is typically presented in a sample that has a lower conductivity than that of the BGE, which could be achieved by using a low-concentration sample buffer. When a voltage is

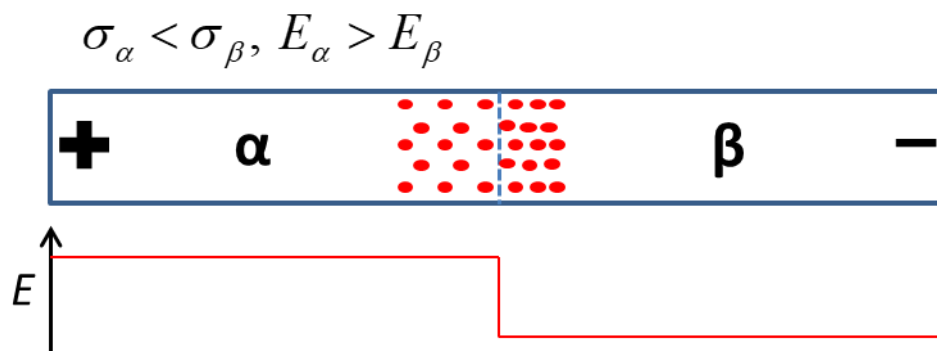


**Figure 1.12.** Illustration of facilitating electric field gradient via conductivity gradient. A smaller conductivity in phase  $\alpha$  causes a larger local electric field in phase  $\alpha$  (i.e.,  $\sigma_{\alpha} < \sigma_{\beta}, E_{\alpha} > E_{\beta}$ ),

applied across the capillary, the stronger electric field in the low-conductivity sample matrix will cause the analyte ions in the sample to stack at the boundary between the sample and the BGE, resulting in an increased local concentration. In FASS, the sensitivity enhancement is determined by the ratio of velocities in the sample zone and BGE zone, which is usually around 10–20 times [109]. There are two major drawbacks to this approach. First, that the sample should have a lower conductivity than that of the BGE, thus FASS is limited to samples with a low-conductivity matrix, or dilution of the sample is required. The other limitation of FASS is that the maximum length of the hydrodynamically injected sample plug is limited to about 3–5% of the capillary volume. The mismatch of the local electroosmotic velocities in the BGE zone and sample zone will cause band broadening if a longer sample zone is injected. FASS has been employed in many routine applications and has become the most popular OSP approach for sensitivity enhancement, despite its limitation.

### 1.3.2.2. Field-amplified sample injection (FASI)

Another OSP techniques that leverages the electric field gradient is field-amplified sample injection (FASI) [110]. In FASI, the sample with lower conductivity than BGE is introduced by electrokinetic injection in contrast to FASS where it is introduced hydrodynamically.

When performing electrokinetic injection, the analytes in the low-conductivity sample matrix are injected into the capillary by the electroosmotic flow as well as its own electrophoretic movement. And the conductivity difference between the sample zone and BGE leads to sample stacking during the injection, leading to an increase in sensitivity. There are four major disadvantages to FASI. The first two are the same as for FASS. The third disadvantage of FASI is that sample ions have different mobilities and are therefore injected to a different extent. This results in more of the higher mobility ions being injected. The final disadvantage is that because of the way injection is performed, the number of analyte ions entering the capillary significantly depends on the conductivity of the matrix and therefore it is susceptible to any samples where the matrix can change. Despite this advantage, FASI can give up to a 1000-fold increase in sensitivity.[110]

### **1.3.2.3. Large-volume sample stacking (LVSS)**

Large-volume sample stacking (LVSS) is another variant of FASS designed to increase the sample volume that can be injected into the capillary with FASS. In this method, a large volume of the low-concentration sample is injected into the capillary, filled up to the entire capillary. The key requirement for this approach to be successful is to slowly push the sample matrix out of the capillary inlet after the analytes are stacked at the sample/BGE interface. It is very important to stop the analytes exiting the inlet of the capillary before the subsequent separation begins. There are two ways to do this, the first is to switch the polarity just before the stacked zone exits the capillary and is typically done when the current reaches 90–95% of the BGE current. This approach was recently employed in recent studies [111–114]. Another way to control sample matrix removal in LVSS is with an EOF pump whereby the sample matrix is removed through the capillary by EOF.[115–116] The key to the success of this method is to ensure that there is a different EOF between the sample and BGE such that as the sample is removed, the net flow through the capillary

changes. When only a small amount of matrix remains, electrophoresis occurs, and the components separate by conventional means. The advantage of this approach is that it is controlled by the chemistry, not by physically switching the polarity based on time. The disadvantage is that it relies on accurate and repeatable control of the EOF, which is very challenging in practice.

#### **1.3.2.4. Isotachophoresis (ITP)**

Among all electrophoretic OSP methods in CE, ITP is well known to be a powerful and robust preconcentration method capable of concentrating trace of component in a high concentration of matrix ions. In ITP, the sample is placed between the leading electrolyte (LE) and trailing electrolyte (TE), which have a higher and lower mobility than the sample ions' mobilities respectively [117–118]. The different in mobility between the LE and TE creates a nonuniform electric field because of the higher conductivity in the higher mobility LE region (**Fig. 1.13**). If a target analyte migrates into the LE zone it encounters a lesser electric field and drops back into its respective zone. Conversely, if the target analyte happens to fall back into the TE zone it encounters a higher electric field strength and is pushed back into the narrow sample zone. As a result, the sample ions with a mobility between the mobility of LE and TE ions stack in front of the TE, but behind of LE in a descending order based on their mobilities. The length of each zone depends on the concentration of each ion and the initial concentration of LE ions defined by Kohlrausch regulating function. Two types of ITP modes can be used, which are the “plateau-mode” and “peak-mode” ITP. Plateau-mode ITP occurs when the analyte is present in large amount allowing the formation of separate contiguous plateau like zones with locally uniform concentrations [119–121]. Peak-mode ITP occurs when the analyte present is an amount that is unable to reach their steady-state concentration, thus unable to form a contiguous zone, and is therefore focused as a sharp peak between two zones [122].

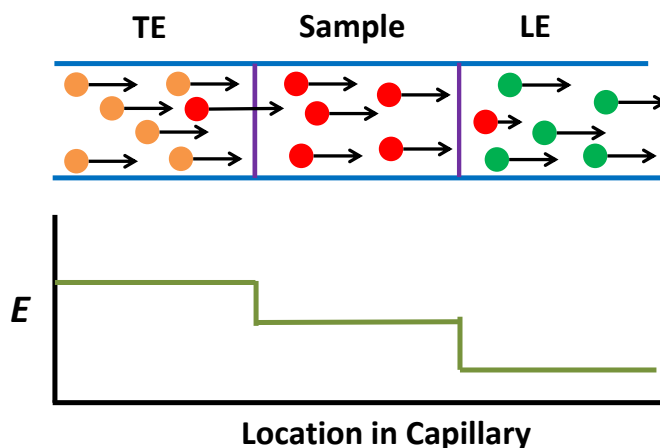


**Figure 1.13.** Illustration of the discontinuous buffer system in ITP. In a discontinuous electrolyte system, when a voltage is applied the TE has a greater local electric field while the LE has a lower local electric field with respect to the target analyte. If the target analyte (red circles) falls back into the TE zone, it encounters a higher electric field and is pushed back towards its narrow window. Similarly, if a target analyte enters the LE zone, it falls back into the narrow window.

Over the past 15 years, Santiago's group has been exceptionally active in the use of peak-mode ITP in the nucleic acid analysis, including purification of nucleic acids from whole blood and rapid in-line hybridization-based analyses of RNA and DNA. In this area, Bercovici *et al.* studied the physicochemical process of preconcentration, mixing, and chemical reaction kinetic by comparing numerical and experimental results [123]. When 20 nM of target DNA was used, a 960-fold acceleration of the hybridization rate was obtained with ITP compared to a standard incubation, which increased to 14,000-fold when the target concentration was 500 pM. While impressive, there is still a background signal from unhybridized nucleotide probe, which migrates with the hybridized DNA. This issue with signal from unhybridized probes can be addressed by the DQAMmiR approach developed in our lab where the unhybridized probes are being shifted by the SSB [89]. Inspired by this work, researchers in our lab incorporated the ITP with DQAMmiR for the miRNA analysis as shown in **Fig. 1.14** [124]. In this approach, both unhybridized ssDNA probes and DNA–miRNA hybrids are concentrated into a narrow zone by ITP prior to CE

separation, resulting in a significant LOD improvement in DQAMmiR without compromising its quantitiveness. This work demonstrated the successful combination of ITP and DQAMmiR in a single capillary using a commercial instrument for simultaneous analysis of multiple miRNAs.

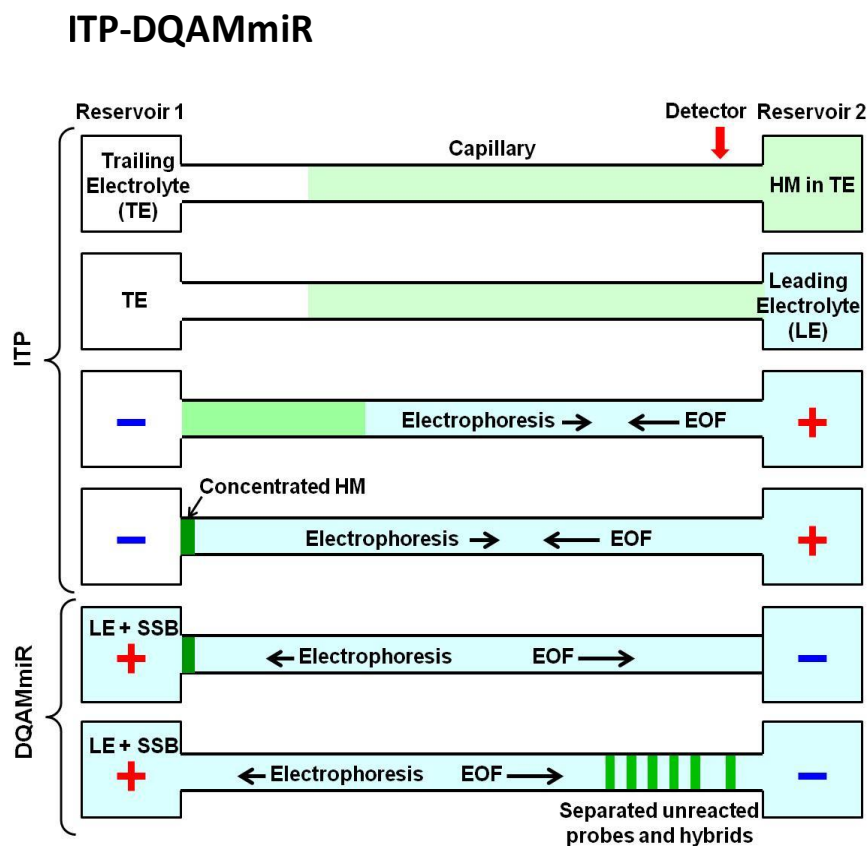


**Figure 1.14.** Conceptual depiction of streamlined combination of isotachopheresis (ITP) and DQAMmiR. The major stages of the ITP-DQAMmiR tandem analysis are shown. In the ITP stage, the capillary is pre-filled with a trailing electrolyte (TE) of low conductivity by a pressure-driven flow from Reservoir 1. The hybridization mixture (HM) is prepared in TE and a large part of the capillary is filled with HM by a pressure-driven flow from Reservoir 2 (detection end of the capillary). HM in Reservoir 2 is replaced with a leading electrolyte (LE) with high conductivity and a voltage is applied with positive electrode being in Reservoir 2. The electroosmotic flow (EOF) from positive to negative electrode is faster than the electrophoretic migration of the hybrids and probes in the opposite direction. This leads to the concentration of probes and hybrids inside the capillary near Reservoir 1. In the DQAMmiR stage, TE in Reservoir 1 is replaced with SSB-containing LE. The voltage is now applied with the positive electrode being in Reservoir 1. Continuously supplied SSB migrates faster than the probes and hybrids and overruns them. The latter facilitates SSB-driven separation of the unreacted probes from the hybrids. (Adapted from [124] by permission of American Chemical Society)

With this method, the LOD was improved by two orders of magnitude (from 100 pM down to 1 pM), making it promising tool for the detection of low abundance miRNAs in practice.

However, this approach is not compatible with the second-generation DQAMmiR with PNA hybridization probes because ITP could not concentrate unreacted PNA probes due to their very low electrophoretic mobilities. Consequently, the unreacted PNA probes eluted from the capillary during ITP, affecting quantitiveness of DQAMmiR, which utilizes the peak(s) of unreacted probes for normalizing the signals from the hybrids. To address this issue, I developed a novel OSP methods that combines the concept of FASS and ITP for the second-generation DQAMmiR with PNA hybridization probes (**Chapter 4**). I showed that the new OSP method can concentrate the miRNA–probe hybrids efficiently without losing the unhybridized PNA probes during the run, which facilitates a comparable LOD improvement (~ 140 times improvement) with the original ITP-DQAMmiR design.

## **CHAPTER 2. ACCURATE MICRORNA ANALYSIS IN CRUDE CELL LYSATE BY CAPILLARY ELECTROPHORESIS-BASED HYBRIDIZATION ASSAY IN COMPARISON WITH QUANTITATIVE REVERSE TRANSCRIPTION-POLYMERASE CHAIN REACTION**

The presented material was published previously and reprinted with permission from “Hu, L.; Stasheuski, A. S.; Wegman, D. W.; Wu, N.; Yang, B. B.; Hayder, H.; Peng, C.; Liu, S. K.; Yousef, G.M.; Krylov, S.N. *Anal. Chem.* **2017**, *89*, 4743–4748”. Copyright 2017 American Chemical Society. My contribution to the article was: (i) planning all experiments, (ii) performing all experiments, (iii) interpreting results, (iv) preparing all figures, (v) writing the manuscript.

### **2.1. Introduction**

Analysis of molecular biomarkers in tissue samples is a promising approach for diagnosis, prognosis, and therapy guidance of cancer and other diseases [125]. Inaccuracies in analysis of molecular biomarkers lead to difficulties with their validation and, consequently, slow down their regulatory approvals for clinical use [126]. Analysis of molecular biomarkers in tissue samples typically involves three major steps: (i) sample collection (tissue excision and storage), (ii) sample preparation (e.g. cell lysis, removal of cell debris, and purification/preconcentration of target molecules), and (iii) sample analysis (quantification of target molecules). Failure to repeat each sample-preparation sub-step in an accurate/reproducible manner is often the main or sole reason for the inaccuracy or irreproducibility of the final analytical result [127]. Minimizing sample preparation is pivotal to making reliable molecular-biomarker analysis of tissue samples. Ideally, the analysis should be applicable to crude cell lysates.

Accurate quantitative analysis of multiple miRNAs is required for validating and using miRNA fingerprints. Accordingly, a significant research effort aims at developing analytical

approaches for quantitative analysis of multiple miRNAs [128–132]. With very few exceptions, sample preparation includes both cell lysis and RNA extraction [131, 133]. The use of commercially-available RNA extraction kits results in varying qualities of isolated RNA and different amounts of residual matrix components in the analytical sample [134–137]. Consequently, the RNA extraction stage introduces systematic errors to quantitation of miRNAs. Ideally, sample preparation should only consist of cell lysis and the analysis should be applicable directly to the lysate. While avoiding errors associated with RNA extraction, the application of miRNA analysis to a crude cell lysate may introduce another type of inaccuracy, which is associated with the interference of the cell lysate with the assay components. This interference is important, in particular, for quantitative reverse-transcription polymerase chain reaction (qRT-PCR), which is a benchmark method for quantitative analysis of multiple miRNAs [138–141].

Researchers in our lab have recently introduced direct quantitative analysis of multiple miRNAs (DQAMmiR), a capillary electrophoresis (CE)-based hybridization assay [89]. In several examples, they demonstrated that sampling the cell lysate did not greatly affect the CE separation pattern [89, 91]. These results led to a hypothesis that DQAMmiR may be robust to changes in the sample matrix and potentially allow highly accurate miRNA analysis in crude cell lysates. Here I test this hypothesis by investigating the influence of the sample matrix on accuracy and precision of the miRNA analysis. To put the results into a context of the benchmark method, I conducted similar experiments for qRT-PCR. The results showed that DQAMmiR quantitates miRNA equally well in a pure buffer, RNA extract from the cell lysate, and the crude cell lysate prepared from MCF-7 cultured cells. The DQAMmiR measurements were accurate to within 13% for miRNA concentrations ranging within 2 orders of magnitude. The standard deviations were below 11%. qRT-PCR, in contrast, revealed multifold inaccuracies and standard deviations of up to 70%.

These results suggest that the complexity of sample matrix has negligible effect on the analytical performance of DQAMmiR. The robustness of DQAMmiR to the changes in sample matrix indicates that this method can directly quantitate miRNAs in crude samples without the need of bias-prone RNA extractions, making DQAMmiR a very promising candidate for validation and clinical use of miRNA-based disease biomarkers.

## **2.2. Materials and Methods**

### **2.2.1. miRNAs and DNA Probe**

MicroRNA (cel-miR-39-3p, 5'-UCA CCG GGU GUA AAU CAG CUU G-3') and its complementary DNA probe (5'-Alexa488-CAA GCT GAT TTA CAC CCG GTG A-3') were custom-synthesized by IDT (Coralville, IA, USA). The concentrations of miRNA and DNA probe in stock solutions were determined from light absorbance at 260 nm measured with a Nano-Drop ND-1000 spectrophotometer (Thermo-Fisher Scientific, Waltham, MA, USA); molar extinction coefficients were provided by IDT. Working solutions were prepared from stock solutions by dilution. "Actual concentrations" of working solutions were calculated as stock concentrations divided by dilution factors.

### **2.2.2. Cell Lysate and RNA Extract**

MCF-7 cells were purchased from American Type Culture Collection (ATCC, Manassas, VA, USA). The cells were grown in the DMEM media (Invitrogen, CA, USA) supplemented with fetal bovine serum (FBS, 10%), penicillin (100 units/mL) and streptomycin (100 µg/mL) at 37 °C in a humidified atmosphere of 5% CO<sup>2</sup> in air. Cells were harvested at 50–70% confluency using trypsin/EDTA (0.25%/0.53 mM) and centrifuged at 1500 rpm (375 × g) for 5 min to form a pellet. The pellet was washed twice with PBS. The cells were counted with a hemocytometer. The cells

were lysed with 1% Triton in a TAE buffer (50 mM Tris-Acetate, 50 mM NaCl, 10 mM EDTA, pH 8.2) with 10  $\mu$ M masking RNA (tRNA library from baker's yeast, Sigma-Aldrich, St. Louis, MO, USA) which was used to suppress the degradation of spiked-in miRNA target (Cel-miR-39-3p) for the following analysis. Total RNA was extracted by mirVana miRNA isolation kit (Ambion, TX, USA).  $1.6 \times 10^6$  cells were used to produce 4 mL cell lysate. The same number of cells was used to generate 4 mL RNA extract. Cell lysates and total RNA extract were aliquoted and stored at  $-80$  °C for further analysis.

### **2.2.3. DQAMmiR**

The hybridization step was carried out in a Mastercycler 5332 thermocycler (Eppendorf, Hamburg, Germany). Cel-miR-39-3p at varying concentrations was incubated with 100 nM DNA probe. For hybridization, a previously demonstrated temperature program was used.<sup>29</sup> The temperature was increased to a denaturing temperature of 80 °C and then lowered to 37 °C at a rate of 20 °C/min and was held at 37 °C to allow annealing. The optimal hybridization time was found experimentally and used for each sample matrix. To minimize miRNA degradation, a nuclease-free environment was used while handling miRNA samples.

We used a P/ACE MDQ capillary electrophoresis system (Beckman-Coulter, Brea, CA, USA) with laser-induced fluorescence detection to carry out separation of the miRNA-probe hybrid from the excess of the probe. Bare fused-silica capillaries with an outer diameter of 365  $\mu$ m, an inner diameter of 75  $\mu$ m, and a total length of 50 cm were utilized. The distance from the injection end of the capillary to the detector was 40 cm. The capillary was flushed prior to every CE run with 0.1 M HCl, 0.1 M NaOH, deionized H<sub>2</sub>O and run buffer (25 mM Borax, pH 9.2) for 1 min each under a 20 psi pressure. Samples were injected by a pressure pulse of 0.5 psi  $\times$  5 s; the volume of the injected sample was 26 nL. Electrophoresis was driven by an electric field of 500

V/cm with positive polarity at the inlet. Fluorescence of the Alexa488 label on the probe was excited by 488 nm light generated with a continuous-wave solid-state laser (JDSU, Milpitas, CA, USA). Electropherograms were analyzed using 32 Karat Software. Peak areas were divided by the corresponding migration times to compensate for the dependence of the residence time in the detector on the electrophoretic velocity of the analyte. Only one miRNA was used in this study; thus, the quantity of miRNA was calculated using the following equation (which is a simplified version of the general equation published elsewhere) [89]:

$$[\text{miRNA}] = [\text{Hybrid}] = \frac{[\text{P}]_0 A_H}{A_H + A_P} \frac{q_H}{q_P} \quad (2-1)$$

where  $[\text{P}]_0$  is the initial concentration of DNA probe,  $A_H$  is the peak area corresponding to the miRNA-probe hybrid,  $A_P$  is the peak area of the SSB-bound DNA probe,  $q_H$  is the relative quantum yield of the hybrid with respect to the free probe, and  $q_P$  is the relative quantum yield of the probe in the presence of SSB with respect to the free probe. The relative quantum yields were determined in a set of separate experiments described in the Supporting Information. The original procedure for finding the quantum yields was described in detail elsewhere [89].

#### 2.2.4. Quantitative Reverse Transcription-Polymerase Chain Reaction (qRT-PCR)

TaqMan MicroRNA Reverse Transcription Kit and the stem-loop RT primers for cel-miR-39-3p were purchased from Applied Biosystems (Foster City, CA, USA) and used to synthesize cDNA according to the manufacturer's instructions. The reaction mix was incubated at 16 °C for 30 min followed by 30 min incubation at 42 °C in the iCycler thermocycler (Bio-Rad, Hercules, CA, USA). The RT products were stored at -20 °C before PCR amplification. Real-time PCR of cDNA from cel-miR-39-3p was performed with an iCycler real-time PCR system (Bio-Rad, CA, USA) using TaqMan-Universal-Master-MixII-no-UNG and TaqMan MicroRNA Assays

(both from Applied Biosystems, Foster City, CA, USA). The PCR was started at 95 °C for 10 min followed by 40 amplification cycles each of 15 s at 95 °C and 1 min at 60 °C. 1.5 µL of RT product was used for each 20 µL of PCR reaction.

### **2.3. Results and Discussion**

DQAMmiR involves 3 major steps: (i) hybridization of miRNAs with the probes (the latter taken in excess), (ii) separation of miRNA-probe hybrids from each other and from the unreacted probes, and (iii) quantitative detection of the separated species. In the hybridization step, the complete binding (>90%) of the target miRNAs by the corresponding probes should be reached without appreciable degradation of the miRNAs or the probes. The slower or incomplete binding and the degradation can affect accuracy of miRNA quantitation in DQAMmiR.

The sample matrix can potentially lead to (i) slower or incomplete hybridization because of the influence of RNA- and DNA-binding proteins, pH, salts, *etc.*, and (ii) the degradation of the target miRNAs and DNA probes by nucleases [142–143]. Thus, for every new sample matrix, the incubation time that is sufficient for the hybridization of >90% of target miRNAs must be found, and insignificant degradation of the target miRNAs and DNA probes during this time must be confirmed.

The adverse effects of the sample matrix on the quality of the hybridization step can be minimized by shortening the incubation time while still ensuring >90% hybridization. The required incubation time can, in turn, be shortened by increasing probe concentrations [93]. Increasing probe concentrations, however, decreases the limit of quantitation (LOQ) of miRNAs because of interferences of signals from the impurities (present in the probes and comigrating with the hybrids) with signals from the hybrids. Therefore, the maximum concentrations of the probes that

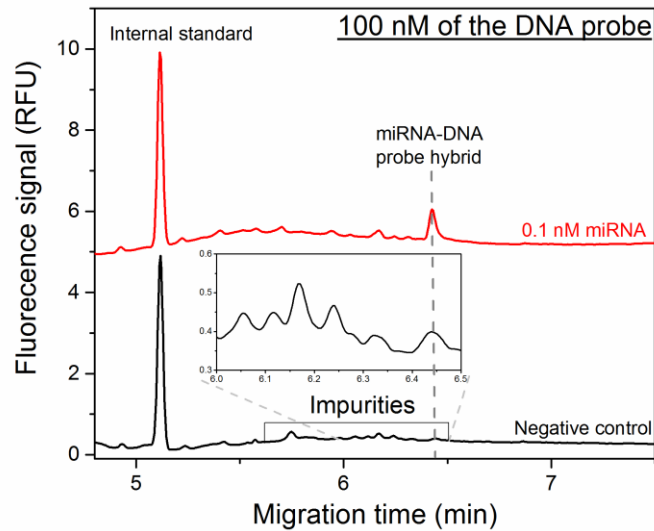


**Figure 2.1.** The impurity level associated with the DNA probes. The impurity level in 100 nM DNA probe compared to the hybrid peak of 0.1 nM target miRNA. According to the results, 100 nM was found to be the maximum DNA probe concentration to quantitate 0.1 nM miRNA with LOQ of 0.1 nM. The inner panel shows zoomed-in impurities of the negative control for clarity.

allow the required LOQ must be chosen first; the incubation time that is sufficient for hybridization of >90% target miRNA must be determined after that.

In this work, we used a single non-human miRNA cel-miR-39-3p as target, which is commonly used as miRNA mimic for human miRNA analysis [144], and, accordingly, a single fluorescently labeled DNA probe complementary to cel-miR-39-3p. We set LOQ at a level of 0.1 nM of cel-miR-39-3p. The impurity level in the DNA probe was measured (**Fig. 2.1**), and the maximum DNA probe concentration that allowed us to achieve the set LOQ was found to be 100 nM. This probe concentration was used in all further experiments.

### 2.3.1. Effect of sample matrix on hybridization

With the probe concentration being defined, we studied the influence of sample matrix on the incubation time required for hybridization of >90% of target miRNA. Three matrices were

investigated: a pure TAE buffer (50 mM Tris-acetate, 50 mM NaCl, 10 mM EDTA, pH 8.2), an RNA extract from the cell lysate of MCF-7 cultured cells (obtained with a commercial miRNA isolation kit), and the crude lysate from the MCF-7 cells. Cel-miR-39-3p, which is foreign for MCF-7 cells, and its fluorescently labeled complementary DNA probe were spiked into the 3 matrices at final concentrations of 10 and 100 nM, respectively. The incubation time varied between 10 and 150 min. CE separation and hybrid quantitation with eq 1 were then conducted. Hybrid concentrations as functions of incubation time for the 3 matrices are shown in Fig. 2.2. Incubation times below 30 min were insufficient for reaching hybrid concentration of 9 nM (90% hybridization of 10 nM miRNA). Upon reaching its maximum hybrid concentration does not change significantly for the pure buffer but gradually decreases for the RNA extract and the cell lysate. The decrease is likely associated with the degradation of the target miRNA which agrees with the fact that the decrease rate is significantly higher for the cell lysate. For our specific case,

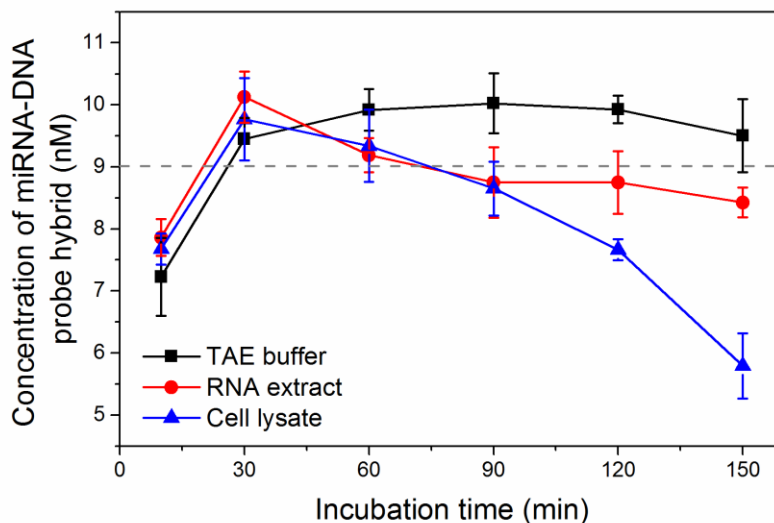


**Figure 2.2.** Effect of sample matrix on miRNA hybridization. Both 10 nM miRNA and 100 nM DNA probe were spiked into the 3 matrices and incubated for varying times; after that, the hybrid was separated from the unreacted probe by CE and hybrid concentration was calculated with eq 1. The dashed line shows the level of 90% hybridization of the spiked 10 nM miRNA. Error bar represents standard deviation of three repetitions.

incubation times in a range of 30–60 min were suitable for all 3 sample matrices—they ensured miRNA integrity and >90% hybridization. For further experiments we chose incubation time of 45 min as the optimum one.

### 2.3.2. Effect of sample matrix on probe degradation

As we mentioned above, the accuracy of miRNA quantitation also depends on the integrity of the DNA probe. We, thus, studied probe degradation in the 3 matrices. 100 nM DNA probe was spiked into each matrix along with fluorescein as an internal standard and incubated for varying times before sampling for CE separation. We found that expectedly probe degradation was very slow in all the matrices (**Fig. 2.3**). Even when incubated in the cell lysate for 2-h, 90% of the probe was still intact suggesting that probe degradation should not significantly affect accuracy of miRNA quantitation by DQAMmiR. If significant probe degradation is observed, the use of masking DNA can suppress this degradation [145]. For the purpose of this work, the above

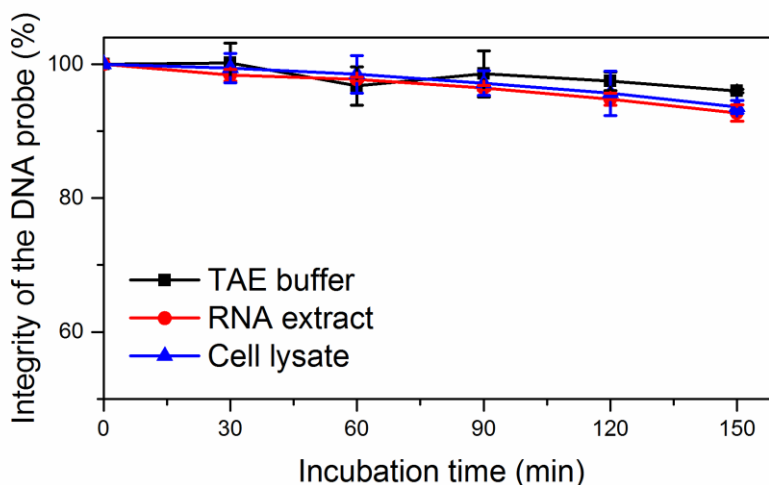


**Figure 2.3.** Integrity of the DNA probe in each matrix over time. 100 nM DNA probe and 50 nM fluorescein (as internal standard) were spiked into the 3 matrices, following incubation for varying times and analyzed by CE. The integrity of the DNA probe was calculated by using the relative peak area of the DNA probe. The integrity of the DNA probe without incubation was set as 100%. Error bar represents standard deviation of three repetitions.

experiments confirmed that the hybridization step with 45 min incubation is sufficient for >90% hybridization and guarantees no significant degradation of the target miRNA or DNA probe.

### 2.3.3. Effect of sample matrix on the performance of DQAMmiR in comparison to qRT-PCR

We further studied the performance of DQAMmiR in different sample matrices by measuring spiked-in miRNA target, cel-miR-39-3p in a range of concentrations. The range of miRNA concentrations was set 0.1–10 nM, while the probe concentration was 100 nM in all experiments. DQAMmiR electropherograms in 3 matrices (**Fig. 2.4**) indicated that there was no significant matrix-associated effect on CE-separation, and quantifiable peaks of the miRNA-probe hybrid for all miRNA concentrations (0.1–10 nM) were successfully produced in all matrices.

The results of DQAMmiR experiments were compared with the results of the qRT-PCR assay, which is a benchmark method for miRNA quantification. According to standard procedures,

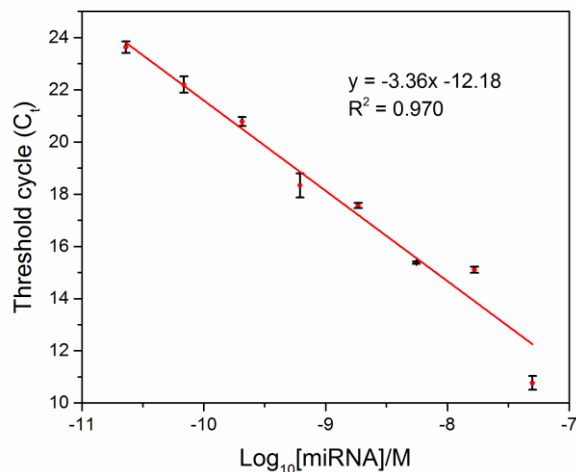


**Figure 2.4.** Example of a standard curve of qRT-PCR. The error bars represent standard deviations of three repetitions on one PCR plate. A standard curve was built in every plate for quantification. Below is an example of a standard curve. All standards were prepared with TAE buffer. 3× serial dilutions were performed with starting concentration of 50 nM, the concentration range of standards was set to cover a range of interest in this study.

a standard curve is required for qRT-PCR for absolute quantification. Here we built the standard curve using standard samples prepared by serial dilution in TAE buffer (**Fig. 2.5**). The concentration range of standards was selected to cover the range of interest in this study (0.1 – 10 nM). The reason why the standard curve must be built for the pure buffer is that in a real case scenario, RNA extract and cell lysate from the real sample contain endogenous target miRNA. Bar graphs in **Fig. 2.6** compare the concentrations of miRNA measured by DQAMmiR and qRT-

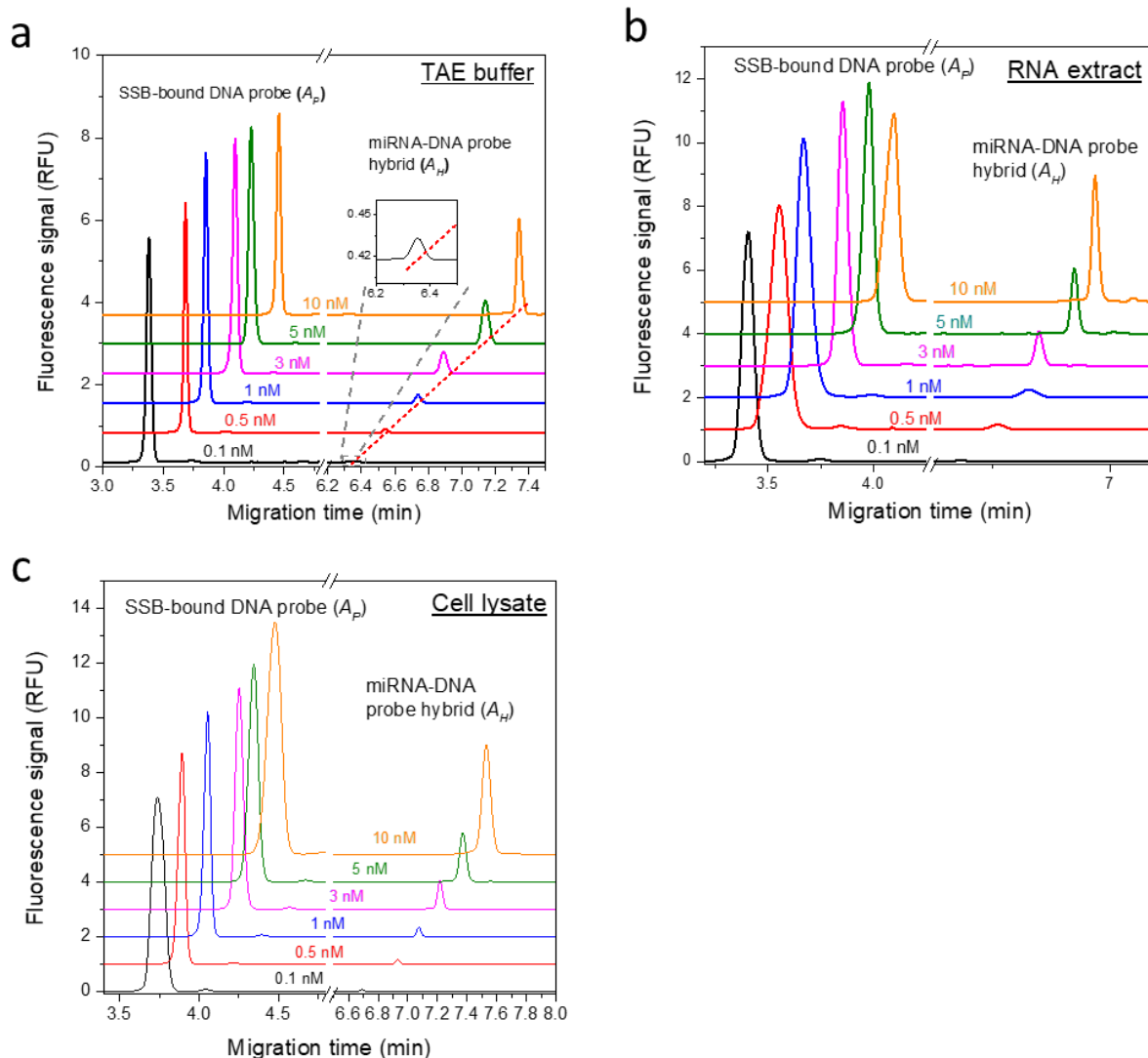


**Figure 2.5.** Electropherograms of DQAMmiR measurements in the (a) TAE buffer, (b) RNA extract, and (c) Cell lysate. Concentration range of miRNA is from 0.1–10 nM. The inset shows the zoom-in of the hybrid peak while [miRNA] = 0.1 nM for clarity.

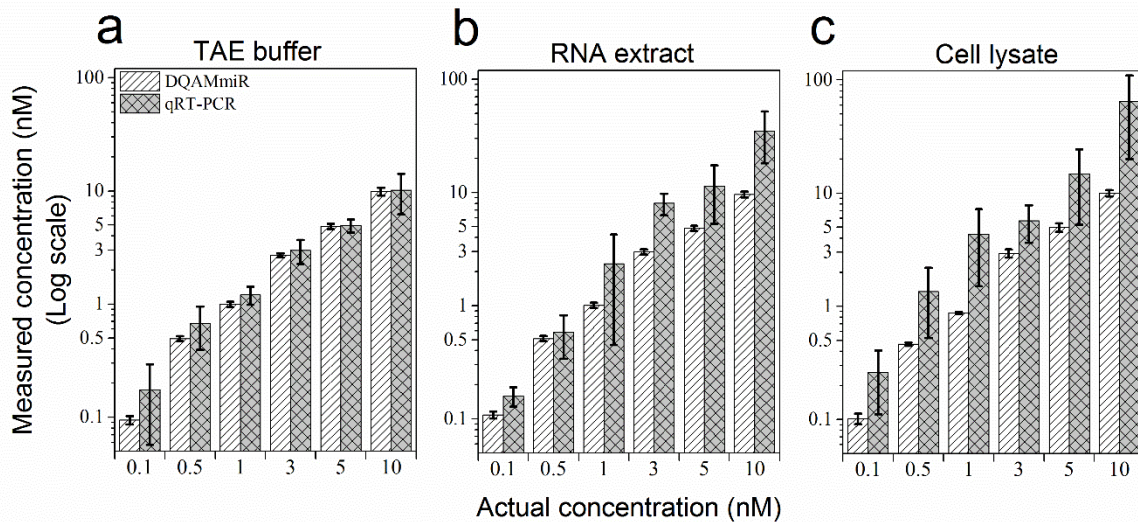


**Figure 2.6.:** Comparison of miRNA recovery in DQAMmiR and qRT-PCR-based for (a) TAE buffer, (b) RNA extract, and (c) cell lysate. Error bar represents the standard deviation of three independent measurements.

PCR with actual concentrations for the three sample matrices. Note that the vertical axis is in the logarithmic scale. In the TAE buffer (**Fig. 2.6a**), DQAMmiR could perfectly recover miRNA concentrations in their whole range with inaccuracy below 10% and relative standard deviation (RSD) below 9%. The results of qRT-PCR showed slightly worse accuracy (inaccuracy of 22%) and precision (RSD of 34%), specifically at lower miRNA concentrations. For miRNA samples in the RNA extract and cell lysate, the differences between DQAMmiR and qRT-PCR were drastic (**Fig. 2.6b and c**). Measurement by DQAMmiR were still accurate (maximum inaccuracy of 13%) and precise (maximum RSD of 11%). In contrast, 5-fold inaccuracies and RSD of up to 70% were observed in the qRT-PCR results. DQAMmiR proved to be perfectly robust to changes of the sample matrix, while qRT-PCR showed the lack of robustness.

In contrast to DQAMmiR, qRT-PCR requires a standard curve for absolute quantification. This requirement makes qRT-PCR an indirect method and can result in profound inaccuracy and

imprecision. In this study, the differences in accuracy between the 3 matrices suggest that the main source of this inaccuracy was from the mismatch of the matrices, the standard curve was built for miRNA spiked in the pure buffer. (We would like to emphasize again that in a real case scenario, it is impossible to build a calibration curve in the matrix of a biological sample as it already contains the target miRNA and, thus, does not allow one to control the concentration of target miRNA.) In contrast to the pure TAE buffer, the crude cell lysate contains molecules (proteins, nucleases, and RNA/DNA, *etc.*) which can influence the activity of the two enzymes (reverse transcriptase and DNA polymerase) employed in qRT-PCR. Typically, preanalytical purifications, such as RNA isolations, are used to purify cell lysates and reduce this interference from the matrices, however, our investigation of samples with RNA extract as a matrix indicated that the extraction kits might not be able to completely remove these interfering contents from crude samples. Moreover, these additional processes for sample preparation could also introduce unpredicted variances in the analyte amount, resulting in an unreliable miRNA expression profile [146]. In contrast, the hybridization in the DQAMmiR assay is an enzyme-free reaction, the conditions of which could be easily altered and optimized without disturbing its quantitative characteristics in crude matrices.

## **2.4. Conclusion**

To conclude, the excellent accuracy and precision of DQAMmiR in cell lysate confirmed that DQAMmiR is applicable to crude cell lysate and is very robust to changes of sample matrices. Therefore, DQAMmiR can facilitate highly accurate analyses of crude clinical samples without additional sample preparation. Such analyses, in turn, will facilitate validation of “miRNA fingerprints” for disease diagnostics.

### **CHAPTER 3. DIRECT QUANTITATIVE ANALYSIS OF MULTIPLE MICRORNA (DQAMMIR) WITH PEPTIDE NUCLEIC ACID HYBRIDIZATION PROBES**

The presented material was published previously and reprinted with permission from “Hu, L.; Anand, M.; Krylova, S. M.; Yang, B. B.; Liu, S. K.; Yousef, G. M.; Krylov, S. N. *Anal. Chem.* **2018**, *90*, 14610–14615”. Copyright 2018 American Chemical Society. My contribution to the article was: (i) ideation, (ii) deriving theoretical models for mobility estimation, (iii) planning all experiments, (iv) performing all experiments, (v) interpreting results, (vi) preparing all figures, (vii) writing the manuscript.

#### **3.1. Introduction to DQAMmiR with PNA probes**

In general, DQAMmiR is a hybridization-based assay in which the excess of hybridization probes (fluorescently-labeled for sensitive detection) is separated from the miRNA–probe hybrids, and the hybrids are separated from each other, by CE with strong EOF [89]. The EOF propels the probes and the hybrids towards the detector at the end of the capillary; quantitative detection of the probes and the hybrids facilitates absolute quantitation of the hybrids without calibration curves.

The first generation of DQAMmiR utilizes ssDNA probes and two types of mobility shifters: (i) SSB added to the running buffer, and (ii) different-length-peptide drag tags conjugated onto the ssDNA probes [89]. SSB facilitates separation of the excess probes from the hybrids by binding the ssDNA probes but not the hybrids. The drag tags induce mobility shifts in the hybrids allowing their separation from each other without interference with the binding affinity of SSB to the ssDNA probes. However, SSB is a protein, and while it is quite stable, involving it in the assay

can potentially decrease assay's robustness and increase its cost making it less suitable for practical clinical use.

To address this issue, here, we introduce the second generation DQAMmiR which does not need SSB and has lesser dependence on drag tags on the probes. The function of SSB, utilized in the first-generation DQAMmiR, is to separate excess ssDNA probes from the ssDNA-miRNA hybrids which have similar electrophoretic mobilities due to negative charges on DNA and RNA. SSB would not be needed if the probes were polymers capable of hybridizing miRNA but not being negatively charged. An example of such polymers is peptide nucleic acid (PNA) which is an electrically neutral analogue of DNA composed of repeating N-(2-amino-ethyl)-glycine units [147]. PNA-miRNA hybrids are negatively charged due to the negative charge on miRNA, although charge density is about a half of that of DNA-miRNA hybrids. Electrically-neutral PNA probes should be separable from the negatively charged PNA-miRNA hybrids without any additional mobility modifier, such as SSB.

To achieve quantitation of multiple targets, separating the hybrids from each other is also essential. A theoretical model was previously developed to predict the electrophoretic mobilities

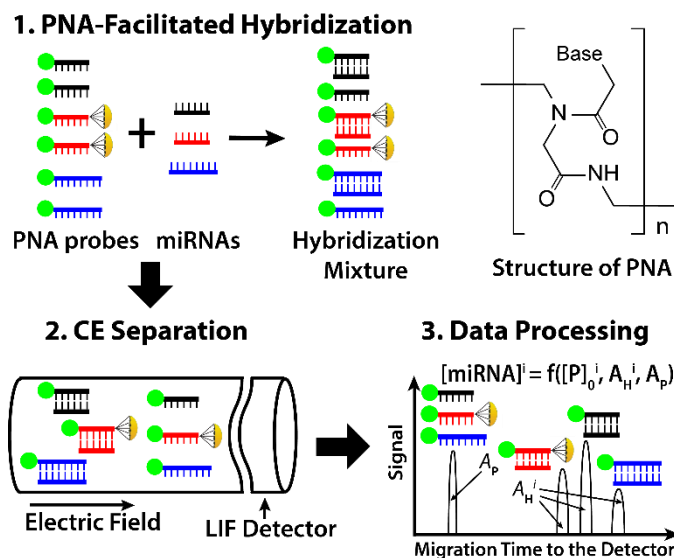


**Figure 3.1.** Schematic depiction of DQAMmiR with PNA hybridization probes. See text for details.

of DNA-RNA hybrids of the first-generation DQAMmiR [92]. Here we adapted this model to PNA-RNA hybrids of the second-generation DQAMmiR. The theoretical results indicated that the PNA-RNA hybrids with different numbers of base pairs could be separated from each other without drag tags, while the peptide drag tags on the PNA probes would still be useful mobility shifters for PNA-RNA hybrids of the same length. The proposed model suggested that using PNA probes in DQAMmiR would simplify the assay via two ways: by making SSB unnecessary and by decreasing the number of probes conjugated with drag tags. The basic schematic of the second-generation DQAMmiR with PNA hybridization probes is shown in **Fig. 3.1**. We proved the feasibility of PNA-facilitated DQAMmiR by analyzing three miRNAs (miR-21, miR147a and miR-378g), which have 20, 20 and 22 nucleotides, respectively. High accuracy and precision along with low LOQ indicate that DQAMmiR with PNA hybridization probes may potentially serve as a tool for practical miRNA analyses in clinical samples.

## **3.2. Materials and Methods**

### **3.2.1. miRNAs and PNA probes**

All miRNAs were custom-synthesized by IDT (Coralville, IA, USA). All PNA probes were custom synthesized by PNA Bio (Thousand Oak, CA, USA). Detail information of miRNAs and PNA probes can be found in **Table 3.1**. Concentrations of miRNA and PNA probes in stock solutions were determined using light absorbance at 260 nm measured with a NanoDrop ND-1000 spectrophotometer (Thermo-Fisher Scientific, Waltham, MA, USA); the extinction coefficients were provided by respective suppliers of miRNA and PNA. Twenty percent (v/v) acetonitrile was added to all buffers to improve PNA solubility.

**Table 3.1.** Detailed sequences of target miRNAs and their complementary PNA hybridization probes.

<b>Targets</b>	<b>Sequence of targets (5'-3')</b>	<b>Sequence of its PNA probe (N'-C')</b>
miR-21	UAG-CUU-AUC-AGA-CUG- AUG-UUG-A	<i>Alexa488-O-TCA-ACA-TCA-GTC-TGA-TAA- GCT-A</i>
miR-147a	GUG-UGU-GGA-AAU-GCU- UCU-GC	<i>Alexa488-O-GCA-GAA-GCA-TTT-CCA-CAC- AC-Gly-Ala-Gly-Thr-Gly</i>
miR-378g	ACU-GGG-CUU-GGA-GUC- AGA-AG	<i>Alexa488-O-CTT-CTG-ACT-CCA-AGC-CCA-GT</i>

### 3.2.2. Hybridization reactions

Hybridization was carried out in a Mastercycler 5332 thermocycler (Eppendorf, Hamburg, Germany). Various concentrations of three miRNAs were incubated with 10 nM of their respective PNA probes in the CE running buffer (20 mM Borax, 120 mM NaCl, 20% acetonitrile, pH 9.0). According to the information provided by the supplier of PNA, all the PNA-miRNA hybrids used in this study have melting temperature ( $T_m$ ) above 80 °C. Thus, we selected 60 °C as hybridization temperature which is about 20 °C lower than their  $T_m$  and favorable for the hybridization reactions.[148] Temperature was first increased to a denaturing level of 95 °C and then lowered to 60 °C at a rate of 20 °C/min. After that the temperature was held at 60 °C for 30 min to allow hybridization. To minimize RNA degradation, a nuclease-free environment was maintained while handling miRNA samples.

### 3.2.3. Capillary electrophoresis

All experiments were performed using a P/ACE MDQ CE instrument (SCIEX, Brea, CA, USA) equipped with a laser-induced fluorescence detector. We used bare fused-silica capillaries

with an outer diameter of 365  $\mu\text{m}$ , an inner diameter of 50  $\mu\text{m}$ , and a total length of 80 cm. The distance from the injection end of the capillary to the detector was 70 cm. The capillary was flushed prior to every CE run with methanol, 0.1 M HCl, 0.3 M NaOH, deionized H<sub>2</sub>O, and the running buffer for 1 min each under a 20 psi pressure. The sample was injected into the capillary by a 5-s pressure pulse of 0.5 psi. Electrophoresis was driven by an electric field of 312.5 V/cm with positive polarity at the capillary inlet. The capillary coolant temperature was kept at 20 °C during CE experiments. Fluorescence of the Alexa488 label on the PNA probes was excited by 488 nm light generated with a continuous-wave solid state laser (JDSU, Milpitas, CA, USA). Electropherograms were analyzed with 32 Karat Software. Peak areas were divided by the corresponding migration times to compensate for the dependence of the residence time in the detector on the electrophoretic velocity of the analyte. The quantity of each miRNA was calculated using these peak areas.

### 3.2.4. Derivation of the equation for the determination of concentrations of multiple miRNAs by PNA facilitated DQAMmiR

The unknown concentration of the  $i$ -th miRNA,  $[\text{miRNA}]_i$ , can be expressed through the area of its respective hybrid peak ( $A_{\text{H},i}$ ), using the unknown coefficient  $a$ , known quantum yield  $q_{\text{H}}^i$  and  $q_{\text{P}}^i$ :

$$[\text{miRNA}]^i = a \left( \frac{A_{\text{H}}^i}{q_{\text{H}}^i q_{\text{P}}^i} \right) \quad (3-1)$$

The known concentration of the  $i$ -th probe,  $[\text{P}]_{0,i}$  can be expressed through the areas of two peaks, the one of unbound PNA probe  $A_{\text{P}}^i$ , and the one of the miRNA-bound probe,  $A_{\text{H}}^i$ , with the same coefficient  $a$  and the known quantum yield  $q_{\text{H}}^i$  and  $q_{\text{P}}^i$ :

$$[\mathbf{P}]_{0,i} = a \left( \frac{A_{\mathbf{P}}^i}{q_{\mathbf{P}}^i} + \frac{A_{\mathbf{H}}^i}{q_{\mathbf{H}}^i q_{\mathbf{P}}^i} \right) \quad (3-2)$$

$$q_{\mathbf{P}}^i [\mathbf{P}]_{0,i} = a \left( A_{\mathbf{P}}^i + \frac{A_{\mathbf{H}}^i}{q_{\mathbf{H}}^i} \right) \quad (3-3)$$

Accordingly, for the situation of  $N$  probes and hybrids, below expression can be obtained:

$$\sum_{i=1}^N (q_{\mathbf{P}}^i [\mathbf{P}]_{0,i}) = a \left( \sum_{i=1}^N A_{\mathbf{P}}^i + \sum_{i=1}^N \frac{A_{\mathbf{H}}^i}{q_{\mathbf{H}}^i} \right) \quad (3-4)$$

Since the peaks of the hybrids are resolved, their corresponding areas  $A_{\mathbf{H}}^i$  can be experimentally determined; accordingly we treated them as known parameters. The peaks corresponding to the unbound PNA probes are overlap, therefore, we can only get the total areas of these peaks  $A_{\mathbf{P}} = \sum_{i=1}^N A_{\mathbf{P}}^i$ . Thus we were able to rewrite the above equation as:

$$\sum_{i=1}^N (q_{\mathbf{P}}^i [\mathbf{P}]_{0,i}) = a \left( A_{\mathbf{P}} + \sum_{i=1}^N \frac{A_{\mathbf{H}}^i}{q_{\mathbf{H}}^i} \right) \quad (3-5)$$

Then we can solve the equation for  $a$ :

$$a = \frac{\sum_{i=1}^N (q_{\mathbf{P}}^i [\mathbf{P}]_{0,i})}{A_{\mathbf{P}} + \sum_{i=1}^N \frac{A_{\mathbf{H}}^i}{q_{\mathbf{H}}^i}} \quad (3-6)$$

By expressing  $a$  from **Eq. 3-6** and incorporating it into **Eq. 3-5** we can finally express the unknown concentration of the  $i$ -th miRNA in the following way:

$$[\text{miRNA}]^i = \frac{A_H^i}{q_H^i q_P^i} \frac{\sum_{i=1}^N (q_P^i [\text{P}]_{0,i})}{A_P + \sum_{i=1}^N \frac{A_H^i}{q_H^i}} \quad (3-7)$$

### 3.3. Results and Discussion

#### 3.3.1. Separation of the PNA probe from PNA–miRNA hybrid in CE

In DQAMmiR, accurate quantitation of multiple miRNAs relies on the separation of the non-hybridized probes from the miRNA-probe hybrids and hybrids from each other by CE. To establish DQAMmiR with PNA probes, it is necessary to investigate the separation of the PNA probe from the PNA-miRNA hybrid. A proof-of-principle experiment was performed using miR-21 and its complementary PNA probe. The result confirmed that the negatively charged PNA-RNA hybrid was separable from the excess of the neutral PNA probe without any mobility shifter (Fig. 3.2). A near 10-min time window was obtained between the PNA probe and the PNA-

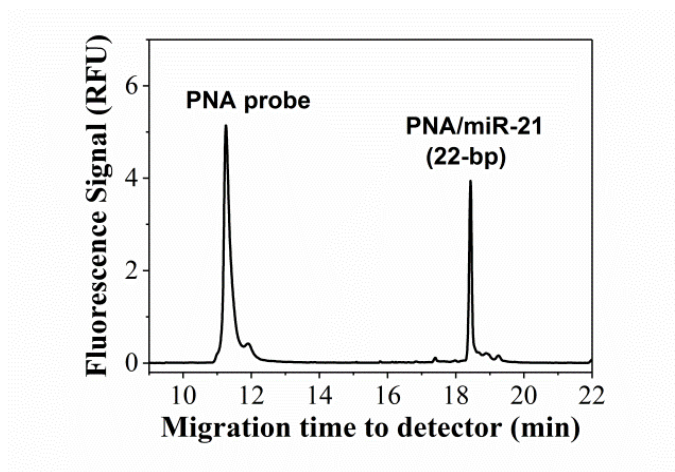


**Figure 3.2.** CE separation of a PNA probe from a PNA-miR-21 hybrid in a running buffer of 20 mM Borax, 20% acetonitrile, pH 9.0. The sample was prepared by incubating 2 nM miR-21 with 10 nM PNA probe with a sequence fully complementary to miR-21. Separation was driven by an electric field of 312.5 V/cm at 20 °C.

miRNA hybrid, which would allow theoretically separation of up to 30 hybrids. The observed quality of separation of the excess PNA probe from the hybrid suggests that this PNA-facilitated assay could analyze miRNAs with high multiplexing capacity.

### 3.3.2. Theoretical estimation of the electrophoretic mobility of PNA–RNA hybrids

Another essential step for PNA-facilitated DQAMmiR was to separate PNA–miRNA hybrids from each other. For this purpose, theoretical estimates of the electrophoretic mobility of PNA–RNA hybrids were found *via* adapting to these hybrids a theoretical model previously developed for DNA–RNA hybrids [92]. In such model, the DNA–RNA duplex was assumed to behave like a rigid rod because the contour lengths  $L_{\text{hyb}} = N_{\text{hyb}}b$  ( $N_{\text{hyb}}$  is the number of base pairs and  $b$  is the helical rise per base) for such short hybrids (18–25 bp) are shorter than their Kuhn length  $b_K$ . For the case of PNA–RNA duplexes,  $b = 0.24$  nm leads to  $4.32 \text{ nm} \leq L_{\text{hyb}} \leq 6 \text{ nm}$  (since  $18 < N_{\text{hyb}} < 25$ ), while the Kuhn length of these helices can be estimated to be larger than 60 nm ( $b_K > 60 \text{ nm}$ ). Thus, the condition of  $L_{\text{hyb}} \ll b_K$  is also satisfied in the case of PNA–RNA duplexes and the rigid-rod model can be adapted to predict the mobilities of PNA–RNA hybrids. Thus, the expressions for the electric force ( $F_{\text{E,hyb}}$ ) and hydrodynamic friction force ( $F_{\text{f,hyb}}$ ) are:

$$F_{\text{E,hyb}} = \frac{eL_{\text{hyb}}}{z_i \lambda_B} E \quad (3-8)$$

$$F_{\text{f,hyb}} = 2\pi\eta L_{\text{hyb}} u_{\text{rel}} \left( \ln \frac{2L_{\text{hyb}}}{d_{\text{hyb}}} - 0.72 \right)^{-1} \quad (3-9)$$

Here  $L_{\text{hyb}} = N_{\text{hyb}}b$  is the length of the hybrid and  $d_{\text{hyb}}$  is the diameter of the hybrid, which is approximately 3.5 nm for PNA–RNA duplexes [149],  $z_i$  is the valence of the counter ions.  $\lambda_B$  and  $\eta$  are the Bjerrum length and viscosity of the solution, which can be found to be 0.79 nm and 1.10 mPa·s, respectively, for the 20% (v/v) acetonitrile containing aqueous solutions at 20 °C

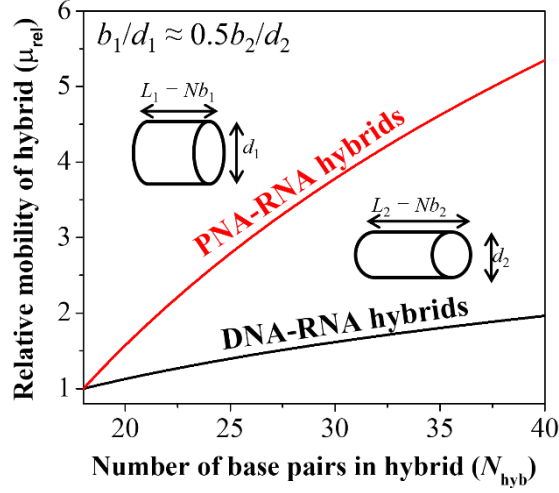


**Figure 3.3.** Dependence of relative mobility of a hybrid ( $\mu_{rel}$ ) with the number of base pairs of the hybrid ( $N_{hyb}$ ). The 18-bp hybrids were used as references. Black trace: DNA-RNA hybrids; Red trace: PNA-RNA hybrids.

[150].  $u_{rel}$  is the velocity of the hybrid with respect to the running buffer. Thus, the mobility of the PNA- hybrid can be found from the balance of the electric force and the hydrodynamic friction force exerted on it:

$$F_{E,hyb} = F_{f,hyb} \quad (3-10)$$

Combining **Eq. 3-8**, **Eq. 3-9**, and **Eq. 3-10**, the expression for electrophoretic mobility  $\mu_{hyb}$  can be written as:

$$\mu_{hyb} = \frac{u_{rel}}{E} = \frac{e}{2\pi z_i \eta \lambda_B} \left( \ln \frac{2N_{hyb}b}{d_{hyb}} - 0.72 \right) \quad (3-11)$$

**Eq. 3-11** suggests that the mobility of a PNA–RNA hybrid depends on the number of base pairs of the hybrid ( $N_{hyb}$ ). Such dependence was also found in our previous model of the DNA–RNA hybrids, although we neglected this effect and assumed that the different length DNA–RNA hybrids have the same mobility for simplicity [92]. On the contrary, this effect is more pronounced for the PNA–RNA hybrids because of the smaller value of  $b/d_{hyb}$  for the PNA–RNA

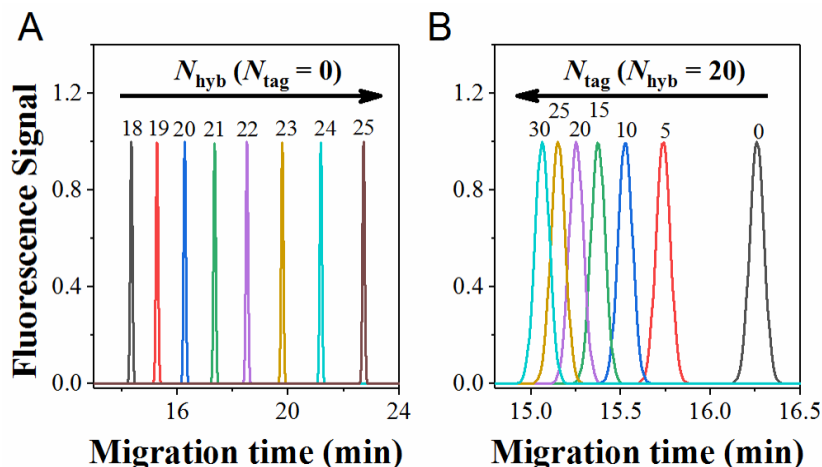


**Figure 3.4.** Simulated electropherograms of different PNA-RNA hybrids. **A)** PNA-RNA hybrids with numbers of base pairs ( $N_{\text{hyb}}$ ) in a range of 18–25. **B)** 20-bp PNA-RNA hybrids with lengths (numbers of amino acids) of peptide tags ( $N_{\text{tag}}$ ) in a range of 0–30. Migration times of peaks shown above were estimated by using  $\mu_{\text{EOF}} = 3.14 \times 10^{-4} \text{ cm}^2 \cdot \text{V}^{-1} \cdot \text{s}^{-1}$  which was experimentally measured for our CE running buffer containing 20 mM Borax and 20% (v/v) acetonitrile at pH 9.0.

helix ( $b = 0.24 \text{ nm}$ ,  $d_{\text{hyb}} = 3.5 \text{ nm}$ ) comparing with the DNA–RNA helix ( $b = 0.34 \text{ nm}$ ,  $d_{\text{hyb}} = 2.6 \text{ nm}$ ) (**Fig. 3.3**).

The validity of this model was tested by theoretically estimating the electrophoretic mobility of PNA–miR-21 hybrid ( $N_{\text{hyb}} = 22$ ) and comparing it with the experimentally measured value. The electrophoretic mobility of PNA–miR-21 hybrid was calculated to be  $1.12 \times 10^{-4} \text{ cm}^2 \cdot \text{V}^{-1} \cdot \text{s}^{-1}$ , while the experimental result led to a value of  $1.20 \times 10^{-4} \text{ cm}^2 \cdot \text{V}^{-1} \cdot \text{s}^{-1}$  (as shown in **Fig. 3.2**). The small deviation of the calculated value from the experimental one suggested the model’s applicability to PNA-RNA hybrids. Simulated electropherograms of PNA–RNA hybrids with different numbers of base pairs were obtained by using  $\mu_{\text{EOF}} = 3.14 \times 10^{-4} \text{ cm}^2 \cdot \text{V}^{-1} \cdot \text{s}^{-1}$  (which corresponds to our running buffer containing 20 mM Borax and 20% acetonitrile at pH 9.0) as shown in **Fig 3.4A**. It is clear that a single-base-pair difference in lengths of PNA-RNA hybrids can cause significant difference in their electrophoretic mobilities.

Such difference in mobilities should allow the separation of different-length PNA–miRNA hybrids from each other.

On the other hand, molecules with similar mobility, such as different same-length PNA-miRNA hybrids, can also be electrophoretically separated from each other by end-labelled free solution electrophoresis (ELFSE) [151]. By using this approach, we have developed universal peptide drag tags conjugated on the ssDNA probes as mobility shifters to separate ssDNA-miRNA hybrids in our first-generation DQAMmiR [91–92]. In this case, these peptide drag tags could also be applied to facilitate separation of different same-length PNA–miRNA hybrids. For this purpose, we also estimated the electrophoretic mobility of PNA–RNA hybrids conjugated with different-length peptide drag tags. When the hydrodynamic friction force acting on the drag tag ( $F_{f,\text{tag}}$ ) is taken into account, **Eq. 3-10** can be rewritten as:

$$F_{E,\text{hyb}} = F_{f,\text{hyb}} + F_{f,\text{tag}} \quad (3-12)$$

The hydrodynamic force,  $F_{f,\text{tag}}$ , acting upon the drag tag can be described *via* expression:

$$F_{f,\text{tag}} = 6\pi\eta R_{H,\text{tag}} u_{\text{rel}} \quad (3-13)$$

where  $R_{H,\text{tag}}$  is the hydrodynamic radius of the drag tag. By substituting expressions of **Eq. 3-8**, **Eq. 3-9**, and **Eq. 3-13** for  $F_{E,\text{hyb}}$ ,  $F_{f,\text{hyb}}$  and  $F_{f,\text{tag}}$ , respectively, into **Eq. 3-12** and by solving the resulting equation, we can obtain the expression for electrophoretic mobility of PNA-RNA hybrids with peptide drag tags:

$$\mu_{\text{hyb+tag}} = \frac{e}{2\pi z_i \eta \lambda_B} \left[ \left( \ln \frac{2N_{\text{hyb}} b}{d_{\text{hyb}}} - 0.72 \right)^{-1} + \frac{3R_{H,\text{tag}}}{N_{\text{hyb}} b} \right]^{-1} \quad (3-14)$$

Studies of unfolded peptides have resulted in the following dependence for the hydrodynamic radius  $R_{H,\text{tag}}$  (in nm) of short peptides by fitting empirical data [152]:

$$R_{H,\text{tag}} = (0.22 \pm 0.11)N_{\text{tag}}^{0.57 \pm 0.02} \quad (3-15)$$

Here,  $N_{\text{tag}}$  is the number of amino acid residues in the peptide chain. The hydrodynamic radius of peptide drag tags with different numbers of amino acid residues can be estimated using **Eq. 3-15**. Thus, mobilities of PNA-RNA hybrids with different-length peptide drag tags could be estimated. As an example, the simulated electropherograms of 20-bp PNA-RNA hybrids with different-length peptide drag tags conjugated on the probe are shown in **Fig. 3.4B**, indicating that the PNA-miRNA hybrids could be separated from each other by either the difference in numbers of nucleotides or lengths of peptide drag tags. The simulation strongly suggests that using PNA probes can simplify DQAMmiR by reducing the need for conjugation of drag tags.

### 3.3.3. DQAMmiR with PNA probes

As proof-of-principle, three miRNA targets, miR-147a, miR-378g, and miR-21, which have the numbers of nucleotides of 20, 20, and 22, respectively, were analyzed by DQAMmiR with PNA hybridization probes. Two PNA probes complementary to miR-378g and miR-21 were custom-synthesized without drag tags, while a PNA probe complementary to miR-147a was conjugated with a five-amino-acid tag.

We first performed CE separation with a running buffer of 20 mM Borax, 20% acetonitrile, pH 9.0 (**Fig. 3.5A**). As a result, the 22-bp PNA-miRNA-21 hybrid exhibited the highest electrophoretic mobility while the PNA-miR-147a (20-bp, 5aa) was found to have the lowest electrophoretic mobility, which agreed well with our theoretical predictions. While deviations of 29%, 24%, and 6% were found between the theoretically predicted mobilities of PNA-miR-147a (20-bp, 5aa), PNA-miR-378g (20-bp), and PNA-miR-21 (22-bp) and their respective experimentally measured mobilities, the qualitative agreement between the theoretical prediction and experimental results was evident: (i) the electrophoretic mobility of the PNA-

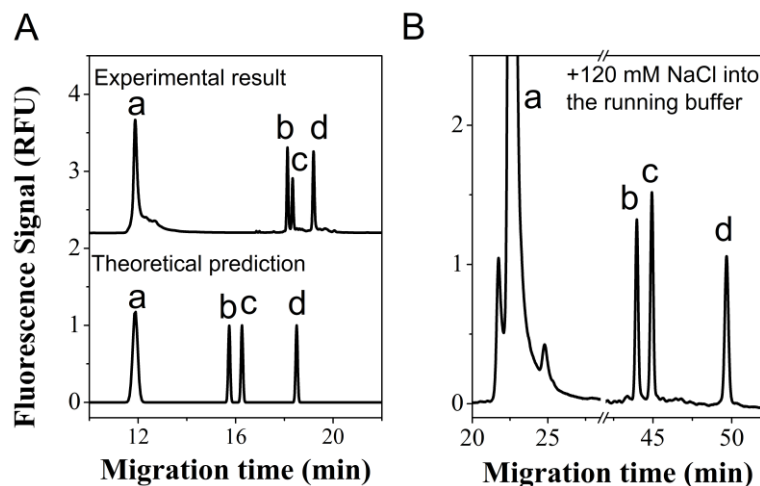


**Figure 3.5.** Experimental implementation of DQAMmiR with PNA probes. **A)** Comparison of experimental and predicted separation of three PNA-miRNA hybrids in 20 mM Borax, 20% acetonitrile, pH 9.0. **B)** Baseline separation of the three hybrids from each other by using a high-ionic-strength CE running buffer: 20 mM Borax, 120 mM NaCl, 20% acetonitrile, pH 9.0. Peak assignment: (a) excess PNA probes, (b) PNA-miR-147a (20-bp, 5aa), (c) PNA-miR-378g (20-bp), and (d) PNA-miR-21 (22-bp).

miRNA hybrid depended on the number of base pairs in the hybrid, and the shorter hybrid had the lower electrophoretic mobility; (ii) the mobility of the hybrid could be altered by conjugating with a peptide drag tag on the PNA probe. However, mobility shift by the 5-aa peptide tag on the PNA-miR-147a hybrid was not sufficient for baseline separation of the two 20-bp hybrids (baseline separation is preferable for high accuracy of miRNA quantitation). The resolution in CE separation can be improved by suppressing the EOF of the running buffer [153], which can be achieved, in particular, by increasing the ionic strength of CE running buffer. Here, we added 120 mM NaCl into the running buffer to suppress EOF and prolong separation. As a result, baseline separation was achieved, leading to a peak resolution of 3.1 between PNA-miR-147a and PNA-miR-378g (**Fig. 3.5B**). Thus, the running buffer for the following experiments was 20 mM Borax, 120 mM NaCl, 20% acetonitrile, pH 9.0.

To study the suitability of PNA-facilitated DQAMmiR for miRNA quantitation, measurements of miR-147a, miR-378g, and miR-21 were performed simultaneously in a concentration range of 32–500 pM, which is of interest for analyzing miRNAs in clinical samples [89]. In all experiments, final concentrations of all three PNA probes in hybridization mixtures were set at 10 nM, which is an excess to all targets. The electropherograms obtained in these experiments are shown in **Fig. 3.6A**. Concentrations of individual miRNAs were calculated by using a simple mathematical strategy as described in section 3.2.4. The quantum yields of the PNA probes for the respective miRNAs can be found in **Table 3.2**. Using equation (2-7), we were able to determine concentrations of the three targets simultaneously by quantitating peak areas from a single electropherogram without building/using a calibration curve.

**Table 3.2.** Relative quantum yields of PNA probes for the respective miRNAs.  $q_P$  is the relative quantum yields of corresponding PNA probes to the PNA probes complementary to miR-21 for signal normalization.  $q_H$  is the relative quantum yield of the corresponding PNA–miRNA hybrid to its unbound PNA probe. Standard deviations from mean values were obtained from three independent experiments.

<b>Quantum Yield</b>	<b>miR-21</b>	<b>miR-147a</b>	<b>miR-378g</b>
$q_P$	1	$0.82 \pm 0.04$	$0.78 \pm 0.04$
$q_H$	$0.27 \pm 0.02$	$0.26 \pm 0.01$	$0.34 \pm 0.05$

**Table 3.3.** Quantification results of DQAMmiR measurements with PNA probes. DQAMmiR-measured concentrations of three miRNAs (miR-21, miR-147a and miR-378g) are shown with respect to their actual concentration as determined by light absorbance at 260 nm. Standard deviations from mean values were obtained from three experiments.

Actual miRNA Concentration (pM)	DQAMmiR-Measured miRNA Concentration (pM, Mean $\pm$ Standard Deviation)		
	miR-21	miR-147a	miR-378g
500	461 $\pm$ 28	538 $\pm$ 11	483 $\pm$ 17
250	229 $\pm$ 25	287 $\pm$ 30	240 $\pm$ 19
125	128 $\pm$ 14	138 $\pm$ 4	118 $\pm$ 6
63	54 $\pm$ 6	69 $\pm$ 5	60 $\pm$ 15
32	28 $\pm$ 4	33 $\pm$ 2	33 $\pm$ 2

The measured concentrations of the three targets (**Table 2.3**) were compared with their actual concentrations as shown in **Fig. 3.6B**. Recoveries between 90–110% with RSD of approximately 10% were observed for measuring all three targets with concentrations varying in a range of 32–500 pM. Also, by studying the signal-to-noise ratio (SNR) of the peaks of hybrids, the lower limit-of-quantitation (LOQ) of this method performed with a commercial CE-LIF instrument was determined to be 14 pM. These results demonstrate that this PNA-facilitated DQAMmiR is capable of quantitating multiple miRNA

s with high accuracy and precision at pico-molar concentrations.

In contrast to DNA probes, PNA probes have greater specificity in hybridizing with DNA or RNA, with a PNA-DNA base mismatch being more destabilizing than a similar mismatch in a DNA-DNA duplex [154]. This property will allow us to establish PNA-facilitated DQAMmiR for analyzing miRNAs with slightly different sequences by simply changing conditions of the hybridization reaction, such as temperature, addition of denaturing reagent, *etc.* PNAs are also resistant to degradation by nucleases or proteases [155], making them perfect hybridization probes

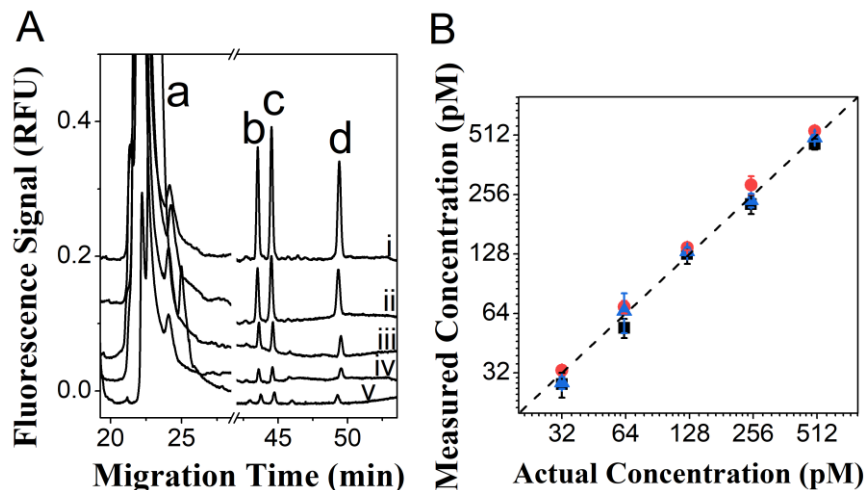


**Figure 3.6.** Results of PNA-facilitated DQAMmiR measurements. **A)** Electropherograms of PNA facilitated measurements. Peak assignment: (a) excess PNA probes, (b) PNA–miR-147a (20-bp, 5aa), (c) PNA–miR-378g (20-bp), (d) PNA–miR-21 (22-bp). Electropherograms i–vi correspond to target concentrations of 500, 250, 125, 63, and 32 pM, respectively. **B)** Quantitation of three miRNAs simultaneously by PNA-facilitated DQAMmiR. Concentrations measured with DQAMmiR are shown with respect to their actual values determined by light absorbance at 260 nm. miR-21, miR-147a, and miR-378g, are represented by black rectangles, red circles, and blue triangles, respectively. The dashed line ( $y = x$ ) represents a line corresponding to 100% recovery. Error bars show one standard deviation from mean values obtained from three experiments.

for analysis of miRNAs in biological samples. As a result, PNA-facilitated DQAMmiR can be potentially a practical tool for quantitation of miRNAs in clinical samples.

### 3.4. Conclusions

In this study, we introduced the second-generation DQAMmiR which utilizes electrically-neutral PNA probes instead of negatively-charged DNA probes. In this approach, the negatively-charged PNA-miRNA hybrids were separated from the neutral PNA probes by CE without any additional mobility shifter, leading to a near 10-min time window, which would allow us to analyze up to 35 miRNAs simultaneously. The theoretical study of the electrophoretic mobility of PNA-miRNA hybrid qualitatively predicted that the separation of the hybrids from each other could be

achieved by utilizing their differences in either (i) the number of base pairs, or (ii) the length of peptide drag tags. This was confirmed by our experimental results. Our proof-of-principle study demonstrated that PNA-facilitated DQAMmiR was able to quantify three miRNAs simultaneously with high accuracy (recovery within 90–110%) and precision (RSD ~ 10%) with LOQ of 14 pM by using a commercial CE instrument, suggesting that DQAMmiR with PNA hybridization probes may facilitate validation and clinical use of miRNA biomarkers.

## CHAPTER 4. NECESSITY AND CHALLENGES OF SAMPLE PRECONCENTRATION IN ANALYSIS OF MULTIPLE MICRORNAS BY CAPILLARY ELECTROPHORESIS

The presented material was published previously and reprinted with permission from “Hu, L.; Krylova, S. M.; Liu, S. K.; Yousef, G. M.; Krylov, S. N. *Anal. Chem.* **2020**, *92*, 14251–14258”. Copyright 2020 American Chemical Society. My contribution to the article was: (i) planning all experiments, (ii) performing all experiments, (iii) interpreting results, (iv) preparing all figures, (v) writing the manuscript.

### 4.1. Introduction

DQAMmiR is a hybridization assay which utilizes fluorescently-labeled hybridization probes complementary to target miRNAs (**Fig. 4.1**). The miRNA–probe hybrids are separated from each other and from the unreacted probes by CE and both the hybrids and the probes are detected with LIF. There are two implementations of DQAMmiR which differ by the nature of hybridization probes: ssDNA in the original implementation, which requires single-strand DNA binding protein (SSB) in the CE running buffer (**Fig. 4.1**, top) [89], and peptide nucleic acid (PNA) in the later implementation, which does not require SSB (**Fig. 4.1**, bottom).

Unlike RT-PCR, DQAMmiR does not involve enzymatic reactions (which are error-prone); therefore, DQAMmiR is more robust than RT-PCR. However, its robustness comes at an expense of relatively high concentration limit of quantitation (LOQ). A typical cell-lysate sample contains miRNAs at sub-pM concentrations, while the LOQ of commercial CE-LIF instruments is in the low pM range at best as shown in the previous chapters. Thus, highly efficient and reproducible preconcentration of the hybrids inside the capillary before CE separation is necessary to address the LOQ issue while maintaining assay robustness.

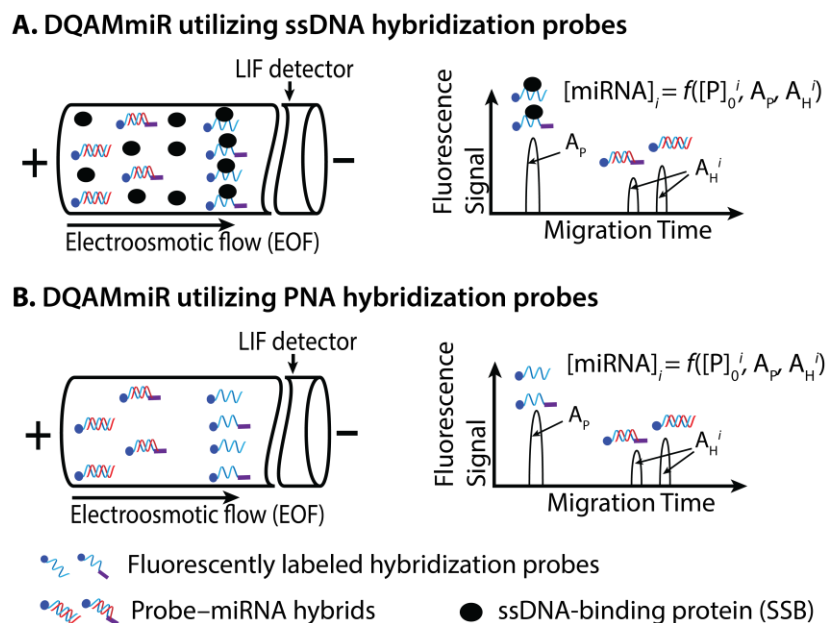


**Figure 4.1.** Schematics of CE separation in two implementations of DQAMmiR: with DNA (A) and PNA probes (B). In both cases, the concentrations of the miRNA targets are determined by analyzing peak areas in the electropherogram with a simple mathematical approach that requires knowing the total concentration of each probe,  $[P]_0^i$ , and a sum peak area of all the unreacted probes,  $A_p$ , as well as a peak area of every hybrid,  $A_H^i$ .

A number of on-column sample preconcentration (OSP) methods have been developed for improving LOQ of CE including field-amplified sample stacking (FASS), dynamic pH junction, sweeping, and isotachopheresis (ITP) [95–100]. All OSP methods use heterogeneous buffer systems to change the analyte’s velocity at interfaces of two adjacent buffer zones. The velocity change, then, can facilitate analyte’s focusing from a large sample plug into a narrow zone, providing up to 10,000-fold improvement in LOQ [156]. However, the OSP methods require suppression of electroosmotic flow (EOF) in the capillary for the best result as the mismatch of the local EOF velocities in the heterogeneous zones causes dispersion of the focused analyte zone [157]. The dispersion, in turn, results in very modest concentration factors, typically less than 10, and poor analyte resolutions in the subsequent CE separation [158]. This drawback limits the

applicability of OSP methods to DQAMmiR because DQAMmiR relies on strong EOF in the capillary for separation of the unreacted probes from the negatively charged miRNA-probe hybrids.

The least EOF-sensitive OSP method is arguably ITP which can concentrate analytes between the leading electrolyte (LE) and the trailing electrolyte (TE) while the electrophoretic mobilities of the analytes are less than that of the LE ion and greater than that of the TE ion [117–118]. Previous works showed that using ITP prior to CE separation could facilitate more than 2 orders of magnitude improvement in LOQ despite the presence of strong EOF [124]. Our previous study also demonstrated that using ITP preconcentration could decrease the LOQ of DQAMmiR with ssDNA hybridization probes by 2 orders of magnitude (see **Fig. 4.2a** for more details). This success inspired us to investigate if the same strategy would also work for DQAMmiR with PNA probes. However, our attempts to implement ITP for DQAMmiR with PNA probes failed because ITP could not concentrate unreacted PNA probes due to their very low electrophoretic mobilities (**Fig. 4.2b**) as discussed in **Chapter 3**. Consequently, the unreacted PNA probes eluted from the capillary during ITP, affecting quantitiveness of DQAMmiR, which utilizes the peak(s) of unreacted probes for normalizing the signals from the hybrids (**Fig. 4.1**). Therefore, a new OSP technique that would be compatible with DQAMmiR utilizing PNA probes was needed.

Here, we introduce a new OSP technique based on the integration of FASS and ITP for DQAMmiR utilizing PNA probes. Although FASS is more sensitive to EOF in contrast to ITP [157], it is a less mobility-selective method which can concentrate all negative charged species regardless of the magnitudes of their electrophoretic mobilities from a low-conductivity zone into a narrow zone at the interface with the high-conductivity zone due to an electric field-amplification phenomenon [158]. Thus, with the addition of FASS to ITP (see **Fig. 4.3** for details), the near-

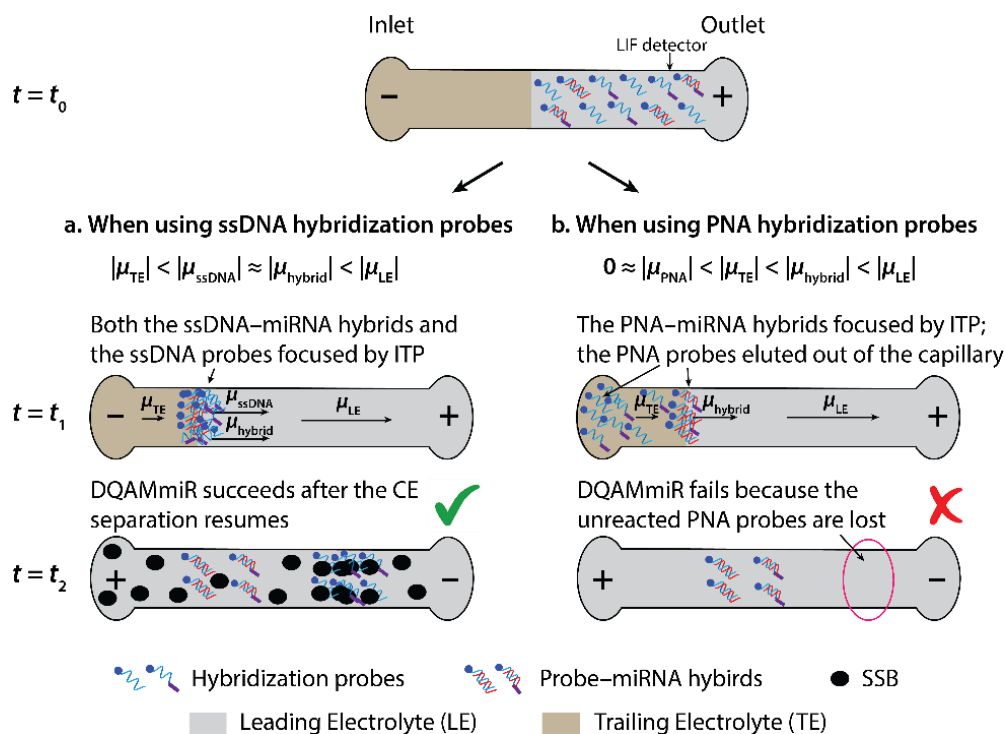


**Figure 4.2.** Conceptual depiction of ITP-CE for DQAMmiR with two different types of hybridization probes: ssDNA (a) and PNA (b). In both cases, a large plug of the hybridization mixture is prepared in the leading electrolyte (LE) and injected into the capillary, which is prefilled with the trailing electrolyte (TE), from the outlet vial. The outlet vial is then replaced with LE and a voltage is applied with the positive polarity being at the outlet ( $t = t_0$ ). In the case of ssDNA hybridization probes (a), because the electrophoretic mobilities of the ssDNA probes,  $\mu_{ssDNA}$ , and the probe-miRNA hybrids,  $\mu_{hybrid}$ , are less than that of the LE ion,  $\mu_{LE}$ , and greater than that of the TE ion,  $\mu_{TE}$ , ( $|\mu_{TE}| < |\mu_{ssDNA}| \approx |\mu_{hybrid}| < |\mu_{LE}|$ ), both the hybrids and the ssDNA probes are focused at the TE/LE interface by ITP ( $t = t_1$ ). The strong EOF from the anode to the cathode propels the focused analytes to near the inlet. The CE separation resumes after reversing the polarity and replacing the inlet vial with the SSB-supplemented LE buffer, which facilitates DQAMmiR ( $t = t_2$ ). However, while using PNA as hybridization probes (b), only the PNA-miRNA hybrids can be focused by ITP because the electrophoretic mobilities of PNA probes,  $\mu_{PNA}$ , are too low ( $0 \approx |\mu_{PNA}| < |\mu_{TE}|$ ). Consequently, unreacted PNA probes in the hybridization mixture elute from the capillary during ITP ( $t = t_1$ ), which leads to their loss and failure of DQAMmiR ( $t = t_2$ ).

neutral PNA probes in the low-conductivity sample plug could also be concentrated into a narrow zone along with the high-mobility PNA-miRNA hybrids despite the probes' very low mobilities,

preventing the probes from eluting from the capillary during the following ITP step. Meanwhile, due to the co-presence of TE and LE in the capillary, the hybrids could still be focused by ITP, which would lead to a significant improvement in LOQ for detecting miRNAs. Unlike the hybrids,

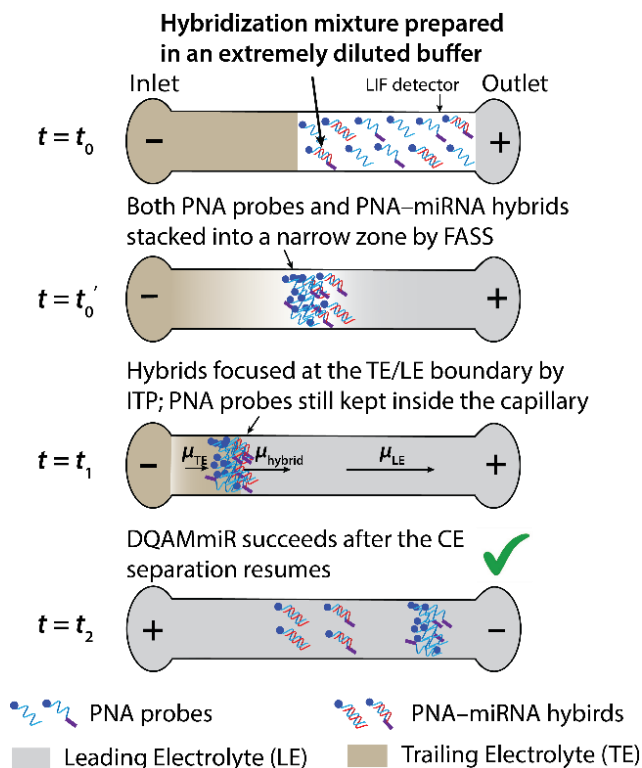


**Figure 4.3.** Conceptual depiction of the proposed FASS-ITP-CE approach for DQAMmiR utilizing PNA probes. The hybridization mixture is prepared in a diluted buffer which has conductivity much lower than those of LE and TE. When a voltage is applied with positive polarity at the capillary outlet ( $t = t_0$ ), the boundary between the sample zone and LE shifts toward the capillary inlet due to the strong EOF from the outlet to the inlet ( $t = t_0'$ ). Meanwhile, because of the conductivity difference between the sample plug and LE, the negatively charged PNA probes and PNA-miRNA hybrids migrate towards and stacked at the sample zone/LE boundary into a narrow zone by FASS regardless of the magnitudes of their electrophoretic mobilities ( $t = t_0'$ ). Due to the co-presence of TE and LE in the capillary, the PNA-miRNA hybrids in the narrow zone can further be focused into a narrower band at the TE/LE interface by ITP, while the stacked PNA probes do not focus further but migrate along with the focused hybrids, keeping them inside the capillary during the step of hybrid concentration by ITP ( $t = t_1$ ). Once the FASS-concentrated probes and FASS-ITP-concentrated hybrids reach near the inlet end of the capillary, the polarity is reversed and the CE separation resumes facilitating DQAMmiR ( $t = t_2$ ).

the unreacted probes do not focus during ITP, but this is an advantage as it keeps peak heights of unreacted probes within the signal dynamic range tuned to detect low concentrations of the hybrids.

In this study, we first proved that the PNA probes were retained in the capillary during preconcentration by FASS-ITP, and, thus, that the FASS-ITP-CE approach could work for DQAMmiR utilizing PNA probes. An LOQ of 0.1 pM was then demonstrated for accurately and precisely quantifying two miRNAs simultaneously, which was 140 times lower than that of the original approach without preconcentration. We also showed that the FASS-ITP-CE approach was able to detect these miRNAs in crude cell lysates directly, indicating that the assay was robust to the presence of biological matrices. Although an LOQ of 0.1 pM is still insufficient to detect all miRNAs in all samples, the 140-fold improvement in LOQ will largely increase the number of putative miRNAs fingerprints that can be validated by this assay. This improvement in LOQ brings DQAMmiR closer to becoming a practical tool for validation and clinical use of miRNA biomarkers of cancer.

## **4.2. Materials and Methods**

### **4.2.1. miRNAs and PNA Probes**

miRNA targets and masking RNA were custom synthesized by IDT (Coralville, IA, USA). All PNA probes were custom synthesized by Panagene Inc. (Daejeon, South Korea). Detail information on miRNAs and PNA probes can be found in **Table 4.1**. Concentrations of miRNAs and PNA probes in stock solutions were determined using light absorbance at 260 nm measured with a NanoDrop ND-1000 spectrophotometer (Thermo-Fisher Scientific, Waltham, MA, USA); extinction coefficients were provided by respective suppliers of miRNA and PNA.

Table 4.1. Sequences of target miRNAs and their fluorescently labeled complementary PNA hybridization probes

Targets	Sequence of targets (5'-3')	Sequence of its complementary PNA probe (N'-C')
miR-20b	CAA-AGU-GCU-CAU- AGU-GCA-GGU-AG	<i>AlexaFluor647</i> -OO-CTA-CCT-GCA-CTA-TGA- GCA-CTT-TG
miR-100	AAC-CCG-UAG-AUC- CGA-ACU-UGU-G	<i>AlexaFluor647</i> -OO-CAC-AAG-TTC-GGA-TCT- ACG-GGT-T- <i>Gly-Thr-Gly-Ala-Gly</i>

#### 4.2.2. Hybridization Reactions

miRNA-PNA hybridization was carried out in a Mastercycler 5332 thermocycler (Eppendorf, Hamburg, Germany). According to the information provided by the supplier of PNA, all the PNA-miRNA hybrids used in this study have melting temperatures ( $T_m$ ) above 80 °C. Thus, we selected 60 °C as hybridization temperature. The temperature was first increased to a denaturing level of 95 °C and then lowered to 60 °C at a rate of 20 °C/min. After that the temperature was held at 60 °C for 30 min to allow hybridization.

#### 4.2.3. Protocol of cell culture

RWPE-1 and 22Rv1 cells were grown in an incubator at 37 °C in the atmosphere of 5% CO<sub>2</sub>. The RWPE-1 cells were grown in Keratinocyte-Serum Free Media (K-SFM) with L-glutamine purchased from ThermoFisher Scientific (Burlington, ON, Canada) supplemented with human recombinant epidermal growth factor and bovine pituitary extract which were supplied with the K-SFM. The 22Rv1 cells were grown in Roswell Park Memorial Institute (RPMI) 1640 Medium purchased from ThermoFisher Scientific (Burlington, ON, Canada) with a supplement of 100 IU·mL<sup>-1</sup> penicillin, 100 µg·mL<sup>-1</sup> streptomycin, and 10% fetal bovine serum purchased from Invitrogen (Burlington, Ontario, Canada). When cells covered roughly 80% of the plate they were washed with PBS, trypsinized to detach them from the bottom of the dish and centrifuged at

150 × g for 5 min. The cells were washed twice with PBS and counted using a hemocytometer. The cells were aliquoted into 100,000 cells per pellet and stored at −80 °C.

#### **4.2.4. CE-LIF Instrument**

All experiments were performed using a P/ACE MDQ CE instrument (SCIEX, Brea, CA, USA) equipped with a laser-induced fluorescence detector. We used bare fused-silica capillaries (Polymicro Technologies, Phoenix, AZ, USA) with an outer diameter of 365 μm, an inner diameter of 75 μm, and a total length of 80 cm. The distance from the detector windows to the capillary inlet and outlet were 70 and 10 cm, respectively (refer to Figure 2 for assignments of capillary inlet and outlet). New capillaries were preconditioned by flushing with methanol, 0.1 M HCl, 0.1 M NaOH, deionized H<sub>2</sub>O, and a CE running buffer (100 mM Tris-Cl, 20% (v/v) acetonitrile (ACN), pH 8.2) under a pressure of 20 psi (138 kPa) for 30, 30, 60, 30, and 120 min, respectively. Twenty percent (v/v) of ACN was added into the running buffer to improve the solubility of PNA probes.<sup>18</sup> The capillary was rinsed prior to every run with 0.1 M HCl, 0.1 M NaOH, deionized H<sub>2</sub>O, and the CE running buffer for 1 min each under a 20-psi pressure. The capillary coolant temperature was kept at 20 °C during all CE experiments. Fluorescence of the Alexa Fluor 647 dye on the PNA probes was excited by 638 nm light generated with a continuous-wave solid state laser (Pavilion Integration Group, San Jose, CA, USA) and detected at 679 nm using an emission filter setup composed of a 655 nm long-pass filter (SCIEX, Brea, CA, USA) and a 679/41 nm bandpass filter (Semrock, Rochester, NY, USA).

#### **4.2.5. Relative quantum yields measurements**

Two aspects must be considered to facilitate accurate quantitation of target miRNAs: (i) the potential difference in the quantum yield between the PNA probes and (ii) the potential

influence of miRNA binding to the PNA probe on the quantum yield of the due on the probe. Thus, relative quantum yield ( $q_H$ ) of each PNA–miRNA hybrid with respect to its unbound PNA probe was determined as explained in our previous work (Table 4.2). The fluorescence intensity of each PNA probe was also normalized by determining its quantum yield ( $q_P$ ) with respect to the PNA probe complementary to miR-100, which was used as a reference (Table 4.3).

**Table 4.2.** Relative quantum yields of PNA–miRNA hybrids ( $q_H$ ) with respect to their unbound PNA probes. Standard deviations from mean values were obtained from three experiments.

PNA–miRNA hybrid	PNA-miR-100	PNA-miR-20b
$q_H$	$0.28 \pm 0.03$	$0.26 \pm 0.01$

**Table 4.3.** Relative quantum yields of the PNA probes ( $q_P$ ) to the PNA probe corresponding to miR-100 for signal normalization. Standard deviations from mean values were obtained from three experiments.

PNA Probe	PNA probe of miR-100	PNA probe of miR-20b
$q_P$	1	$0.88 \pm 0.02$

#### 4.2.6. Standard CE-Based DQAMmiR

The hybridization mixture was injected into the capillary by a pressure pulse of 0.5 psi (3.4 kPa) for 5 s from the capillary inlet. Electrophoresis was driven by an electric field of 375 V/cm with a positive polarity at the sample-injection end. Electropherograms were analyzed with 32 Karat Software (SCIEX, Brea, CA, USA).

#### 4.2.7. ITP-CE for DQAMmiR

The capillary was prefilled with the TE buffer with pressure of 20 psi (137.9 kPa) for 1 min. Sample in the LE buffer (100 mM Tris-Cl, 20% (v/v) ACN, pH 8.2) was injected from the capillary outlet by a pressure pulse of 3 psi for 99 s. The buffer in the outlet was switched to a

clean LE buffer and an electric field of 375 V/cm was applied with positive polarity at the capillary outlet. The voltage was turned off at the time point when the displacement of TE with LE was completed, which can be determined by observing the current profile of the run. Buffer in the inlet was switched to LE buffer and an electric field of 375 V/cm was applied with positive polarity at the capillary inlet. The unreacted PNA probes and the PNA–miRNA hybrids were then separated and detected by CE-LIF as in the standard CE-based DQAMmiR.

#### **4.2.8. FASS-ITP-CE for DQAMmiR**

The capillary was prefilled with the TE buffer (20 mM Tris-HEPES, pH 8.2) with a pressure of 20 psi (137.9 kPa) for 1 min. The sample in a low-conductivity buffer (1 mM Tris-Cl, 20% (v/v) ACN, pH 8.2) was injected from the capillary outlet by a pressure pulse of 3 psi (20.7 kPa) for 99 s, which gives a sample plug length of 44.9 cm. A LE buffer of 100 mM Tris-Cl, 20% (v/v) ACN, pH 8.2 was used in the vial at the capillary outlet while the inlet end was kept in a vial containing TE buffer; an electric field of 375 V/cm was applied with positive polarity at the capillary outlet to facilitate FASS-ITP preconcentration as described in Figure 2B. The FASS-ITP was stopped when the concentrated analytes reach near the capillary inlet by turning off the voltage. The stop time for the FASS-ITP step was determined by observing the electrical current profile of the run. The buffer at the capillary inlet was then replaced with LE and an electric field of 375 V/cm was applied with positive polarity at the capillary inlet to resume CE separation. The unreacted PNA probes and the PNA–miRNA hybrids were then separated by CE and detected with LIF as in the standard DQAMmiR approach.

#### 4.2.9. Quantitation of miRNA

Peak areas were divided by the corresponding migration times to compensate for the area dependence on the species residence time while its passing the capillary detection window with different velocities. Concentrations of miRNAs were determined using the following equation:

$$[\text{miRNA}]^i = \frac{A_H^i \sum_{i=1}^N (q_P^i [P]_0^i)}{q_H^i q_P^i A_P + \sum_{i=1}^N \frac{A_H^i}{q_H^i}} \quad (4-1)$$

where  $[P]_0^i$  is the total concentration of the  $i$ -th PNA probe (composed of the hybrid and the excess probe),  $A_H^i$  is the area corresponding to the  $i$ -th hybrid,  $A_P$  is the cumulative area of the unbound probes,  $q_P^i$  is a relative quantum yield of the  $i$ -th PNA probe to normalize the quantum yield differences between the probes, and  $q_H^i$  is the relative quantum yield of the  $i$ -th hybrid with respect to that of the unbound probe. These relative quantum yields,  $q_P^i$  and  $q_H^i$ , were found experimentally.

#### 4.2.10. Analyzing miRNAs in crude cell lysates

Each cell pellet containing 10,000 cells was lysed by adding a 100- $\mu$ L volume of lysis solution composed of 0.1% (v/v) Triton X-100, 5 nM PNA-20b, 1 nM PNA-100 in the buffer of 1 mM Tris-Cl, 20% (v/v) ACN, pH 8.2, giving a final concentration of the cell contents in the lysate equivalent to 100,000 cells per 1 mL. The lysate was then mixed with the probes, and the mixture was incubated for hybridization and analyzed by FASS-ITP-CE according to the Materials and Methods in the main text.

### 4.3. Results and Discussion

#### 4.3.1. ITP-CE for DQAMmiR with PNA probes

The insufficiently low LOQ of CE-LIF-based DQAMmiR limits its utility for validation of miRNA fingerprints. This issue could be potentially resolved by incorporating OSP techniques, such as ITP, prior to CE separation. Our previous study demonstrated that using ITP preconcentration before CE separation could decrease LOQ of DQAMmiR with ssDNA probes by two orders of magnitudes, which inspired us to investigate whether the same ITP-CE strategy would be applicable to DQAMmiR with PNA hybridization probes.

In ITP, analytes can be concentrated only if they have electrophoretic mobilities greater than that of the TE ion and lower than that of the LE ion [159]. Because the miRNA quantitation in DQAMmiR requires accurate detection of both unreacted probes and the miRNA–probe hybrids, it is essential to have TE/LE chemistry that can concentrate both the PNA probes and the hybrids in ITP-CE for DQAMmiR with PNA probes. Thus, the following conditions need to be satisfied for electrophoretic mobilities:

$$|\mu_{\text{TE}}| < |\mu_{\text{PNA}}| < |\mu_{\text{hybrid}}| < |\mu_{\text{LE}}| \quad (4-2)$$

where  $\mu_{\text{TE}}$ ,  $\mu_{\text{PNA}}$ ,  $\mu_{\text{hybrid}}$ , and  $\mu_{\text{LE}}$  are mobilities of the TE ion, PNA probes, PNA–miRNA hybrids, and the LE ion, respectively. However, the mobilities of PNA probes are near zero ( $|\mu_{\text{PNA}}| \approx 0$ ) due to their electrically neutral backbones. Only the C-terminus and a fluorescent dye provide a small negative charge resulting in small net electrophoretic mobilities for PNA probes, making it very challenging to find a suitable TE ion to satisfy inequalities in **Eq. 4-2**. A previous study by Bercovici *et al.* demonstrated that the PNA probes could not be focused by ITP where they used 2-morpholin-4-ium-4-ylethanesulfonate ion (MES) as a TE ion and  $\text{Cl}^-$  as an LE ion [160].

In order to investigate the feasibility of implementing ITP-CE for DQAMmiR with PNA probes, we also experimentally tested another two common TE ions: 2-[4-(2-hydroxyethyl)piperazin-1-yl]ethanesulfonic ion (HEPES) and Tricine, which have smaller net mobilities than MES according to the AnglerFish software [161], while using the high-mobility  $\text{Cl}^-$  ion as the LE ion. In these experiments, a hybridization mixture of two miRNA targets, miR-20b and miR-100, and their complementary PNA probes, named here as PNA-20b and PNA-100, taken in excess was prepared and subjected to ITP-CE. The results (**Fig. 4.4**) showed that the peaks for the unreacted PNA probes either were unexpectedly small or disappeared in experiments using either of the two different TE ions despite the PNA probes being more than ten times in excess of miRNAs in the hybridization mixture. These results proved that the unreacted PNA probes eluted

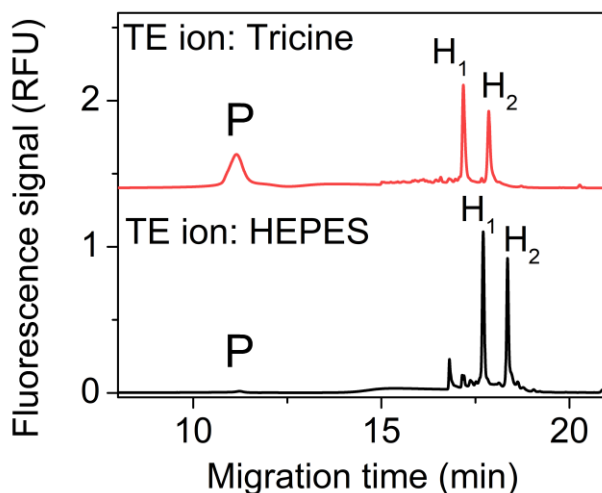


**Figure 4.4.** Investigation of two TE ions — Tricine and HEPES — in ITP-CE for DQAMmiR with PNA hybridization probes. A hybridization mixture of 0.1 nM miR-20b, 0.1 nM miR-100, 5 nM PNA-20b, and 1 nM PNA-100 were prepared in the LE buffer composed of 100 mM Tris-Cl, 20% (v/v) ACN, pH 8.2 and analyzed by ITP-CE. The TE buffers composed of 10 mM Tris, 50 mM Tricine, pH 7.3 (top trace) and 20 mM Tris, 10 mM HEPES, pH 8.2 (bottom trace) were used in these experiments, respectively. P stands for excess PNA probes;  $\text{H}_1$  stands for the PNA–miR-100 hybrid; and  $\text{H}_2$  stands for the PNA–miR-20b hybrid.

from the capillary during sample preconcentration by ITP, indicating that net electrophoretic mobilities of both tested TE ions were larger than that of the PNA probes. Since the quantitation of miRNAs in DQAMmiR requires detection of not only the hybrids but also the unreacted probes, ITP as a sole preconcentration method is not compatible with DQAMmiR utilizing PNA probes. Therefore, we had to find a new OSP technique that could decrease the LOQ of DQAMmiR while utilizing PNA probes.

To address this issue, we explored other alternative OSP techniques and realized that integrating FASS with ITP could be a potential solution to preconcentrate the hybrids efficiently while preventing the loss of the unreacted PNA probes. In contrast to ITP, FASS is a less mobility-selective process for sample concentration, *i.e.* it can concentrate all negative or positive charged species regardless of the magnitude of their mobilities from a low-conductivity plug into a narrow zone at the interfaces with a high-conductivity zone due to an electric field-amplification effect. As described in **Fig. 4.2**, the FASS-ITP-CE approach can be implemented by preparing the hybridization in an extremely diluted buffer with the conductivity significantly lower than that of both TE and LE. Thus, an amplified electric field can be facilitated in the sample plug once the high voltage is applied, leading to concentration of both the low-mobility PNA probes and the high-mobility PNA–miRNA hybrids at the sample/LE interface by FASS. On the other hand, a diffused TE zone is also formed by the counter broadening effect at the TE/sample plug boundary. As a result, a discontinued TE-analytes-LE pattern, which is required for ITP, is formed in the capillary. Therefore, the PNA–miRNA hybrids would be concentrated at the TE/LE interface into a narrower band as the condition of  $|\mu_{TE}| < |\mu_{hybrid}| < |\mu_{LE}|$  is satisfied. In theory, the stacked PNA probes should be slowly separated from the ITP-focused hybrids because their net mobilities are smaller than that of the TE ion. However, this separation of the stacked PNA probes from the ITP-

focused hybrids would be limited because the electric field in the analyte zone at the TE/LE interface is low due to the presence of the low-conductivity diluted TE zone in the capillary. Thus, the unreacted PNA probes would be kept along with the concentrated hybrids in the capillary for the subsequent CE separation after reversing the polarity, which would allow us to facilitate accurate quantitation of miRNAs like in the standard CE-based DQAMmiR.

#### **4.3.2. FASS-ITP-CE for DQAMmiR with PNA probes**

In order for this FASS-ITP-CE approach to work, four requirements must be satisfied:

1) PNA probes must hybridize with their miRNA targets in the low-concentration buffer as a low-conductivity sample plug is required for FASS-ITP-CE; 2) unreacted PNA probes must be kept inside the capillary during the sample preconcentration process, as they are essential for accurate miRNA quantitation; 3) PNA–miRNA hybrids must be concentrated efficiently to achieve low LOQ for analyzing miRNAs in cell lysates; 4) the assay must be suitable for quantifying multiple miRNAs with high accuracy and precision.

##### **4.3.2.1. Effect of sample buffer concentration on PNA/miRNA hybridization**

As FASS-ITP requires a sample plug with low conductivity, it is essential to investigate if PNA probes can still bind their miRNA targets tightly in low-concentration buffers. It is known that low-concentration buffers are typically not favored by nucleic acid hybridization [162]. However, thanks to the neutral backbone of PNA, PNA–RNA duplexes are much more stable than the DNA–RNA duplexes in low-concentration buffers due to the lack of coulomb repulsion forces between the two strands [163]. Relative neutrality of PNA with respect to DNA should make it possible to perform PNA–miRNA hybridization reactions in low-concentration buffers. To confirm this, we prepared hybridization mixtures in Tris-Cl buffers with concentrations of 100, 10,

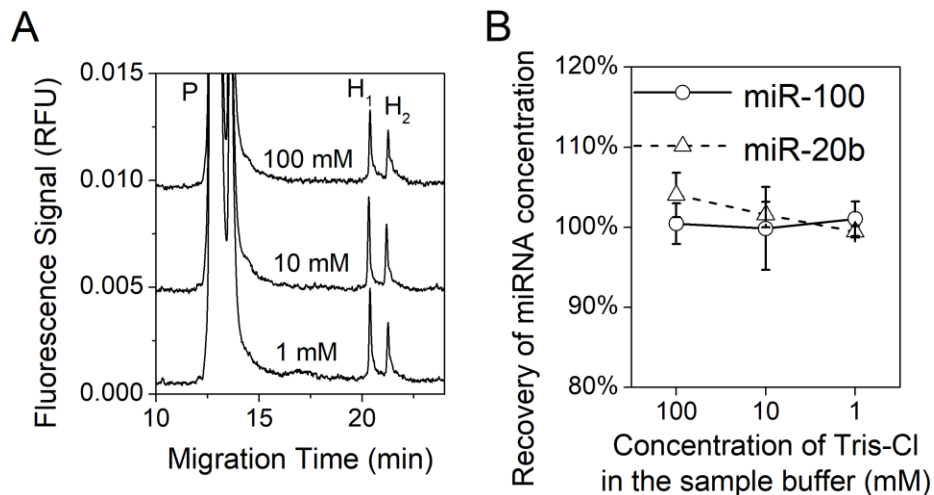


**Figure 4.5.** The effect of sample buffer concentration on PNA–miRNA hybridization. A hybridization mixture of 50 pM miR-20b, 50 pM miR-100, 5 nM PNA-20b, and 1 nM PNA-100 were prepared in buffers composed of 1 to 100 mM Tris-Cl, 20% (v/v) ACN, at pH 8.2. They were then analyzed by standard CE-based DQAMmiR. Electropherograms (A) and the quantitation results (B) are shown here. P stands for excess PNA probes; H<sub>1</sub> stands for the PNA–miR-100 hybrid; and H<sub>2</sub> stands for PNA–miR-20b hybrid. Error bars represent one standard deviation from three independent runs.

and 1 mM. These hybridization mixtures were analyzed by standard CE-based DQAMmiR as described in Materials and Methods. The results in **Fig. 4.5A** show that the separation of unreacted PNA probes from the hybrids and the hybrids from each other was not affected by the low concentrations of the sample buffer, which allowed us to facilitate DQAMmiR in these buffers. Quantitation results from triplicated measurements in **Fig. 4.5B** showed recoveries of 95% to 105% for measuring two miRNAs in all samples with RSD of less than 5%. It indicates that the concentration of the sample buffer has negligible effect on PNA–miRNA hybridization. PNA probes could still bind their complementary miRNA targets tightly in a very diluted buffer of 1 mM Tris-Cl, 20% (v/v) ACN, pH 8.2, which would qualify for the low-conductivity sample buffer required in FASS-ITP.

#### 4.3.2.2. Ability of retaining excess PNA probes in FASS-ITP-CE

We then had to prove that combining FASS with ITP would prevent the loss of the low-mobility PNA probes in the preconcentration process. In FASS-ITP-CE, the preconcentration step should be stopped before the concentrated analytes reach the capillary end to prevent them from eluting from the capillary before the start of the separation step (Figure 2B in main text). Our task was to find a way to stop FASS-ITP before the concentrated analytes leave the capillary with as little residual TE remaining as possible as it could deteriorate the quality of CE separation. After exploring a number of options, we focused on the value of electric current as an indicator of completion of the FASS-ITP step and that can be used to determine stop time,  $t_{st}$ . The displacement of both the low-conductivity sample matrix and TE by LE in the capillary during FASS-ITP is accompanied by a gradual increase in the electric current. There is a time-point on the current versus time dependence where the slope abruptly changes from finite to zero (Fig. 4.6). This time is thought to correspond to the exact moment of the completion of electrolyte displacement. Thus, we could stop FASS-ITP at this time and resume the CE separation subsequently.

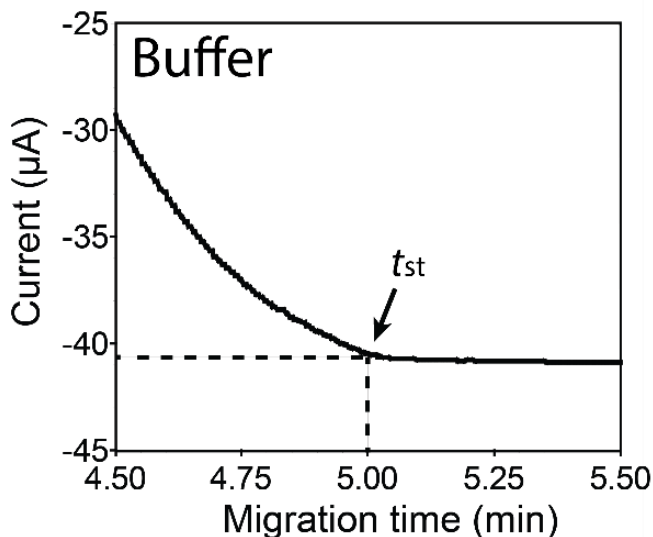


**Figure 4.6.** Determination of the time-point ( $t_{st}$ ) for stopping in preconcentration by FASS-ITP and starting CE by applying an electric field with a reversed polarity.

As any loss of PNA probes would result in decreasing of their fluorescence signal in the electropherogram, we designed experiments in which the same sample containing only PNA probes would be analyzed by FASS-ITP-CE and CE in parallel. Thus, we could evaluate if FASS-ITP-CE retained the PNA probes by comparing the fluorescence signal of the PNA probes obtained from FASS-ITP-CE with that obtained from CE (which would be used as a reference). In this FASS-ITP-CE experiment, two buffers, 20 mM Tris-HEPES at pH 8.2 and 100 mM Tris-Cl with 20% (v/v) ACN at pH 8.2, were used as TE and LE, respectively. The diluted buffer composed of 1 mM Tris-Cl and 20% (v/v) ACN at pH 8.2, which has the conductivity much lower than those of both TE and LE buffer, was used as sample buffer. The sample was analyzed by FASS-ITP-CE as described in Materials and Methods. In parallel, another sample with the same concentrations of PNA probes was prepared in LE and analyzed by CE with LE as a running buffer. In this CE experiment, a 44.9-cm-long plug of the sample was injected by pressure; the same plug length was used in FASS-ITP-CE. Thus, the quantities of PNA probes injected into the capillary were identical in these two runs. Because the running buffer in this experiment was LE and was identical to the running buffer in FASS-ITP-CE. The velocities of the PNA probes passing through the detector were also identical in these two runs. Therefore, we could examine if the PNA probes were retained in FASS-ITP-CE by directly comparing the peak area of the PNA probes with that obtained from the CE run. A ratio between peak areas in FASS-ITP-CE and CE runs was equal to 1.03 (**Fig. 4.7**), suggesting that the PNA probes were kept inside the capillary in the FASS-ITP preconcentration process. The 3% difference results from errors in the volume of injected sample. This excellent recovery proves that the combination of FASS with ITP prevents the unreacted PNA probes from eluting from the capillary (as expected). Retaining the probes, in turn, allows us to

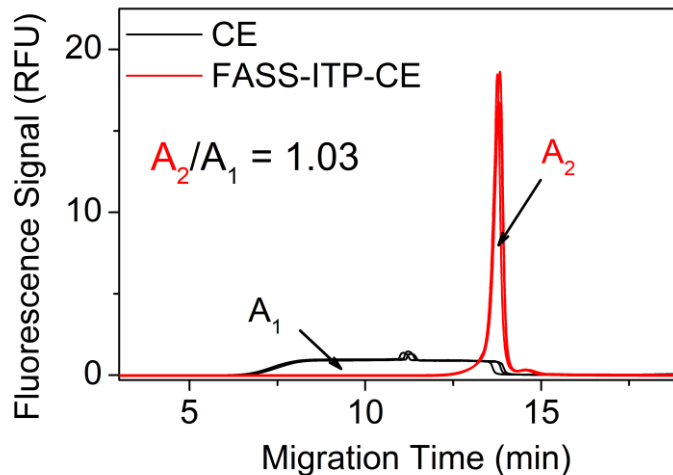


**Figure 4.7.** Proof of the ability to retain PNA probes in FASS-ITP-CE. A mixture of 5 nM PNA-20b and 1 nM PNA-100 were prepared and analyzed by CE (black traces with an average peak area of  $A_1$ ) and FASS-ITP-CE (red traces with an average peak area of  $A_2$ ). Samples were injected by pressure of 3 psi for 99 s in both cases. Three repeated runs of each experiment shown here indicate good reproducibility.

perform accurate miRNA quantitation after CE separation of the hybrids from each other and the unreacted probes and LIF detection of all these analytes.

#### 4.3.2.3. Evaluation the preconcentration efficiency of FASS-ITP-CE

We also evaluated the efficiency of FASS-ITP-facilitated preconcentration of the PNA–miRNA hybrids. As shown in **Fig. 4.8A**, the separation of the unreacted PNA probes from the hybrids and two PNA–miRNA hybrids from each other in DQAMmiR were not affected by the additional preconcentration step. Very sharp peaks were detected for both hybrids, producing peaks with heights 100 times greater than those obtained without preconcentration, suggesting that the LOQ of FASS-ITP-CE could be more than 2 orders of magnitude lower than that of the standard CE for detecting miRNAs. It was also noticed that these peak heights were comparable with those in Figure , indicating that the combination of FASS with ITP provided preconcentration

efficiency similar to that of ITP alone for concentrating the PNA–miRNA hybrids. It's worth noticing that a previous study reported that the combination of ITP with FASS in a coated capillary (with suppressed EOF) could provide a preconcentration efficiency higher than that of ITP alone [164]. In our case of an uncoated capillary with strong EOF, the addition of FASS to ITP didn't further improve the efficiency of concentrating the PNA–miRNA hybrids. Most importantly, however, FASS did not interfere with the concentration efficiency of ITP for the PNA–miRNA hybrids and could still greatly decrease the LOQ of the assay for detecting multiple miRNAs. On the other hand, we noticed that the impurities associated with the PNA probes and the synthetic miRNA targets were also pre-concentrated by the FASS-ITP process, resulting in some impurity peaks in the electropherogram of the FASS-ITP-CE measurement in Figure 6A. To minimize their effects on miRNA quantification, a purification procedure was employed to remove the impurities from the PNA probes as described below.

#### **4.3.2.4. Purification of the PNA probes using FASS-ITP-CE**

The presence of fluorescent impurities in the PNA probes significantly increases the LOQ for miRNA detection in FASS-ITP-CE. As evident from **Fig. 4.9**, bottom trace, the PNA probes from the supplier contained a significant amount of impurities overlapping with the hybrids in the electropherograms. This would influence the accuracy of the peak areas of the hybrids while target concentrations are low, and consequently, lead to errors in quantitation and poor (high) LOQ. Ideally, the impurities in the PNA probe stocks can be removed by collecting fractions at the CE outlet as they are separable from the PNA probes in CE. However, because only a small volume of sample can be injected in CE for separation, the probes in the collected fractions would be

diluted by multiple orders of magnitude, which makes it difficult to be used PNA purified in such

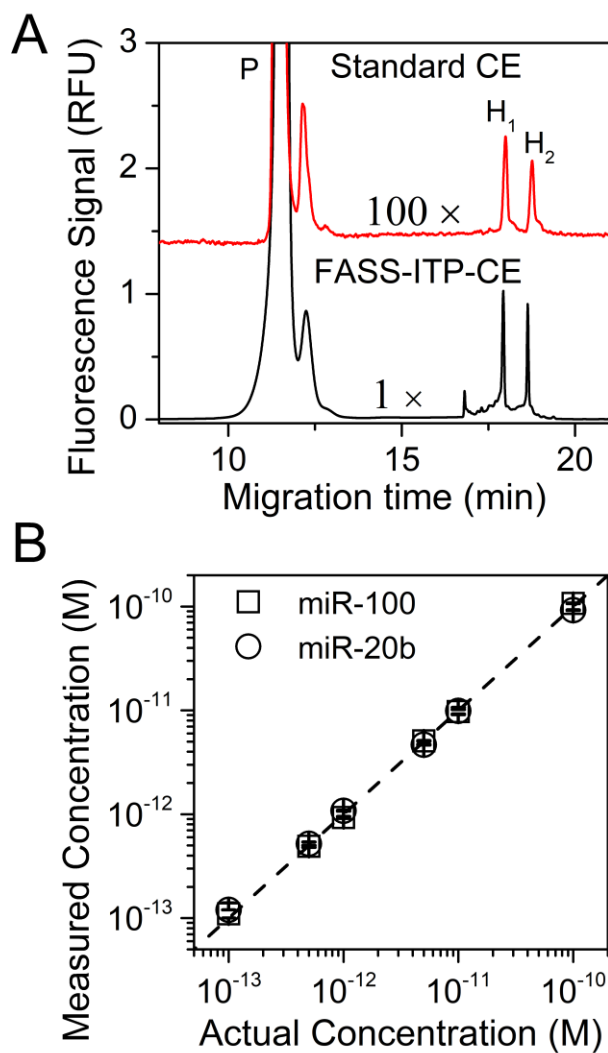


**Figure 4.8.** Evaluation of the preconcentration efficiency and the analytical performances of FASS-ITP-CE. A) Electropherograms for measurements by standard CE and FASS-ITP-CE for DQAMmiR. A hybridization mixture of 0.1 nM miR-20b, 0.1 nM miR-100, 5 nM PNA-20b and 1 nM PNA-100 were analyzed by the standard CE approach and the FASS-ITP-CE approach in parallel. The trace of the standard CE approach was zoomed in by a factor of 100 along the vertical axis for its easy comparison with the FASS-ITP-CE trace. P stands for unreacted PNA probes; H<sub>1</sub> stands for the PNA–miR-100 hybrid; and H<sub>2</sub> stands for the PNA–miR-20b hybrid. B) Quantification of the two miRNAs, miR-20b and miR-100, by the FASS-ITP-CE approach in a concentration range of 0.1 to 100 pM. Measured concentrations are plotted with respect to their actual concentrations, determined by UV absorbance at 260 nm. The dashed line ( $y = x$ ) represents the recovery of 100%. The error bars represent one standard deviation of three independent replications.

a way in the following FASS-ITP-CE experiments.

To address this issue, we developed a protocol to remove the impurities in the PNA probe stocks based not on CE but on our FASS-ITP-CE procedure. In FASS-ITP-CE, the injected sample volume is 120 times greater than that in a standard CE run. PNA probes in a large sample plug are concentrated into a narrow zone by FASS while the impurities are being focused by the hyphenated process of FASS-ITP. Thus, the PNA probes can be separated from the impurities in the subsequent CE. Thus, we could remove the impurities by collecting the fraction of the concentrated PNA probes at the capillary outlet during CE separation. As a 120-time volume was injected, the PNA probes in the collected fraction in this method would supposedly be approximately 120 times less diluted than that in normal CE. Furthermore, we can increase the concentration of the purified

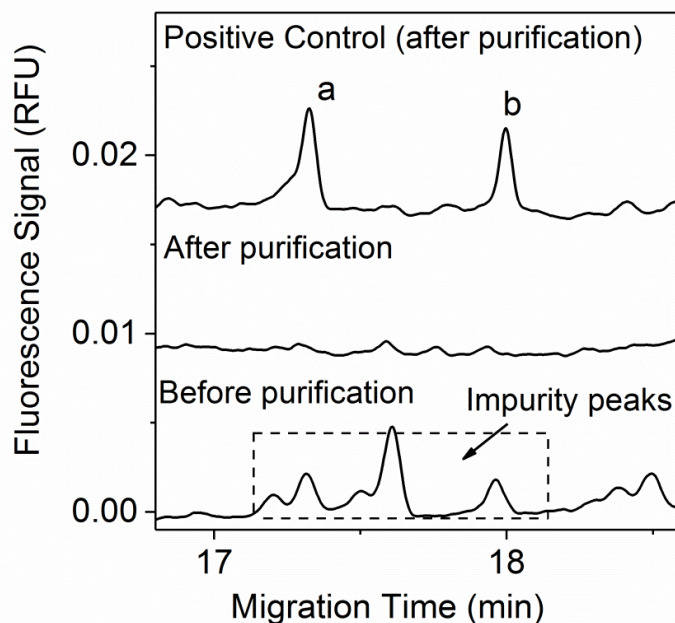


**Figure 4.9.** Electropherograms of the negative control samples before purification (bottom trace) and after purification (middle trace). The negative control samples were composed of 5 nM PNA-20b and 1 nM PNA-100 only without miRNA targets. Samples composed of 1 pM miR-20b, 1 pM miR-100, 5 nM PNA-20b and 1 nM PNA-100 was also analyzed as positive control (top trace). The purified PNA probes were used in this positive control sample. Peak assignment: a) PNA–miR-100 hybrid; b) PNA–miR-20b hybrid.

PNA probes by collecting the fractions of the PNA probes from multiple runs into a single tube. For example, by collecting the fractions from 5 repeated runs, we successfully obtained a solution of purified PNA probe for miR-100 with a concentration of 1.2  $\mu\text{M}$  from a stock with a concentration of 6  $\mu\text{M}$ . The high-concentration purified probes could then be quantified by UV-absorbance and stored for their use in the following analysis. In **Fig. 4.9**, we also show the result of an experiment in which we analyzed a sample containing purified PNA probes only (middle trace). It was clear that the impurity levels in the PNA probes of the same concentrations were significantly lower than those before purification. We also analyzed a sample containing each miRNA target at a concentration of 1 pM by using the purified PNA probes. The result (**Fig. 4.9**, top trace) demonstrated that the miRNA targets of 1 pM could be accurately quantitated by using the purified PNA probes. This result clearly indicated that lowering the level of impurities via purification of PNA probes provided by a supplier would allow us to quantitate hybrids peaks with concentrations below 1 pM accurately.

#### **4.3.2.5. FASS-ITP-CE for DQAMmiR with PNA probes**

Although some noise peaks are still present in the electropherogram (*e.g.* the peak near 17 min) after purification, these peaks are relatively small comparing to the hybrid peaks, and, more importantly, they are separable from the peaks of the hybrids. Therefore, the presence of these impurity peaks does not influence miRNA quantification. The analytical performance of the FASS-ITP-CE assay was then evaluated by quantifying miR-20b and miR-100 with varying concentrations. The electropherograms (**Fig. 4.10**) obtained from these measurements demonstrated good repeatability of the migration times of the hybrid peaks. Although no internal standard was used in these measurements, the impurity peak at near 17 min could be used as a migration time reference to calibrate small shifts in migration times of the hybrid peaks between

the runs. The quantitation results (Fig. 4.8B) demonstrate that the miRNA concentrations measured by the FASS-ITP-CE approach agree well with the known concentrations of the spiked-in targets in a concentration range of 0.1 to 100 pM, giving recoveries within a range of 90 to 110% with  $RSD \leq 10\%$  for all concentrations. These experiments revealed that the FASS-ITP-CE approach was applicable to DQAMmiR utilizing PNA probes. The results show that FASS-ITP-CE can quantify two miRNAs accurately and precisely with LOQ of 0.1 pM, which is 140-times lower than that of the standard approach as reported in the previous study.<sup>18</sup> Although an LOQ of

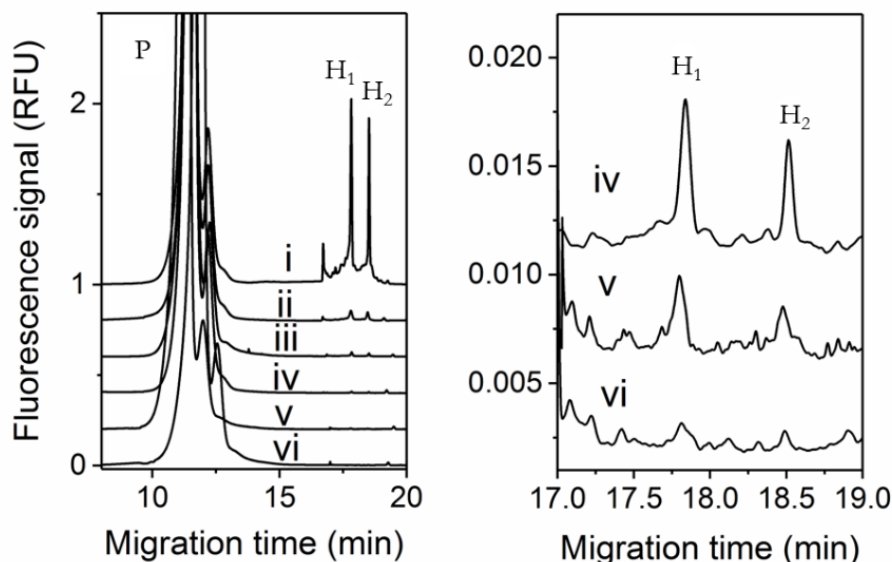


**Figure 4.10.** Electropherograms for FASS-ITP-CE of samples in pure buffer. P stands for excess PNA probes; H<sub>1</sub> stands for PNA–miR-100 hybrid; and H<sub>2</sub> stands for PNA–miR-20b hybrid. Electropherograms i–vi (left panel) correspond to target concentrations of 100, 10, 5, 1, 0.5, and 0.1 pM, respectively. Electropherograms for targets concentrations of 1, 0.5, and 0.1 pM are zoomed-in (right panel) for clarity.

0.1 pM is still insufficient to detect low-abundance miRNAs, the 140-times improvement in LOQ will facilitate validation of putative miRNAs fingerprints with a greater variability in miRNA concentrations in the sample.

**Table 4.4.** Quantitation results of the measurements. Measured concentrations of two miRNAs (miR-100 and miR-20b) shown with respect to their actual concentration as determined by light absorbance at 260 nm; standard deviations from mean values were obtained from three independent experiments.

Actual miRNA Concentration (pM)	Measured miRNA Concentration (pM, Mean $\pm$ Standard Deviation)	
	miR-20b	miR-100
100	92.1 $\pm$ 0.7	107.0 $\pm$ 0.6
10	9.9 $\pm$ 0.8	9.7 $\pm$ 0.5
5	4.7 $\pm$ 0.1	5.1 $\pm$ 0.1
1	1.1 $\pm$ 0.1	0.9 $\pm$ 0.1
0.5	0.52 $\pm$ 0.02	0.50 $\pm$ 0.01
0.1	0.11 $\pm$ 0.01	0.11 $\pm$ 0.01

#### 4.3.2.6. Analysis of endogenous miRNAs in crude cell lysates by FASS-ITP-CE

Finally, in order to assess the feasibility and applicability of FASS-ITP-CE for analyzing miRNAs in a biological matrix, we applied this method to analyze two endogenous miRNAs (miR-100 and miR-20b) in two cell lines: a prostate cancer-derived cell line, 22Rv1, and a normal prostate cell line, RWPE-1. In these experiments, measurements were conducted by determining the miRNA concentrations in the crude cell lysate directly, *i.e.*, the cultured cells were lysed and analyzed without additional sample purification. The results (**Fig. 4.11**) show that both miR-100 and miR-20b were detected in the 22Rv1 cell lysate, while only miR-100 was detectable by the current assay in the RWPE-1 cell lysate. The quantification results for measuring miR-100 and miR-20b are shown in **Table 4.5**. It revealed that the expression level of miR-20b is greater in the cancer cells than in the normal cells, while the expression levels of miR-100 were similar in the

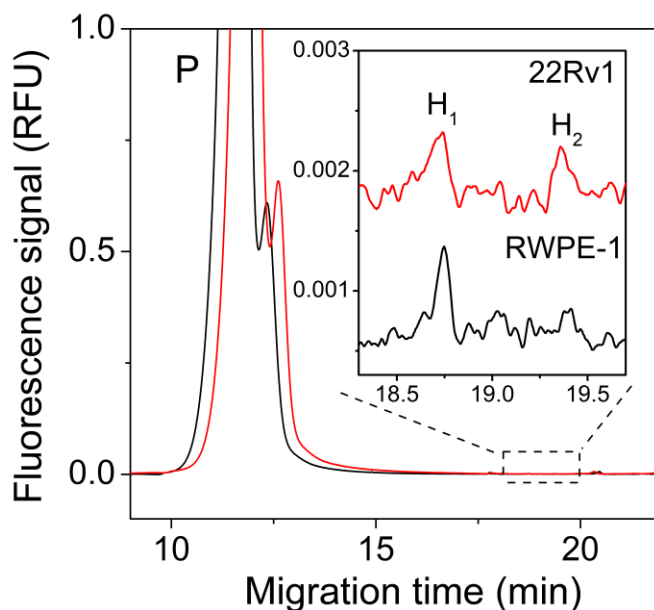


**Figure 4.11.** FASS-ITP-CE analysis of miR-100 and miR-20b in 22Rv1 cell lysate (red trace) and RWPE-1 cell lysate (black trace). The inset shows the zoomed-in area of the PNA–miRNA hybrid peaks. P marks a peak corresponding to the unreacted PNA probes, H<sub>1</sub> marks a peak of the PNA–miR-100 hybrid, and H<sub>2</sub> marks a peak of the PNA–miR-20b hybrid.

cancer and normal cells. This result agrees well with the previous report of miR-20b being an oncogene in prostate cancer [165]. Known concentrations of the two miRNAs were also spiked into cell lysates to account for any effect the cell contents could have on quantification; the effect was found to be negligible. Despite the fact that the current LOQ of the assay may still limit its applicability to quantifying low-expression miRNAs in practice, the success of directly measuring two miRNAs simultaneously in crude cell lysates indicates that our FASS-ITP-CE approach is not affected by the contents of the sample matrix. This suggests that FASS-ITP-CE can be a feasible tool for validation of some putative miRNA fingerprints in patient samples in practice.

**Table 4.5.** Concentrations of two miRNAs (miR-100 and miR-20b) in RWPE-1 cell lysates and 22Rv1 cell lysates determined by FASS-ITP-CE.

		Rep1 (pM)	Rep2 (pM)	Rep3 (pM)	Mean (pM)	Standard Deviation (pM)
RWPE-1 Cell lysate	[miR-100]	0.08*	0.08*	0.09*	0.08	0.01
	[miR-20b]	Below LOD	Below LOD	Below LOD	Not applicable	Not applicable
22Rv1 Cell lysate	[miR-100]	0.12	0.12	0.14	0.13	0.01
	[miR-20b]	0.09*	0.10	0.11	0.10	0.01

\*Below LOQ but higher than LOD.

#### 4.4. Conclusions

In this study, I introduced a sample preconcentration technique for DQAMmiR utilizing PNA probes for analysis of multiple miRNAs. This preconcentration technic combines FASS with ITP prior to CE to greatly decrease LOQ of DQAMmiR. We demonstrated that FASS-ITP could efficiently concentrate PNA–miRNA hybrids while preventing the loss of PNA probes, proving that FASS-ITP-CE is applicable to DQAMmiR utilizing PNA probe in principle. Using FASS-ITP-CE for simultaneous analysis of two miRNAs showed that an LOQ of 0.1 pM could be

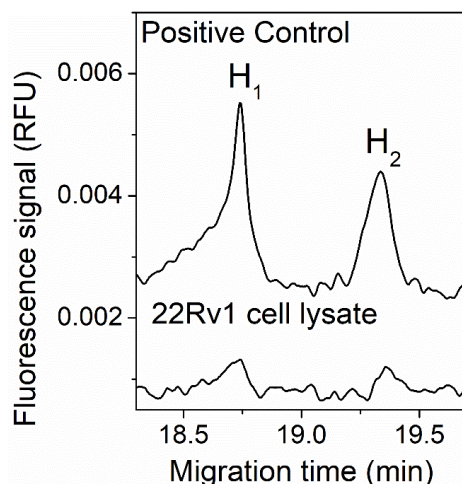


**Figure 4.12.** Electropherograms for FASS-ITP-CE measurements of miR-100 and miR-20b in the 22Rv1 cell lysate (bottom trace) and a positive control sample (top trace). H<sub>1</sub> stands for the PNA–miR-100 hybrid and H<sub>2</sub> stands for the PNA–miR-20b hybrid. The positive control sample was prepared by spiking 50 pM miR-20b and miR-100 into the 22Rv1 cell lysate.

achieved. This LOQ is about 140 times lower than that of the standard CE-based DQAMmiR. We also showed that FASS-ITP-CE was suitable for analyzing endogenous miRNAs in crude cell lysates directly, suggesting that the method was robust to variations in the sample-matrix components. Although, an LOQ of 0.1 pM is still insufficient to detect low-abundance miRNAs, lowering LOQ by a factor of 140 and methods robustness to sample-matrix contents will largely expand the utility of DQAMmiR, bringing it closer to becoming a practical tool for validation and clinical use of miRNA biomarkers.

## **CHAPTER 5. RATIOMETRIC ANALYSIS OF MICRORNAS IN URINE BY CAPILLARY ELECTROPHORESIS ENABLES THEIR CLINICAL USE AS NON-INVASIVE BIOMARKERS**

The presented material is a draft version of a manuscript currently under development. My contribution to the article was: (i) planning all experiments, (ii) performing all experiments, (iii) interpreting results, (iv) preparing all figures, (v) writing the manuscript.

### **5.1. Introduction**

Recent findings of disease-specific miRNAs in biological fluids, such as blood, urine, and saliva, etc., has shown that the detection of deregulated miRNAs can be used for less-invasive diagnosis and prognosis of diseases [28–29]. Among miRNAs in different biological fluids, urinary miRNAs are an ideal source of biomarkers since urine is the most readily obtainable and non-invasive biological fluids. Moreover, urinary miRNAs are also found to be relative stable, which supports their clinical utility as biomarkers [166]. And many urinary miRNA signatures have been reported as potential biomarkers of a variety of urological diseases [167–170].

However, none of these tentative biomarkers have been used in clinical applications yet. One of the major challenges of miRNA analyses in urine is that their quantities can vary drastically depending on the time of urine sampling and miRNA-extraction procedure. This challenge can be overcome if a ratiometric approach is used in which two or more miRNAs are analyzed simultaneously and the quantity of the one of them is used for normalization of the quantities of others. But simultaneously quantitation of multiple miRNAs also poses a major challenge. Due to the low abundance of miRNAs in clinical samples, the methods for miRNA analysis are required to have LOD at sub-picomolar level, which exceeds the capability of most published methods. And most of the sufficiently sensitive methods, such as electrochemical sensing and optical

resonance, usually allow for reliable quantitation of a single miRNA only. For other amplification-based methods, including RT-PCR, while they in theory can analyze multiple targets in parallel and detect as low as a single copy of miRNAs, they are prone to amplification bias. And because the amplification efficiency typically varies different target sequences in PCR, it is challenging to compare the analyses results for different targets making it unsuitable for ratiometric measurements of multiple miRNAs.

This problem can be potentially addressed by using our capillary electrophoresis-based DQAMmiR methods, which is capable of direct quantitative analysis of multiple miRNAs, as introduced in previous chapters. As a hybridization-based method, DQAMmiR has shown capability of analyzing multiple miRNAs simultaneously with LOD of sub-picomolar with online sample preconcentration. Moreover, the quantitation in DQAMmiR is direct, *i.e.* it doesn't require any modification and amplification on miRNA targets, which minimize bias for analyzing different targets. And in previous chapter, I also demonstrated that the biological sample matrices, such as RNA extracts and crude cell lysates, would have minimized impact on the quantitiveness of the DQAMmiR, making it an promising method for ratiometric analysis of multiple miRNAs in clinical samples. In this study, I explored the applicability of DQAMmiR for ratiometric analysis of multiple miRNAs in urine samples. For this purpose, I applied the first-generation DQAMmiR, which utilizes ssDNA as hybridization probes and SSB and peptide drag tags as separation enhancers, to analyze two miRNAs, miR-16 and miR-21, in urine sediments. We demonstrated that DQAMmiR, with sample preconcentration by ITP prior to CE, could successfully detect endogenous miR-16 and miR-21 in the crude lysates of urine sediments collected from a volunteer. To study the utility of ratiometric analysis of multiple miRNAs as biomarkers, I attempted to measure the concentrations of these miRNAs in several urine sediments collected from the same

volunteer but at different times. The results confirmed that the abundance of endogenous miR-16 and miR-21 could vary greatly intraindividually in these samples, although the quantitiveness of the SSB-mediated DQAMmiR was interfered by the impurities presented in the crude sample matrices. This results indicated that it would be very challenging to use the individual miRNA concentrations or quantity in urine as clinical biomarkers. However, we found that the concentration ratio between the two targets remained almost consistent for the volunteer, suggesting that the ratiometric measurements between multiple miRNAs would serve as better biomarkers than individual miRNA concentrations in clinical tests for diagnosis and prognosis. And DQAMmiR would be an ideal analytical methodology for the development and use of such tests.

## **5.2. Materials and Methods**

### **5.2.1. miRNAs and DNA probes**

MicroRNA and its complementary DNA probe were custom-synthesized by IDT (Coralville, IA, USA). To allow separation of the 2 hybrids, a 15-aa peptide tag was conjugated to the DNA probe which is complementary to miR-16 via a thioester bond. The conjugation reaction, which is described in our previous work [91], occurred between the thiol group on the 5' end of the DNA probe and a maleimide group on the N-terminus of the peptide tag. All maleimide modified peptides were synthesized by Canpeptide (Pointe-Clare, QC, Canada).

The concentrations of miRNA and DNA probe in stock solutions were determined from light absorbance at 260 nm measured with a Nano-Drop ND-1000 spectrophotometer (Thermo-Fisher Scientific, Waltham, MA, USA); molar extinction coefficients were provided by IDT.

Working solutions were prepared from stock solutions by dilution. “Actual concentrations” of working solutions were calculated as stock concentrations divided by dilution factors.

### **5.2.2. Standard CE-Based DQAMmiR**

The hybridization mixture was injected into the capillary (50 cm in length, 75  $\mu$ m in diameter) by a pressure pulse of 0.5 psi (3.4 kPa) for 5 s from the capillary inlet. Electrophoresis was driven by an electric field of 500 V/cm with a positive polarity at the sample-injection end. Electropherograms were analyzed with 32 Karat Software (SCIEX, Brea, CA, USA).

### **5.2.3. ITP-CE for DQAMmiR**

The capillary (80 cm in length, 75  $\mu$ m in diameter) was prefilled with the TE buffer with pressure of 20 psi (137.9 kPa) for 1 min. Sample in the TE buffer (20 mM Tris-HEPES, pH 8.3) was injected from the capillary outlet by a pressure pulse of 3 psi for 99 s. The buffer in the outlet was switched to a clean LE buffer (50 mM Tris-Acetate, 50 mM Sodium Acetate, pH 9.2) and an electric field of 375 V/cm was applied with positive polarity at the capillary outlet. The voltage was turned off at the time point when the displacement of TE with LE was completed, which can be determined by observing the current profile of the run. Buffer in the inlet was switched to LE buffer and an electric field of 375 V/cm was applied with positive polarity at the capillary inlet. The unreacted DNA probes and the DNA–miRNA hybrids were then separated and detected by CE-LIF as in the standard CE-based DQAMmiR.

### **5.2.4. Urine Sample Collection and Processing**

50-mL fresh urine sample was collected from a volunteer in a 50-mL centrifuge tube. Centrifuge urine at 2000g for 30 minutes at room temperature. Remove the supernatant to within approximately 1 mL of the sediment. Resuspend the sediment in the remaining 1 supernatant and

transfer the contents to a 2-mL sample tube. Centrifuge at 2000g for 10 minutes at room temperature and remove the supernatant and leave the sediment pellet in the tube. To lysis the sediment pellet, add 100  $\mu$ L of lysis buffer (0.1% Triton X-100, 20 mM Tris-HEPES, pH 8.3) into the tube. After vortexing, incubate the lysate at 95°C for 5 minutes. For each analysis, add 10  $\mu$ L of this lysate into a hybridization mixture with final volume of 100  $\mu$ L.

### **5.3. Results and Discussion**

#### **5.3.1. Implementing DQAMmiR for simultaneous quantitation of miR-16 and miR-21**

I firstly designed fluorescently labelled ssDNA probes that are complementary to miR-16 and miR-21 respectively. To analyze two targets simultaneously, the DNA probe complementary to miR-16 was labelled with a 15-aa peptide tag to facilitate separation of two probe-miRNA hybrids from each other in CE. By using the synthetic miRNA as targets, the experimental results in **Fig. 5.1A** showed that the two probe-miRNA hybrids were well separated in CE. I also evaluated the quantitiveness of the method by quantitating these synthetic miRNAs in a buffer solution as sample matrix. 90–110% recoveries and RSD < 15% were obtained for measuring both miRNAs in a concentration range from 5–1000 pM without any preconcentration. These results (**Fig. 5.1B**) demonstrated that the designed probes could be used in DQAMmiR to quantitate these two miRNAs accurately and precisely. And these ssDNA probes would be used to analyze endogenous miR-16 and miR-21 in urine samples in the following study. However, the concentrations of these two endogenous miRNAs in urine samples could be lower than this concentration range. Thus, there is a need for ITP preconcentration to improve the LOD of the method.

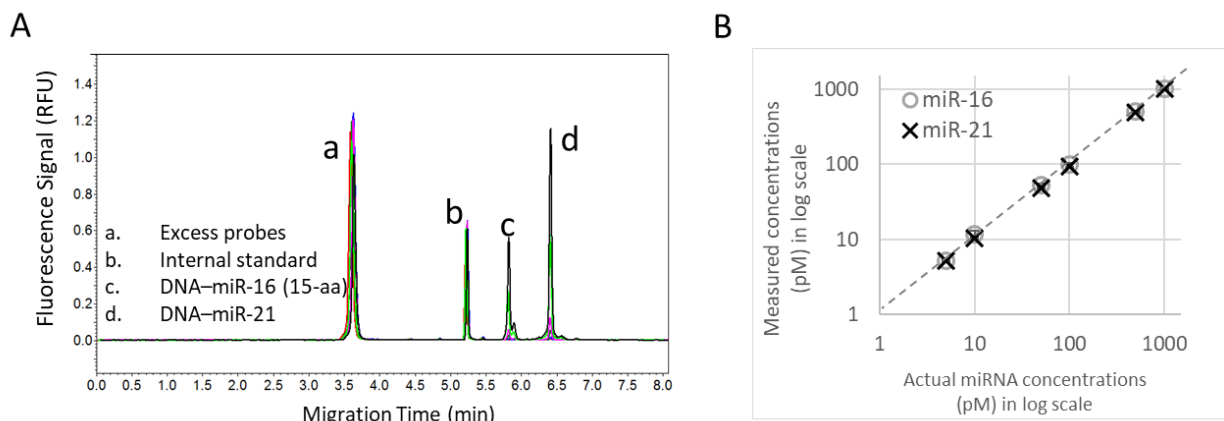


**Figure 5.1.** Implementation of DQAMmiR for simultaneously analysis of miR-16 and miR-21. A) Illustration of electropherograms of DQAMmiR analysis of miR-16 and miR-21. B) Quantitation results of DQAMmiR for analysis of various concentrations of miR-16 and miR-21 in a range of 5–1000 pM without sample preconcentration. These measurements were conducted in a 50-cm capillary, with a running buffer of 25mM Borax, pH 9.2 (50nM SSB) and a sample buffer of 50 mM Tris-Ac, 150mM NaCl, 10mM EDTA, pH 8.3. 5nM of DNA probes are used in each sample as excess, along with 0.5 nM of fluorescein as an internal standard.

### 5.3.2. Implementing ITP-DQAMmiR for simultaneous quantitation of miR-16 and miR-21

To establish ITP-DQAMmiR, I employed the two buffers: 1) 50 mM Tris-Acetate, 50 mM Sodium Acetate, pH 9.2 as LE for ITP and running buffer (with 10 nM SSB) for CE separation; 2) 20 mM Tris-HEPES, pH 8.3 as TE for ITP and sample buffer. The results in **Fig. 5.2** showed that the ITP-DQAMmiR with these buffer systems worked well, i.e., the separation between the two DNA-miRNA hybrids was not affected by the ITP preconcentration. However, the preconcentration step also concentrated the impurities associated with DNA probes, which would interfere with the detection of DNA-miRNA hybrids below at sub-pM levels as shown in **Fig. 5.2C**.

To resolve this problem, I decided to decrease the concentrations of DNA probes for the analysis of miRNAs at such low concentrations. One concern for decreasing the concentrations of

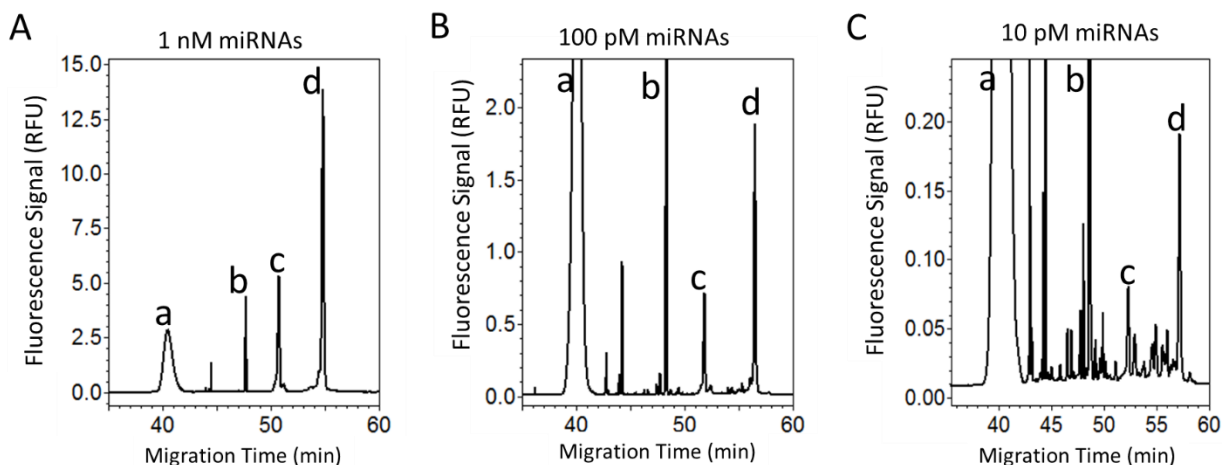


**Figure 5.2.** Implementation of DQAMmiR with ITP preconcentration for the analysis of miR-16 and miR-21 at different concentrations: A) 1 nM, B) 100 pM, and C) 10 pM. Peak assignment: (a) excess DNA probes (SSB bound), (b) fluorescein, (c) DNA–miR-16 (15aa) hybrid, and (d) DNA–miR-21 hybrid. 5nM of DNA probes are used in each sample as excess, along with 0.5 nM of fluorescein as an internal standard.

DNA probes is that the hybridization efficiency between the DNA probes and miRNAs might be impacted. However, our experimental results (shown in **Fig. 5.3**) that such impact is minimized. This could be explained by the efficient ITP concentration, which concentrated both the DNA probes and miRNA targets into a very narrow band, resulting in a very high local concentrations in that band, which facilitated the efficient DNA/miRNA hybridization in the capillary. Similar effect has been leveraged by Bercovici et al. to establish rapid on-column nucleic acid hybridizations [123]. With this effect, I was able to decrease the concentrations of DNA probes to 100 pM, which significantly decreased the level of impurities in the samples. This would allow me to detect miRNAs at much lower concentrations. I then used this approach to detect miRNAs below 10 pM as shown in **Fig 5.4**. The results in **Table 5.1** demonstrated that could quantified miR-16 and miR-21 simultaneously with LOQ of 500 fM and 100 pM respectively.

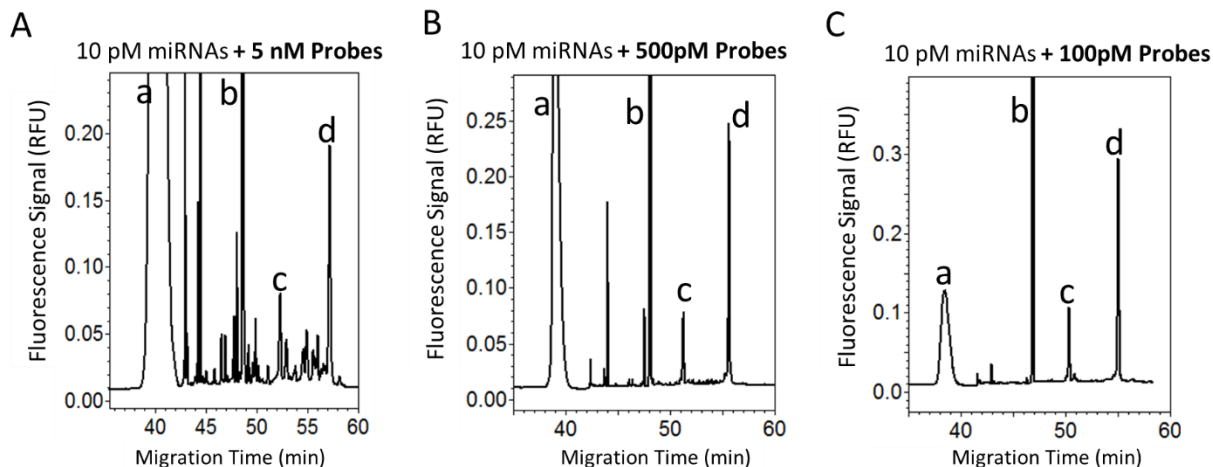


**Figure 5.3.** Implementation of DQAMmiR with ITP preconcentration for the analysis of miR-16 and miR-21 with different concentrations of DNA probes: A) 5 nM, B) 500 pM, and C) 100 pM. Peak assignment: (a) excess DNA probes (SSB bound), (b) fluorescein, (c) DNA–miR-16 (15aa) hybrid, and (d) DNA–miR-21 hybrid. 10 pM of miRNAs were used in each sample as excess, along with 0.5 nM of fluorescein as an internal standard.

**Table 5.1.** Quantitation results of ITP-DQAMmiR for the analysis of miR-16 and miR-21 at different concentrations

Actual concentration (pM)	Measured concentration (pM)	
	miR-16	miR-21
10	11.4 ± 0.5	11.5 ± 0.4
5	4.0 ± 0.5	4.8 ± 0.3
1	0.72 ± 0.15	0.86 ± 0.10
0.5	0.44 ± 0.10	0.45 ± 0.08
0.1	Below LOQ	0.12 ± 0.05

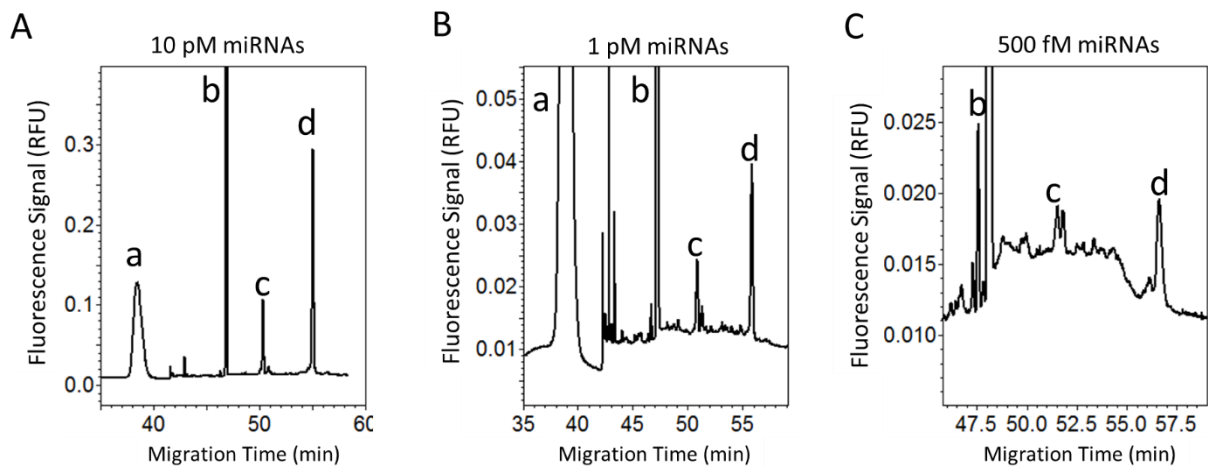


**Figure 5.4.** DQAMmiR with ITP preconcentration for quantitation of miR-16 and miR-21 at different concentrations: A) 10 pM, B) 1 pM, and C) 500 fM. Peak assignment: (a) excess DNA probes (SSB bound), (b) fluorescein, (c) DNA–miR-16 (15aa) hybrid, and (d) DNA–miR-21 hybrid. 100 pM of DNA probes are used in each sample as excess, along with fluorescein as an internal standard.

### 5.3.3. Analysis of miR-16 and miR-21 in urine sediments with ITP-DQAMmiR

I then attempted to apply the ITP-DQAMmiR to detect the endogenous miR-16 and miR-21 in urine samples, or more specifically, in urine sediments which contain miRNAs originated from the urinary tissues and cells according to the recent studies. For this purpose, I first developed

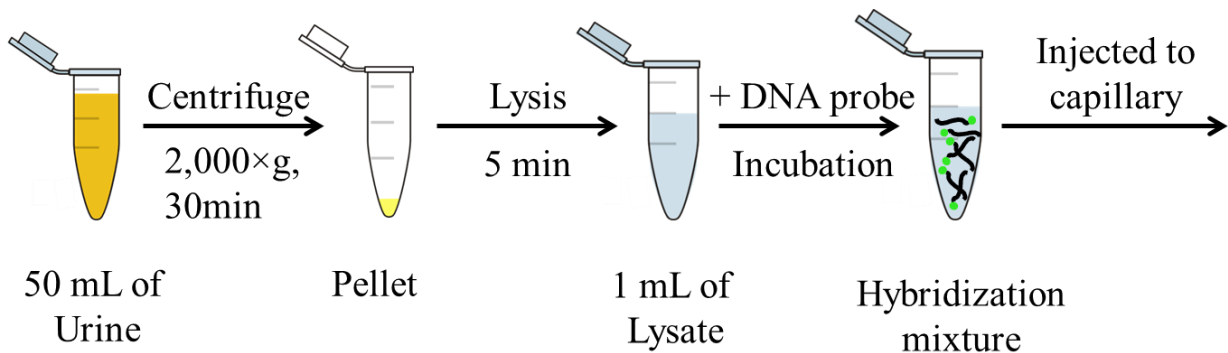


**Figure 5.5.** Sampling procedures for the analysis of endogenous miRNAs in urine sediments. Lysis buffer is composed of 0.1% Triton X-100, 20 mM Tris-HEPES, pH 8.3.

a simple sampling procedure as shown in **Fig 5.5**. Since DQAMmiR is robust to the biological matrices as highlighted in Chapter 2, I was able to eliminate the RNA extraction step which was typically required for other miRNA detection methods. With this procedure, I successfully detected the endogenous miR-16 and miR-21 in the crude lysates of urine sediments that were collected from a volunteer as shown in **Fig. 5.6**, indicating that the sample matrices in the urine sediment lysates didn't affect the ITP preconcentration and CE separation. However, the contents in such complicated samples interfered with the identification of peaks for excess DNA probes (SSB-bound) the electropherogram as shown in **Fig. 5.7**, which in turn affected the quantitiveness of DQAMmiR. This is because many metabolisms presented in urine can be detected by the LIF detection setup I used here. Moreover, the SSB-mediated separation of DNA probes could be interfered by the sample matrices, which leading to irreproducible peaks for the excess DNA probes across different samples as shown here.

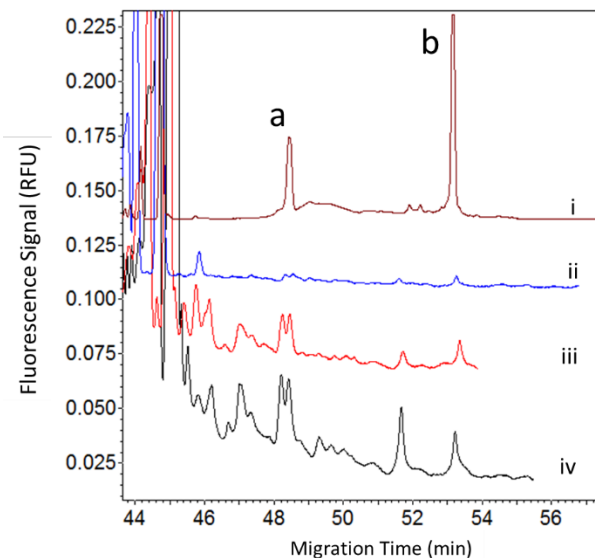


**Figure 5.6.** DQAMmiR with ITP preconcentration for quantitation of miR-16 and miR-21 in crude lysates of urine sediments: i) positive control (10 pM miRNAs), ii) urine sample 1, iii) urine sample 2, and iii) urine sample 3. Peak assignment: (a) DNA–miR-16 (15aa) hybrid, and (b) DNA–miR-21 hybrid. 100 pM of DNA probes are used in each sample.

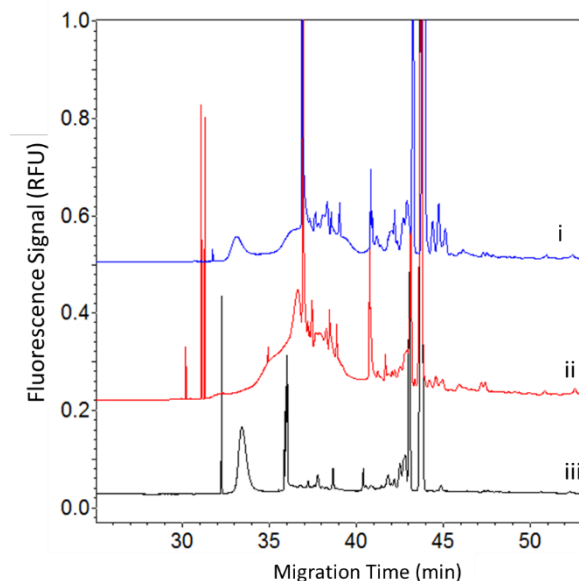


**Figure 5.7.** Illustration of complicated matrices in crude lysates of urine sediments interfering with DQAMmiR quantification. Traces: i) urine sample 1, ii) urine sample 2, and iii) urine sample 3.

Due to this impact, I was not able to accurately determine the exact concentrations of each miRNAs in the lysate samples. It was clear (**Fig. 5.6**) that peak areas of both DNA–miR-16 (15aa) hybrid, and DNA–miR-21 hybrid varied significantly in trace ii–iv, which indicates that the endogenous abundance of miR-16 and miR-21 varied significantly in the three urine sediment samples that were collected from a same volunteer on the same day. This suggests that it would not be practical to use the any individual urinary miRNAs as biomarkers because their quantity could vary intraindividually.

While the peaks areas of both miRNAs varied significantly in three samples, it was noticeable that the ratio between the peak area of DNA–miR-16 (15aa) hybrid and the peak area of DNA–miR-21 hybrid was relatively consistent ( $\frac{A_{\text{DNA-miR-16}}}{A_{\text{DNA-miR-21}}} = 2.1 \pm 0.1$ ) across three samples. This results proved that my hypothesis that the concentration ratios between two urinary miRNAs could be consistent intraindividually, which would serve as better biomarkers than individual

miRNA concentrations in clinical diagnostic tests. And DQAMmiR, would be a very promising tool for the use of such ratiometric approaches in practice.

#### **5.4. Conclusions**

In this study, I developed simple sampling procedures for the analysis of urinary miRNAs by DQAMmiR. With such simple sampling procedures, I was able to detect both endogenous miR-16 and miR-21 in urine sediment samples collected from a volunteer, which demonstrated that the complex matrices in the urine sediment lysates didn't interfere with the ITP preconcentration and CE separation. By analyzing three urine sediment samples collected from the same volunteer on the same day but at different times, I showed that the concentrations of individual miRNAs could varied significantly (up to 10 fold) intraindividually, the concentration ratio between miR-16 and miR-21, however, remained almost constant in these samples. This results suggested that using the ratio between two urinary miRNAs could serve as better biomarkers than individual urinary miRNA concentrations in clinical diagnostic tests. And DQAMmiR could be an ideal platform for the use of such ratiometric biomarkers.

## CONCLUDING REMARKS

A robust miRNA detection method is needed for the validation and clinical use of miRNA-based biomarkers. In my project, I proved that the CE separation in DQAMmiR is robust to various biological matrices including crude cell lysates, as compared to the benchmark methods RT-PCR. This suggests that it is possible to apply DQAMmiR to analyze endogenous miRNAs in a variety of biological samples with minimal sample preparation steps, making it a promising platform for analyzing miRNA-based biomarkers. I introduced a new generation of DQAMmiR which utilizing electrically neutral PNA as hybridization probes. In this approach, the negatively-charged PNA-miRNA hybrids were separated from the neutral PNA probes by CE without any additional mobility shifter, which eliminates the need for SSB, which further improves the robustness of DQAMmiR. However, the electrically neutral PNA probes in DQAMmiR makes it incompatible with the ITP for sample preconcentration which is necessary for the detection of low abundance miRNAs in clinical samples. To overcome this issue, I introduced a new sample preconcentration methods which combines FASS with ITP prior to CE separation to greatly decrease LOQ of DQAMmiR. I demonstrated that FASS-ITP could efficiently concentrate PNA-miRNA hybrids while preventing the loss of PNA probes, proving that FASS-ITP-CE is applicable to DQAMmiR utilizing PNA probe in principle. Using FASS-ITP-CE for simultaneous analysis of two miRNAs showed that an LOQ of 0.1 pM could be achieved. This LOQ is about 140 times lower than that of the standard CE-based DQAMmiR. I also showed that FASS-ITP-CE was suitable for analyzing endogenous miRNAs in crude cell lysates directly, suggesting that the method was robust to variations in the sample-matrix components. I also explored the applicability of DQAMmiR to the analysis of urinary miRNAs. By using a simple sampling procedures, I demonstrated that the DQAMmiR could successfully detect two endogenous miRNAs, miR-16

and miR-21. In this study, I noticed that the abundance of miRNAs in urine samples could vary significantly (up to 10 fold) in different urine samples collected from the same person on the same day but at different times. Such intraindividual variability illustrates that it would be inappropriate to use individual miRNA concentrations as biomarkers in practice. In contrast, I noticed that the concentration ratio between two miRNAs could be relatively stable in these samples, suggesting that the ratiometric measurements between multiple miRNAs would serve as better biomarkers than individual miRNA concentrations in clinical diagnostic tests. And DQAMmiR would be an ideal analytical methodology for the development and use of such tests.

In conclusion, I have further proved and improved the robustness of DQAMmiR which I believe is a very promising method for use in a variety of clinical applications. In addition, I have added a few new tools/methods, such as electrically neutral PNA as hybridization probe and FASS-ITP for preconcentration, into the pre-existing tools (e.g., SSB-mediated mobility shifting, universal peptide drag tags, ITP preconcentration). With this versatile toolsets, future users can easily customize their methods and assays depending on their use cases. The next step for this work is to test the clinical validity of DQAMmiR with some clinically relevant use cases.

## **FUTURE PLANS**

DQAMmiR continues to be developed in the Krylov lab, with the future focus on testing its analytical validity in clinical applications, such as validation of urinary miRNA biomarkers. The proper validation will lead to the application of DQAMmiR to real clinical use cases with our collaborators here at York University and at Sunnybrook hospital.

In order to test the analytical validity of DQAMmiR, we are planning to apply DQAMmiR to analyze a few tentative miRNA biomarkers in urine samples. There will be two purposes for this work. First, we will investigate the optimal sample preparation procedures for the analysis of urine samples. Secondly, we can test whether the ratiometric analysis approach with DQAMmiR would improve the clinical utility of the miRNA-based biomarkers in urine. In this work, we are planning to validate a disease-relevant miRNA-based biomarker in a variety of urine samples collected from patients with low-risk and high-risk prostate cancers.

Other than that, we are also planning to explore the utility of DQAMmiR in analyzing miRNA-based biomarkers in other types of biological fluids, such as blood, saliva etc. For this purpose, we will first test the robustness of DQAMmiR as well as the OSP techniques (ITP and FASS-ITP) in these different types of biological matrices. Once that being proved, we would be able to expand the applicability of DQAMmiR to a large variety of use cases. We are also actively seeking collaboration in this space to ensure we can get variety of clinical samples going forward.

## LIST OF PUBLICATIONS

1. **Hu, L.**; Stasheuski, A. S.; Wegman, D. W.; Wu, N.; Yang, B. B.; Hayder, H.; Peng, C.; Liu, S. K.; Yousef, G.M.; Krylov, S.N. Accurate miRNA analysis in crude cell lysate by capillary electrophoresis-based hybridization assay in comparison with quantitative reverse transcription-polymerase chain reaction. *Anal. Chem.* **2017**, *89*, 4743–4748.
2. **Hu, L.**; Anand, M.; Krylova, S. M.; Yang, B. B.; Liu, S. K.; Yousef, G. M.; Krylov, S. N. Direct quantitative analysis of multiple microRNAs (DQAMmiR) with peptide nucleic acid hybridization probes. *Anal. Chem.* **2018**, *90*, 14610–14615
3. Wang, T.Y.; **Hu, L.**; Krylov, S.N. Empirical Predictor of Conditions which Support Ideal-Filter Capillary Electrophoresis. *Electrophoresis* **2020**, *41*, 1225–1229.
4. **Hu, L.**; Krylova, S. M.; Liu, S. K.; Yousef, G. M.; Krylov, S. N. Necessity and Challenges of Sample Pre-concentration in Analysis of Multiple MicroRNAs by Capillary Electrophoresis. *Anal. Chem.* **2020**, *92*, 14251–14258.
5. **Hu, L.**; Krylova, S. M.; Krylov, S. N. Ratiometric Analysis of MicroRNAs in Urine by Capillary Electrophoresis Enables their Clinical Use as Non-invasive Biomarkers. *Manuscript In Preparation*

## REFERENCE

1. Lee, R. C.; Feinbaum, R. L.; Ambros, V. *Cell* **1993**, *75*, 843–854.
2. Friedman, R. C.; Farh, K. K.-H.; Burge, C. B.; Bartel, D. P. *Genome Res.* **2009**, *19*, 92–105.
3. Lee, Y.; Kim, M.; Han, J.; Yeom, K. H.; Lee, S.; Baek, S. H.; Kim, V. N. *The EMBO journal* **2004**, *23*, 4051–4060.
4. Denli, A. M.; Tops, B. B.; Plasterk, R. H.; Ketting, R. F.; Hannon, G. J. *Nature* **2004**, *432*, 231–235.
5. Hutvagner, G.; McLachlan, J.; Pasquinelli, A. E.; Bálint, É.; Tuschl, T.; Zamore, P. D. *Science* **2001**, *293*, 834–838.
6. Khvorova, A.; Reynolds, A.; Jayasena, S. D. *Cell* **2003**, *115*, 209–216.
7. Bartel, D. P. *Cell* **2004**, *116*, 281–297.
8. Helwak, A.; Kudla, G.; Dudnakova, T.; Tollervey, D. *Cell* **2013**, *153*, 654–665.
9. Buscaglia, L. E. B.; Li, Y. *Chin. J. Cancer* **2011**, *30*, 371–380.
10. Papagiannakopoulos, T.; Shapiro, A.; Kosik, K. S. *Cancer Res.* **2008**, *68*, 8164–8172.
11. Lee, I.; Ajay, S. S.; Yook, J. I.; Kim, H. S.; Hong, S. H.; Kim, N. H.; Dhanasekaran, S. M.; Chinnaiyan, A. M.; Athey, B. D. *Genome Res.* **2009**, *19*, 1175–1183.
12. Place, R. F.; Li, L.-C.; Pookot, D.; Noonan, E. J.; Dahiya, R. *Proc. Natl. Acad. Sci. U.S.A.* **2008**, *105*, 1608–1613.
13. Qin, W.; Shi, Y.; Zhao, B.; Yao, C.; Jin, L.; Ma, J.; Jin, Y. *PLoS ONE* **2010**, *5*, e9429.
14. Visone, R.; Rassenti, L. Z.; Veronese, A.; Taccioli, C.; Costinean, S.; Aguda, B. D.; Volinia, S.; Ferracin, M.; Palatini, J.; Balatti, V.; Alder, H.; Negrini, M.; Kipps, T. J.; Croce, C. M. *Blood* **2009**, *114*, 3872–3879.
15. Calin, G. A.; Dumitru, C. D.; Shimizu, M.; Bichi, R.; Zupo, S.; Noch, E.; Aldler, H.; Rattan, S.; Keating, M.; Rai, K.; Rassenti, L.; Kipps, T.; Negrini, M.; Bullrich, F.; Croce, C. M. *Proc. Natl. Acad. Sci. U.S.A.* **2002**, *99*, 15524–15529.
16. Iorio, M. V.; Ferracin, M.; Liu, C.-G.; Veronese, A.; Spizzo, R.; Sabbioni, S.; Magri, E.; Pedriali, M.; Fabbri, M.; Campiglio, M.; Menard, S.; Palazzo, J. P.; Rosenberg, A.; Musiani, P.; Volinia, S.; Nenci, I.; Calin, G. A.; Querzoli, P.; Negrini, M.; Croce, C. M. *Cancer Res.* **2005**, *65*, 7065–7070.
17. Lu, J.; Getz, G.; Miska, E. A.; Alvarez-Saavedra, E.; Lamb, J.; Peck, D.; Sweet-Cordero, A.; Ebert, B. L.; Mak, R. H.; Ferrando, A. A.; Downing, J. R.; Jacks, T.; Horvitz, H. R.; Golub, T. R. *Nature* **2005**, *435*, 834–838.

18. Yanaihara, N.; Caplen, N.; Bowman, E.; Seike, M.; Kumamoto, K.; Yi, M.; Stephens, R. M.; Okamoto, A.; Yokota, J.; Tanaka, T.; Calin, G. A.; Liu, C.-G.; Croce, C. M.; Harris, C. C. *Cancer Cell* **2006**, *9*, 189–198.
19. Meng, F.; Henson, R.; Wehbe-Janek, H.; Ghoshal, K.; Jacob, S. T.; Patel, T. *Gastroenterology* **2007**, *133*, 647–658.
20. Johnson, S. M.; Grosshans, H.; Shingara, J.; Byrom, M.; Jarvis, R.; Cheng, A.; Labourier, E.; Reinert, K. L.; Brown, D.; Slack, F. J. *Cell* **2005**, *120*, 635–647.
21. McDermott, A. M.; Miller, N.; Wall, D.; Martyn, L. M.; Ball, G.; Sweeney, K. J.; Kerin, M. J. *PLoS ONE* **2014**, *9*, e87032.
22. Mar-Aguilar, F.; Luna-Aguirre, C. M.; Moreno-Rocha, J. C.; Araiza-ChÁVez, J.; Trevino, V.; RodrÍGuez-Padilla, C.; ResÉNdez-PÉRez, D. *Asia Pac. J. Clin. Oncol.* **2013**, *9*, 53–59.
23. Srinivasan, M.; Sedmak, D.; Jewell, S. *Am. J. Clin. Pathol.* **2002**, *161*, 1961–1971.
24. Wester, K.; Wahlund, E.; Sundström, C.; Ranefall, P.; Bengtsson, E.; Russell, P. J.; Ow, K. T.; Malmström, P.-U.; Busch, C. *Applied Immunohistochemistry & Molecular Morphology* **2000**, *8*, 61–70.
25. Chung, J.-Y.; Braunschweig, T.; Williams, R.; Guerrero, N.; Hoffmann, K. M.; Kwon, M.; Song, Y. K.; Libutti, S. K.; Hewitt, S. M. *J. Histochem. Cytochem.* **2008**, *56*, 1033–1042.
26. Xi, Y.; Nakajima, G.; Gavin, E.; Morris, C. G.; Kudo, K.; Hayashi, K.; Ju, J. *RNA* **2007**, *13*, 1668–1674.
27. Varnholt, H.; Drebber, U.; Schulze, F.; Wedemeyer, I.; Schirmacher, P.; Dienes, H.-P.; Odenthal, M. *Hepatology* **2008**, *47*, 1223–1232.
28. Mitchell, P. S.; Parkin, R. K.; Kroh, E. M.; Fritz, B. R.; Wyman, S. K.; Pogosova-Agadjanyan, E. L.; Peterson, A.; Noteboom, J.; O'Briant, K. C.; Allen, A.; Lin, D. W.; Urban, N.; Drescher, C. W.; Knudsen, B. S.; Stirewalt, D. L.; Gentleman, R.; Vessella, R. L.; Nelson, P. S.; Martin, D. B.; Tewari, M. *Proc. Natl. Acad. Sci. U.S.A.* **2008**, *105*, 10513–10518.
29. Chen, X.; Ba, Y.; Ma, L.; Cai, X.; Yin, Y.; Wang, K.; Guo, J.; Zhang, Y.; Chen, J.; Guo, X.; Li, Q.; Li, X.; Wang, W.; Zhang, Y.; Wang, J.; Jiang, X.; Xiang, Y.; Xu, C.; Zheng, P.; Zhang, J.; Li, R.; Zhang, H.; Shang, X.; Gong, T.; Ning, G.; Wang, J.; Zen, K.; Zhang, J.; Zhang, C.-Y. *Cell Res.* **2008**, *18*, 997–1006.
30. Liu, J.; Gao, J.; Du, Y.; Li, Z.; Ren, Y.; Gu, J.; Wang, X.; Gong, Y.; Wang, W.; Kong, X. *Int. J. Cancer* **2012**, *131*, 683–691.
31. Ohtsuka, E.; Nishikawa, S.; Fukumoto, R.; Tanaka, S.; Markham, A. F.; Ikehara, M.; Sugiura, M. *European J. Biochem.* **1977**, *81*, 285–291.
32. McLaughlin, L. W.; Romaniuk, E.; Romaniuk, P. J.; Neilson, T. *European J. Biochem.* **1982**, *125*, 639–643.
33. Weiss, E. A.; Gilmartin, G. M.; Nevins, J. R. *EMBO J.* **1991**, *10*, 215–219.

34. Liu, C.-G.; Calin, G. A.; Meloon, B.; Gamliel, N.; Sevignani, C.; Ferracin, M.; Dumitru, C. D.; Shimizu, M.; Zupo, S.; Dono, M.; Alder, H.; Bullrich, F.; Negrini, M.; Croce, C. M. *Proc. Natl. Acad. Sci. U.S.A.* **2004**, *101*, 9740–9744.
35. Lao, K.; Xu, N. L.; Yeung, V.; Chen, C.; Livak, K. J.; Straus, N. A. *Biochem. Biophys. Res. Commun.* **2006**, *343*, 85–89.
36. Wegman, D.W.; Krylov, S.N. *TrAC* **2013**, *44*, 121–130
37. Morin, R. D.; O'Connor, M. D.; Griffith, M.; Kuchenbauer, F.; Delaney, A.; Prabhu, A.-L.; Zhao, Y.; McDonald, H.; Zeng, T.; Hirst, M.; Eaves, C. J.; Marra, M. A. *Genome Res.* **2008**, *18*, 610–621.
38. Wu, Q.; Wang, C.; Lu, Z.; Guo, L.; Ge, Q., Analysis of serum genome-wide microRNAs for breast cancer detection. *Clin. Chim. Acta* **2012**, *413*, 1058–1065.
39. Wyman, S. K.; Parkin, R. K.; Mitchell, P. S.; Fritz, B. R.; O'Briant, K.; Godwin, A. K.; Urban, N.; Drescher, C. W.; Knudsen, B. S.; Tewari, M. *PLoS ONE* **2009**, *4*, e5311.
40. Stoddart, D.; Heron, A. J.; Mikhailova, E.; Maglia, G.; Bayley, H. *Proc. Natl. Acad. Sci. U.S.A.* **2009**, *106*, 7702–7707.
41. Manrao, E. A.; Derrington, I. M.; Laszlo, A. H.; Langford, K. W.; Hopper, M. K.; Gillgren, N.; Pavlenok, M.; Niederweis, M.; Gundlach, J. H. *Nat. Biotechnol.* **2012**, *30*, 349–353.
42. Driskell, J. D.; Seto, A. G.; Jones, L. P.; Jokela, S.; Dluhy, R. A.; Zhao, Y. P.; Tripp, R. A. *Biosens. Bioelectron.* **2008**, *24*, 917–922.
43. Izumi, Y.; Takimura, S.; Yamaguchi, S.; Iida, J.; Bamba, T.; Fukusaki, E. *J. Biosci. Bioeng.* **2012**, *113*, 412–419.
44. Sforza, S.; Scaravelli, E.; Corradini, R.; Marchelli, R. *Chirality* **2005**, *17*, 515–521.
45. Gao, Z.; Yang, Z. *Anal. Chem.* **2006**, *78*, 1470–1477.
46. Yang, H.; Hui, A.; Pampalakis, G.; Soleymani, L.; Liu, F.-F.; Sargent, E. H.; Kelley, S. O. *Angew. Chem. Int. Ed.* **2009**, *48*, 8461–8464.
47. Wang, Z.; Zhang, J.; Guo, Y.; Wu, X.; Yang, W.; Xu, L.; Chen, J.; Fu, F. *Biosens. Bioelectron.* **2013**, *45*, 108–113.
48. Boriachek, K.; Umer, M.; Islam, M. N.; Gopalan, V.; Lam, A. K.; Nguyen, N. T.; Shiddiky, M. J. A. *Analyst* **2018**, *143*, 1662–1669.
49. Luo, L.; Wang, L.; Zeng, L.; Wang, Y.; Weng, Y.; Liao, Y.; Chen, T.; Xia, Y.; Zhang, J.; Chen, J. *Talanta* **2020**, *207*, p120298
50. Sabahi, A.; Salahandish, R.; Ghaffarinejad, A.; Omidinia, E. *Talanta* **2020**, *209*, p120595.
51. Hong, C. Y.; Chen, X.; Liu, T.; Li, J.; Yang, H. H.; Chen, J. H.; Chen, G. N. *Biosens. Bioelectron.* **2013**, *50*, 132–136.
52. Fan, Y.; Chen, X.; Trigg, A. D.; Tung, C.-h.; Kong, J.; Gao, Z. *J. Am. Chem. Soc.* **2007**, *129*, 5437–5443.

53. Zhang, G.-J.; Chua, J. H.; Chee, R.-E.; Agarwal, A.; Wong, S. M. *Biosens. Bioelectron.* **2009**, *24*, 2504–2508.
54. Baker, M. B.; Bao, G.; Searles, C. D. *Nucleic Acids Res.* **2012**, *40*, e13.
55. Kang, W. J.; Cho, Y. L.; Chae, J. R.; Lee, J. D.; Choi, K.-J.; Kim, S. *Biomaterials* **2011**, *32*, 1915–1922.
56. Paiboonskuwong, K.; Kato, Y. *Nucleic Acids Symposium Series* **2006**, *50*, 327–328.
57. Persat, A.; Santiago, J. G. *Analytical Chemistry* **2011**, *83*, 2310–2316.
58. Hartig, J. S.; Grune, I.; Najafi-Shoushtari, S. H.; Famulok, M. *J. Am. Chem. Soc.* **2004**, *126*, 722–723.
59. Neely, L. A.; Patel, S.; Garver, J.; Gallo, M.; Hackett, M.; McLaughlin, S.; Nadel, M.; Harris, J.; Gullans, S.; Rooke, J. *Nat. Meth.* **2006**, *3*, 41–46.
60. Yin, B.-C.; Liu, Y.-Q.; Ye, B.-C. *J. Am. Chem. Soc.* **2012**, *134*, 5064–5067.
61. Varallyay, E.; Burgyan, J.; Havelda, Z. *Nat. Protocols* **2008**, *3*, 190–196.
62. Kim, S. W.; Li, Z.; Moore, P. S.; Monaghan, A. P.; Chang, Y.; Nichols, M.; John, B. *Nucleic Acids Res.* **2010**, *38*, e98.
63. Yang, W.-J.; Li, X.-B.; Li, Y.-Y.; Zhao, L.-F.; He, W.-L.; Gao, Y.-Q.; Wan, Y.-J.; Xia, W.; Chen, T.; Zheng, H.; Li, M.; Xu, S.-q. *Anal. Biochem.* **2008**, *376*, 183–188.
64. Roy, S.; Soh, J. H.; Gao, Z. *Lab Chip* **2011**, *11*, 1886–1894.
65. Wang, Y.; MacLachlan, E.; Nguyen, B. K.; Fu, G.; Peng, C.; Chen, J. I. L. *Analyst* **2015**, *140*, 1140–1148.
66. Wang, Q.; Li, Q.; Yang, X.; Wang, K.; Du, S.; Zhang, H.; Nie, Y. *Biosens. Bioelectron.* **2016**, *77*, 1001–1007.
67. Joshi, G. K.; Deitz-McElyea, S.; Liyanage, T.; Lawrence, K.; Mali, S.; Sardar, R.; Korc, M. *ACS Nano* **2015**, *9*, 11075–11089.
68. Chang, P.-L.; Chang, Y.-S.; Chen, J.-H.; Chen, S.-J.; Chen, H.-C. *Anal. Chem.* **2008**, *80*, 8554–8560.
69. Khan, N.; Cheng, J.; Pezacki, J. P.; Berezovski, M. V. *Anal. Chem.* **2011**, *83*, 6196–6201.
70. Kemp G. *Biotechnol. Appl. Biochem.* **1998**, *27*, 9–17.
71. Frazier, R. A.; Ames, J. M.; Nursten, H. E. *Electrophoresis* **1999**, *20*, 3156–3180.
72. Kleparník, K.; Bocek, P. *Chem. Rev.* **2007**, *107*, 5279–5317.
73. Dabek-Zlotorzynska, E. *Electrophoresis* **1997**, *18*, 2453–2464.
74. Desai, M. J.; Armstrong, D. W. *Microbiol. Mol. Biol. Rev.* **2003**, *67*, 38–51.
75. Giddings, J. C. *Sep. Sci.* **1969**, *4*, 181–189.

76. Bharadwaj, R.; Santiago J. G.; Mohammadi, B. *Electrophoresis* **2002**, *23*, 2729–2744.
77. Baba, Y.; Tsuchiko, M.; Enomoto, S.; Chin A. M.; Dubrow, R. S. *High Resolut. Chromatogr.* **1991**, *14*, 204–206.
78. Cohen, A. S.; Vilenchick, M.; Dudley, J. L.; Gemborys, M. W.; Bourque, A. J. *J. Chromatogr.* **1993**, *638*, 293–301.
79. Swinney, K.; Bornhop, D. J. *Electrophoresis* **2000**, *21*, 1239–1250.
80. Kuban, P.; Hauser, P. C. *Anal. Chim. Acta* **2008**, *67*, 15–29.
81. Jung, B.; Zhu, Y.; Santiago, J. G. *Anal. Chem.* **2007**, *79*, 345–349.
82. van den Beld, C. M. B.; Tjaden, U. R.; Reinhoud, N. J.; Stegehuis, D. D.; van der Greef, J. *J. Controlled Release* **1990**, *13*, 129–139.
83. Albin, M.; Weinberger, R.; Sapp, E.; Moring, S. *Anal. Chem.* **1991**, *63*, 417–422.
84. Krylova, S. M.; Wegman, D. W.; Krylov, S. N. *Anal. Chem.* **2010**, *82*, 4428–4433.
85. Berezovski, M.; Krylov, S. N. *J. Am. Chem. Soc.* **2003**, *125*, 13451–13454.
86. Al-Mahrouki, A. A.; Krylov, S. N. *Anal. Chem.* **2005**, *77*, 8027–8030.
87. Li, T.; Zhang, D.; Luo, W.; Lu, M.; Wang, Z.; Song, Y.; Wang, H. *Anal. Chem.* **2010**, *82*, 487–490.
88. Dedionisio, L.; Raible, A. M.; Gryaznov, S. M. *Electrophoresis* **1998**, *19*, 1265–1269.
89. Wegman, D. W.; Krylov, S. N. *Angew. Chem. Int. Ed.* **2011**, *50*, 10335–10339.
90. Zhang, H.; Li, X.-F.; Le, X. C. *J. Am. Chem. Soc.* **2007**, *130*, 34–35.
91. Wegman, D. W.; Cherney, L. T.; Yousef, G.; Krylov, S. N. *Anal. Chem.* **2013**, *85*, 6518–6523.
92. Cherney, L. T.; Krylov, S. N. *Analyst* **2013**, *138*, 553–558.
93. Ghasemi, F.; Wegman, D. W.; Kanoatov, M.; Yang, B. B.; Liu, S. K.; Yousef, G. M.; Krylov, S. N. *Anal. Chem.* **2013**, *85*, 10062–10066.
94. Wegman, D. W.; Ghasemi, F.; Stasheuski, A. S.; Khorshidi, A.; Yang, B. B.; Liu, S. K.; Yousef, G. M.; Krylov, S. N. *Anal. Chem.* **2016**, *88*, 2472–2477.
95. Chien, R. L.; Burgi, D. S. *J. Chromatogr.* **1991**, *559*, 141–152.
96. Jacobson, S. C.; Ramsey, J. M. *Electrophoresis* **1995**, *16*, 481–486.
97. Aebersold, R.; Morrison, H. D. *J. Chromatogr.* **1990**, *516*, 79–88.
98. Britz-Mckibbin, P.; Chen, D. D. Y. *Anal. Chem.* **2000**, *72*, 1242–1252.
99. Kaniansky, D.; Marak, J. *J. Chromatogr.* **1990**, *498*, 191–204.
100. Krivankova, L.; Gebauer, P.; Bocek, P. *J. Chromatogr. A* **1995**, *716*, 35–48.

101. Zhang, H.; Zhang, W.; Zhang, Z.; Shi, Z.; Liu, W. *J. Liq. Chromatogr. Relat. Technol.* **2014**, *37*, 1145–1162.
102. Tang, W.; Ge, S.; Gao, F.; Wang, G.; Wang, Q.; He, P.; Fang, Y. *Electrophoresis* **2013**, *34*, 2041–2048.
103. Hsieh, B. C.; Chen, R. L. C.; Tsai, T. *J. Sep. Sci.* **2013**, *36*, 803–808.
104. Zhu, G.; Sun, L.; Yan, X.; Dovichi, N. J. *Anal. Chem.* **2014**, *86*, 6331–6336.
105. Terabe, S.; Otsuka, K.; Ando, T. *Anal. Chem.* **1985**, *57*, 834–841.
106. Terabe, S.; Otsuka, K.; Ichikawa, K.; Tsuchiya, A.; Ando, T. *Anal. Chem.* **1984**, *56*, 111–113.
107. Quirino, J. P.; Terabe, S. *Science* **1998**, *282*, 465–468.
108. Quirino, J. P.; Terabe, S. *J. High Resol. Chromatogr.* **1999**, *22*, 367–372.
109. Breadmore, M. C. *Electrophoresis* **2007**, *28*, 254–281.
110. Deng, D.; Deng, H.; Zhang, L.; Su, Y. *J. Chromatogr. Sci.* **2014**, *52*, 357–362.
111. Chen, Z.; Lin, Z.; Zhang, L.; Cai, Y. *Analyst* **2012**, *137*, 1723–1729.
112. Cheng, Y. C.; Wang, C. C.; Chen, Y. L.; Wu, S. M. *Electrophoresis* **2012**, *33*, 1443–1448.
113. Wang, C. C.; Chen, J. L.; Chen, Y. L.; Cheng, H. L.; Wu, S. M. *Anal. Chim. Acta* **2012**, *744*, 99–104.
114. Lin, Y. Y.; Wang, C. C.; Ho, Y. H.; Chen, C. S.; Wu, S. M. *Anal. Bioanal. Chem.* **2013**, *405*, 259–266.
115. Kawai, T.; Ueda, M.; Fukushima, Y.; Sueyoshi, K.; Kitagawa, F.; Otsuka, K. *Electrophoresis* **2013**, *34*, 2303–2310.
116. Tu<sup>o</sup>ma, P.; Š<sup>u</sup>stková<sup>´</sup> -Fis<sup>ˇ</sup>erova<sup>´</sup> ,M.; Opekar, F.; Pavl<sup>´</sup>ic<sup>ˇ</sup>ek, V.; M<sup>´</sup>alkov<sup>´</sup> a, K. *J. Chromatogr. A* **2013**, *1303*, 94–99.
117. Everaerts, F. M.; Beckers, J. L.; Verheggen, T. P. E. M.; *Isotachophoresis—Theory, Instrumentation and Applications*, Elsevier, Amsterdam, **1976**.
118. Garcia-Schwarz, G.; Rogacs, A.; Bahga, S. S.; Santiago, J. G. *J. Visualized Exp.* **2012**, *61*, e3890.
119. Breadmore, M. C.; Shallan, A. I.; Rabanes, H. R.; Gstoettenmayr, D.; Abdul Keyon, A. S.; Gaspar, A.; Dawod, M.; Quirino, J. P. *Electrophoresis* **2013**, *34*, 29–54.
120. Bahga, S. S.; Santiago, J. G. *Analyst* **2013**, *138*, 735–754.
121. Smejkal, P.; Bottenus, D.; Breadmore, M. C.; Guijt, R.M.; Ivory, C. F.; Foret, F.; Macka, M. *Electrophoresis* **2013**, *34*, 1493–1509.
122. Khurana, T. K.; Santiago, J. G. *Anal. Chem.* **2008**, *80*, 6300–6307.

123. Bercovici, M.; Han, C. M.; Liao, J. C.; Santiago, J. G. *Proc. Natl. Acad. Sci. U. S. A.* **2012**, *109*, 11127–11132.
124. Wegman, D. W.; Ghasemi, F.; Khorshidi, A.; Yang, B. B.; Liu, S. K.; Yousef, G. M.; Krylov, S. N. *Anal. Chem.* **2015**, *87*, 1404–1410.
125. Hayes, D. F. *Ann. Oncol.* **1993**, *4*, 807–819.
126. Pennello, G. A. *Clin. Trials* **2013**, *10*, 666–676.
127. Horvatovich, P.; Mischoff, R. *Eur. Mass Spectrom.* **2010**, *16*, 101–121.
128. Arefian, E.; Kiani, J.; Soleimani, M.; Shariati, S. A. M.; Aghaee-Bakhtiari, S. H.; Atashi, A.; Gheisari, Y.; Ahmadbeigi, N.; Banaei-Moghaddam, A. M.; Naderi, M.; Namvarasl, N. et al. *Nucleic Acids Res.* **2011**, *39*, e80.
129. Labib, M.; Khan, N.; Ghobadloo, S. M.; Cheng, J.; Pezacki, J. P.; Berezovski, M. V. *J. Am. Chem. Soc.* **2013**, *135*, 3027–3038.
130. Hong, C.; Baek, A.; Hah, S. S.; Jung, W.; Kim, D. E. *Anal. Chem.* **2016**, *88*, 2999–3003.
131. Lee, H.; Shapiro, S. J.; Chapin, S. C.; Doyle, P. S. *Anal. Chem.* **2016**, *88*, 3075–3081.
132. Qavi, A. J.; Bailey, R. C. *Angew. Chem., Int. Ed.* **2010**, *49*, 4608–4611.
133. Ren, Y.; Deng, H.; Shen, W.; Gao, Z. *Anal. Chem.* **2013**, *85*, 4784–4789.
134. Mráz, M.; Malinova, K.; Mayer, J.; Pospisilova, S. *Biochem. Biophys. Res. Commun.* **2009**, *390*, 1–4.
135. Jahn, C. E.; Charkowski, A. O.; Willis, D. K. *J. Microbiol. Methods* **2008**, *75*, 318–324.
136. Wang, W. X.; Wilfred, B. R.; Baldwin, D. A.; Isett, R. B.; Ren, N.; Stromberg, A.; Nelson, P. T. *Biochim. Biophys. Acta, Gene Regul. Mech.* **2008**, *1779*, 749–757.
137. Nagy, Z. B.; Wichmann, B.; Kalmár, A.; Barták, B. K.; Tulassay, Z.; Molnár, B. *Pathol. Oncol. Res.* **2016**, *22*, 505–513.
138. Tichopad, A.; Didier, A.; Pfaffl, M. W. *Mol. Cell. Probes* **2004**, *18*, 45–50.
139. Pfaffl, M. W. In *Quantitative Real-Time PCR in Applied Microbiology*; Filion, M., Ed; Caister Academic Press: Norfolk, **2012**; pp 53–62.
140. Chen, C.; Ridzon, D. A.; Broomer, A. J.; Zhou, Z.; Lee, D. H.; Nguyen, J. T.; Barbisin, M.; Xu, N. L.; Mahuvakar, V. R.; Andersen, M. R.; Lao, K. Q. *Nucleic Acids Res.* **2005**, *33*, e179.
141. Shi, R.; Chiang, V. L. *BioTechniques* **2005**, *39*, 519–525.
142. Wetmur, J. G.; Fresco, J. *Crit. Rev. Biochem. Mol. Biol.* **1991**, *26*, 227–259.
143. Ibberson, D.; Benes, V.; Muckenthaler, M. U.; Castoldi, M. *BMC Biotechnol.* **2009**, *9*, 102.
144. Labib, M.; Khan, N.; Berezovski, M. V. *Anal. Chem.* **2015**, *87*, 1395–1403.

145. Javaherian, S.; Musheev, M. U.; Kanoatov, M.; Berezovski, M. V.; Krylov, S. N. *Nucleic Acids Res.* **2009**, *37*, e62.
146. Podolska, A.; Kaczkowski, B.; Litman, T.; Fredholm, M.; Cirera, S. *Acta Biochim. Polym.* **2011**, *58*, 535–540.
147. Egholm, M.; Buchardt, O.; Nielsen, P. E.; Berg, R. H. *J. Am. Chem. Soc.* **1992**, *114*, 1895–1897.
148. Weiler, J.; Gausepohl, H.; Hauser, N.; Jensen, O. N.; Hoheisel, J. D., *Nucleic Acids Res.* **1997**, *25*, 2792–2799.
149. Kiliszek, A.; Banaszak, K.; Dauter, Z.; Rypniewski, W. *Nucleic Acids Res.* **2016**, *44*, 1937–1943.
150. Gagliardi, L. G.; Castells, C. B.; Ràfols, C.; Rosés, M.; Bosch, E. *J. Chem. Eng. Data* **2007**, *52*, 1103–1107.
151. Heller, C.; Slater, G. W.; Mayer, P.; Dovichi, N.; Pinto, D.; Viovy, J.-L.; Drouin, G. *J. Chromatogr. A* **1998**, *806*, 113–121.
152. Wilkins, D. K.; Grimshaw, S. B.; Receveur, V.; Dobson, C. M.; Jones, J. A.; Smith, L. J. *Biochemistry* **1999**, *38*, 16424–16431.
153. Kaneta, T.; Tanaka, S.; Yoshida, H. *J. Chromatogr. A* **1991**, *538*, 385–391.
154. Nielsen, P. E. *Annu. Rev. Biophys.* **1995**, *24*, 167–183.
155. Demidov, V. V.; Potaman, V. N.; Frank-Kamenetskii, M. D.; Egholm, M.; Buchard, O.; Sonnichsen, S. H.; Nielsen, P. E. *Biochem. Pharmacol.* **1994**, *48*, 1310–1313.
156. Hirokawa, T.; Ohmori, A.; Kiso, Y. *J. Chromatogr.* **1993**, *634*, 101–106.
157. Bharadwaj, R.; Santiago, J. G. *J. Fluid Mech.* **2005**, *543*, 57–92.
158. Burgi, D. S.; Chien, R. L. *Anal. Chem.* **1991**, *63*, 2042–2047.
159. Stegehuis, D. S.; Irth, H.; Tjaden, U. R.; Van der Greef, J. *J. Chromatogr.* **1991**, *538*, 393–402.
160. Ostromohov, N.; Schwartz, O.; Bercovici, M. *Anal. Chem.* **2015**, *87*, 9459–9466.
161. Malý, M.; Boublík, M.; Pocrnić, M.; Ansorge, M.; Lorinčíková, K.; Svobodová, J.; Hruška, V.; Dubský, P.; Gaš, B. *Electrophoresis* **2020**, *41*, 493–501.
162. Owczarzy, R.; You, Y.; Moreira, B. G.; Manthey, J. A.; Huang, L.; Behlke, M. A.; Walder, J. A. *Biochemistry* **2004**, *43*, 3537–3554.
163. Chim, W.; Sedighi, A.; Brown, C. L.; Pantophlet, R.; Li, P. C. H. *Can. J. Chem.* **2018**, *96*, 241–247.
164. Kawai, T.; Ota, N.; Imasato, A.; Shirasaki, Y.; Otsuka, K.; Tanaka, Y. *J. Chromatogr. A* **2018**, *1565*, 138–144.
165. Guo, J., Xiao, Z., Yu, X., Cao, R. *Oncol. Lett.* **2017**, *14*, 6895–6900

166. Mall, C.; Rocke, D. M.; Durbin-Johnson, B.; Weiss, R. H. *Biomark. Med.* 2013 7, 623–631.
167. Giannakodimos, I. *Curr Med Chem.* **2022**;29, 4311–4313.
168. Mahtal, N.; Lenoir, O.; Tinel, C.; Anglicheau, D.; Tharaux, P. L. *Nat. Rev. Nephrol.* **2022**, 18, 643–662.
169. Lin, H.; Shi, X.; Li, H.; Hui, J.; Liu, R.; Chen, Z.; Lu, Y.; Tan, W. *BMC Cancer.* **2021**, 21, e1293.
170. Duan, Z. Y.; Cai, G. Y.; Bu, R.; Lu, Y.; Hou, K.; Chen, X. M. *Sci. Rep.* **2016**, 6, 23498.